学位申請論文

上原　真一

主論文1

Permeability Structure of the Median Tectonic Line in Oshika-mura, Nagano Prefecture, central Japan

UEHARA Shin-ichi

December, 2001

Department of Geology and Mineralogy,
Graduate School of Science, Kyoto University

Abstract

Fluid motion in and across fault zones has received much attention in various problems in earth science such as fault mechanics, mechanism of earthquakes, and fault-seal of hydrocarbons. However, the permeability structures of fault zones have not been studied systematically. This paper thus reports permeability measurements of faults rocks along the Median Tectonic Line (MTL), the largest strike-slip fault in Japan, using a gas-medium triaxial deformation apparatus. Internal structures of the MTL fault zone were described at Kitagawa and Ankoh outcrops of the MTL and their neighboring areas in Ohshika-mura, Kami-ina-gun, Nagano Prefecture, central Japan. The fault zone consists of mylonites (about 1000 m wide), cataclasite (about 50–200 m wide) and incohesive fault rocks (about 5–30 m wide). The host rock to the west is mostly Hiji tonalite in Ryoke Metamorphic Belt and incohesive MTL fault rocks are adjacent directly to Sambagawa metamorphic rocks (mostly pelitic schist) to the east. Samples of fault rocks and their host rocks were collected at Kitagawa and Ankoh. The testing machine is equipped with a servo-controlled pore-pressure controlling system, and permeability has been measured with the pore-pressure oscillation method at room temperature and under a pore pressure of 20 MPa and confining pressures to 200 MPa (i.e., effective pressures to 180 MPa), using nitrogen gas as a confining medium. A simple gas-flow method for easy permeability measurements was developed herein and has also been used at confining pressures to 200 MPa.

An increase in the effective pressure from 10 to 180 MPa decreases permeability of all granular fault rocks measured here by about three orders of magnitudes, by closing cracks and/or compaction. Permeability of fault gouge is greater than those of cemented cataclasites and mylonites by more than 2 orders of magnitudes at a given effective

pressure so that the incohesive fault zone near the material boundary between the Ryoke and Sambagawa belts must have acted as a conduit for fluid motion. Clayey (sticky) fault gouge zone has permeability as low as 10^{-19} m^2 at high effective pressures, but such impermeable fault gouge is developed very locally and does not constitute a continuous zone (clayey gouge zone is likely to have been destroyed by latest MTL movement). Thermal pressurization is unlikely in this incohesive fault zone unless clayey gouge is formed pervasively at deeper parts of the MTL. Incohesive fault rocks exhibit large hysteresis upon pressure cycling and samples tend to remember the low permeability values at the largest pressure, suggesting nearly permanent compaction of gouge and breccia. Whereas cataclasites and mylonites display moderate hysteresis suggesting closing and opening of fractures upon pressure cycling. Thus the past history is important for evaluating permeability of incohesive fault rocks.

Triaxial compression experiments revealed marked effects of deformation on the permeability of fault rocks. Permeability of fault gouge decreases rapidly by about 2 orders of magnitude during initial loading and continues to decrease slowing even during inelastic deformation. The initial drop in permeability is much smaller for cataclasite and the permeability of this rock abruptly increases upon failure, and the overall change correlate well with the initial, nearly elastic contraction and subsequent dilatancy upon the initiation of inelastic deformation. If cemented cataclasite deform prior to or during earthquakes, cataclasite zone can be a site of fluid flow. But the gouge zone is unlikely to switch to permeable zone upon the initiation of fault slip. Thus permeability structures may change abruptly prior to or during earthquakes; the permeability of the fault gouge zone may decrease, while that of the cataclasite zone may increase. Fault gouge and cataclasite have internal angle of friction of about 36 and 45 degrees, respectively, as

typical of brittle rocks.

Fractures play vital role in fluid flow in fractured rocks and highly fractured zone can be the most permeable zone in a fault zone. But the evaluation of natural fractured rocks at great depths is not easy because of the complexity of fracture geometry and the scale effect of fractures. As a first step to this goal, this paper examined permeability of a single fracture, ground surface or natural fracture through integrated study of measurements of fracture permeability at effective pressures to 180 MPa, surface roughness measurements and contact analyses of surface asperities using the Hertzian theory. Apertures of ground surface and natural fracture in Sambagawa pelitic schist and Ryoke mylonite were estimated from measured permeability at effective pressures to 180 MPa assuming the cubic law. Aperture of contacting fractures has also been calculated from contact analyses of representative asperities. The agreements are not perfect, but the overall features of progressive reduction in aperture upon an increase in effective pressure were predicted. The deviation is probably due to be complex deformation of multiple contacting asperities.

The present paper thus revealed permeability structure of the MTL, demonstrated how permeability structure can change with deformation prior to and during earthquakes, and attempted to evaluate the fluid flow along fractures. The results will provide useful constraints for fluid flow analyses within fault zones. For full understanding of permeability structures and their changes during complete earthquake cycles, future studies must cover, at least, the effect of large shearing deformation within fault zones, effects of temperature, complete evaluation of the effects of fractures at deeper conditions, mechanical and chemical cementation of fault rocks during interseismic period.

Key words: Median Tectonic Line, fault permeability, fault-zone structure, fluid flow, deformation-fluid flow experiments, earthquake.

Contents

1. INTRODUCTION

Fault zones are regarded as passage ways for fluid flow in the Earth, but only several studies describe internal structures of faults and report permeability values of fault rocks such as fault gouge and breccia (Caine et al., 1996; Evans et al., 1997; Seront et al., 1998; Lockner et al., 2000; Falkner and Rutter, 2000; Mizoguchi et al., 2000; Wibberley and Shimamoto, 2001). Permeability structures of fault zones can be quite variable depending on tectonic setting, nature of host rocks, maturity and scale of a fault and associated internal structures, and depth of a fault (shallow to deep parts of a fault zone with different deformation mechanisms). Our current understanding of permeability structures of faults is far from adequate to cover the wide range of fault zones in nature.

This paper presents field and experimental studies on the permeability structures of Median Tectonic Line (MTL) in Ohshika-mura, Nagano Prefecture, central Japan. MTL is the largest strike-slip fault in Japan and was selected for this study since large scale faults are particularly important for understanding mechanisms of large and great earthquakes. MTL has a long tectonic history (Hara et al., 1980; Takagi, 1983, 1984; Michibayashi & Masuda, 1993; Michibayashi, 1993; chapter 2 of this paper) and its fault zone consists of mylonite, cataclasite and incohesive fault rocks. Hence this fault is ideal not only for studying a large-scale fault zone, but also for studying fault zone at shallow to great depths. Ohshika-mura is characterized by the development of a typical shear-zone structure in mylonites on the side of Ryoke Belt indicating left-lateral displacement (Hara et al., 1980). MTL fault zone at the boundary between Sambagawa and Ryoke Belts consists of incohesive fault rocks and a wide cataclasite zone. MTL in Ohshika-mura is thus suitable for studying permeability structures of a large fault. Chapter 2 describes internal structures of MTL fault zone in Ohshika-mura.

Brace et al. (1968) introduced a pulse-decay technique and opened a way to measure very low permeability of intact, crystalline rocks. An oscillation method was then proposed

independently by Kranz et al. (1990) and Fisher and Paterson (1992). In the latter method, the pore pressure on the upstream side of a specimen is oscillated sinusoidally with its response is measured on the downstream side, and the permeability and storage capacity can be estimated by the amplitude change and phase delay of the pore pressure. I used the oscillation method in most permeability measurements in this paper with N_2 pore fluids, using a triaxial deformation-fluid flow gas apparatus at Kyoto University. This machine is equipped with a fast operating servo-controlled system for controlling pore pressure and permeability ranging about 6 orders of magnitudes (10^{-14} to 10^{-20} m^2) can be measured. Using a gas as pore fluid enables quick permeability measurements even if permeability is as low as 10^{-20} m^2 (about 1,000 s for one measurement). A simple flow method is used in some measurements. Chapter 3 summarizes experimental procedures for permeability measurements.

Effective pressure (confining pressure minus pore pressure) is known to have drastic effects on permeability via closing cracks in cohesive fault rocks and/or compaction of granular aggregates such as incohesive fault rocks. In fact, previous studies examined fault-zone permeability by measuring permeability of fault rocks only at pressures (Caine et al.,1996; Evans et al., 1997; Lockner et al., 2000). Chapter 4 of this paper presents MTL permeability structures based on much more detailed data under pressure cycling conditions. Present work combined with recent work by Wibberley and Shimamoto (2001) will delineate complexity and variation of permeability structure of a large scale fault.

Fault rocks are subjected to deformation due to fault motion, and deformation is also a very important factor in controlling permeability of rocks and granular aggregates (e.g., Zoback and Byerlee, 1975; Zhu and Wong, 1997; Zhang and Cox, 2000). Effects of deformation would be particularly significant in evaluating long-term evolution of permeability structures during the formation and development of a fault, as well as in estimating short-term changes in fault-zone permeability structures due to precursory slip prior to an earthquake.

Chapter 5 of this paper reports permeability measurements of cohesive (rock-like) cataclasite and black fault gouge during triaxial deformation at different effective pressures. Contrasting behaviors of the two fault rocks, occupying significant proportions of MTL fault zone, are indeed remarkable and its implications for temporal change in permeability structures during a pre-seismic period will be discussed at the end of this paper.

Highly fractured zones (fractured cohesive fault rocks, fractured host rocks at the marginal parts of a fault zone) are likely to be a highly permeable zone and are probably important as conduits of fluid motion. However, the evaluation of their permeability is very difficult because of complex geometry of fractures and possible scale effects of fractures. As a first step to estimate permeability of fractured zones, chapter 6 of this paper presents an integrated analyses of fluid flow analyses along a single fracture (either ground surface or natural fracture), based on the laboratory measurements of fracture permeability, measurements of surface topography and contact analyses of measured surfaces using the Herzian theory (Johnson, 1985; Brown and Scholz, 1985; Yoshioka and Scholz, 1989). The agreements are reasonable, though not perfect.

The final section discusses the characteristic features of MTL permeability structures, discusses implications of the present results to fluid flow and thermal pressurization due to frictional heating, and suggests future tasks for complete understanding of fluid flow in fault zones.

2. INTERNAL STRUCTURES OF THE MEDIAN TECTONIC LINE IN OHSHIKA-MURA

2.1 Geological Setting

The MTL is the largest strike-slip fault in Japan, extending from Kanto to Kyushu (Fig. 2.1(a)). It forms the boundary between two contrasting metamorphic belts; the Ryoke belt (low P/ high T) and the Sambagawa belt (high P/ low T). These two metamorphic belts have each had a separate geotectonic evolution, both of which have controlled the geotectonic history of the MTL (e.g. Hara et al., 1977, 1980; Takagi, 1986).

There has been a great amount of debate on the history of the MTL. The age of the mylonitization has been investigated in many studies, and is considered to be before 60Ma. The MTL has been active recently around Southwest Japan. Topography caused by dextral active fault motion has been also reported around the Ankoh outcrop (Sakamoto, 1977), studied in this thesis. However, as shown later, the fault plane of the MTL is not clear at the Ankoh and Kitagawa outcrops, which suggests that the MTL has not been active recently at these outcrops.

The Ryoke belt consists of Hiji tonalite and metamorphic rocks, while the Sambagawa belt consists mainly of pelitic schist and basic schist around our study area (Fig. 2.1(b)). Towards the MTL, tonalite and metamorphic rocks of the Ryoke belt grade into mylonites characterized by grain-size reduction of quartz (Hara et al., 1977, 1980; Takagi, 1984; Michibayashi, 1993). A mylonite zone, several hundreds to a thousand meters in width, is distributed along the MTL in the Ryoke belt. The mylonitization of Ryoke rocks is considered to have finished before Ryoke and Sambagawa belts become juxtaposed against each other, as suggested by the following, for example (Takagi, 1984);

(1) Such gradation of quartz grain-size as shown at Ryoke is not found in the Sambagawa belt.

(2) The distribution of the quartz grain-size belt in the presently preserved Ryoke mylonite

zone is not symmetrical, suggesting that an eastern part of the mylonite zone existed but has been removed.

Ryoke mylonitic rocks and Sambagawa rocks along the MTL are overprinted by cataclastic deformation structures. Takagi (1983) thus suggested that cataclasites in the Ryoke belt formed after the mylonitization during the exhumation process. The attitudes of stretching lineation and asymmetric microstructures observed in the mylonites indicate that sinistral strike-slip shearing mainly took place during mylonitization (Hara et al., 1980; Takagi, 1986).

2.2 Internal Structures of the MTL

The distribution of fault rocks was investigated and samples collected for permeability measurements at the Kitagawa and Ankoh areas in Ohshika-mura. The MTL runs approximately N-S, and dips almost vertically around these areas. The outcrops of these areas were studied in detail by Matsushima (1994) and Tanaka et al. (1996). In both areas, the gouge zone is bounded on the Ryoke side by partially brecciated cataclasite zones derived probably from tonalitic mylonite in which few colored minerals are found, and those derived from mylonites of pelitic and silicic metamorphic rock. Along the MTL, black sandy gouge zones, a few meters in width, are observed at both these places. There are many minor faults around these outcrops studied in detail by Matsushima (1994).

Kitagawa outcrop and its vicinity

As Takagi (1984) and Michibayashi (1993) reported, there are clear grain-size changes of quartz in mylonites along the Nishi kobanazawa stream in Ryoke belt (Figs. 2.2 and 2.6).

Small amounts of brecciated cataclasite derived from tonalitic and metamorphic mylonite in the Ryoke belt and brecciated schist are observed at the Kitagawa outcrop (Fig. 2.3). Cataclasite in the Ryoke belt along the gouge zone is cemented by calcite or dolomite (Fig. 2.7). Sambagawa rocks adjacent to the gouge zone are brecciated.

A black sandy gouge zone is observed along the MTL at both the Kitagawa and the Ankoh outcrops and the microfabric and composition described in the following are close to each other. This zone is one to two meters in width, and consists of cohesive portion with a sandy matrix of identical composition (Fig. 2.9). X-ray-diffraction data revealed that this gouge consists of quartz, mica minerals and other clay minerals. Thin section observation showed that irregular-shape-minerals, which may be calcite or dolomite, surrounded the aggregates of clay minerals (Fig. 2.8(e)). Heterogeneities are partially present such as a clast and matrix microstructure which are both composed of the same minerals, although dolomite or calcite seems to be denser in clasts than in the matrix (Fig. 2.10). In places clear shear bands can be observed, although they do not form a clear microfabric. However, the protolith structure has been completely destroyed. A clayey gouge zone 1 to 2 cm thick was found at the top of the outcrop in a black sandy gouge zone, but this is not continuous and the thickness of the zone is variable. This clayey gouge zone is likely to have been destroyed by latest MTL movement.

The white gouge is relatively coarse. Under the optical microscope, we can observe fine-grained quartz (<15μm) covered by fine needle-like minerals (< 30μm) distributed densely, determined as mica minerals by the XRD analysis, and calcite.

Sambagawa schist next to the black gouge zone is brecciated strongly, and the boundary between them is not clear. X-ray-diffraction data revealed that this breccia consists of mica clay minerals and chlorite.

Ankoh outcrop and its vicinity

Fractured mylonite and cataclasite are observed in Ryoke belts around this area as reported by Tanaka et al. (1996) (Fig. 2.4). Next to the black gouge zone, a little brecciated Ryoke cataclasite is observed, which is cemented by calcite (Fig. 2.8(d)) and there are few colored minerals in this cataclasite. On the Sambagawa side, we can find fine-grained cataclasite which has dense veins of calcite nearly parallel to the fault plane (Fig. 2.8(f)), and

berecciated Sambagawa rocks are observed along Aoki river.

At the Ankoh outcrop, two black sandy gouge zones are observed, which are about 8 m apart from each other (Fig. 2.5). A clay gouge zone one to a few cm thick was observed, although the boundaries are not sharp and it is not continuous. The composition of clay minerals and the microstructure of the gouge are similar to those of the black gouge at the Kitagawa outcrop.

(a)

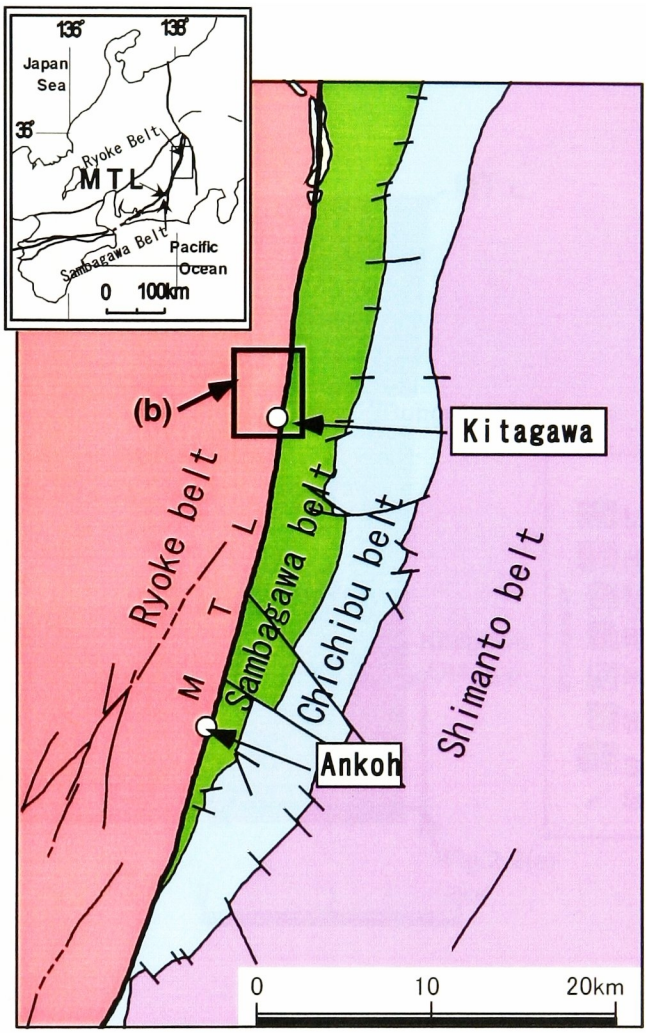

Fig. 2.1. (a) Location of the study area and regional setting of the Median Tectonic Line and metamorphic belts in central Japan.

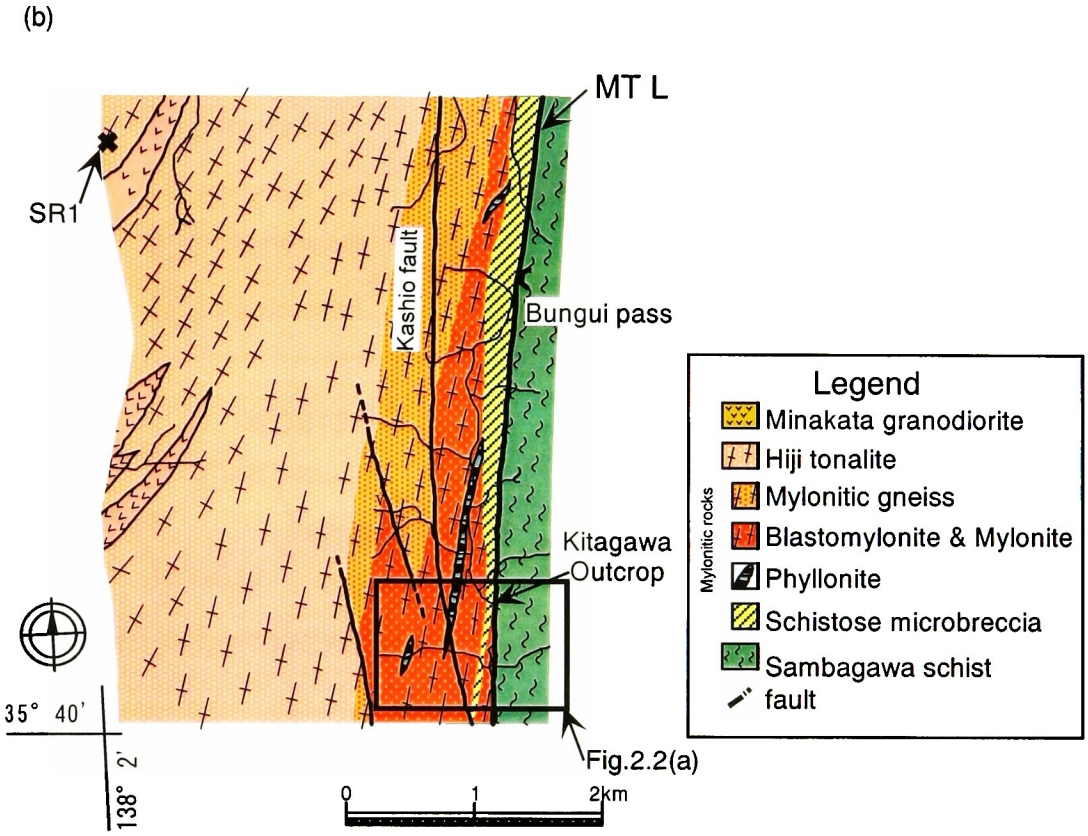

Fig. 2.1. (b) Geological map modified from Hayashi and Takagi (1987). The location of this area is indicated in (a). The sampling location of SR1(Tonalite) is also shown.

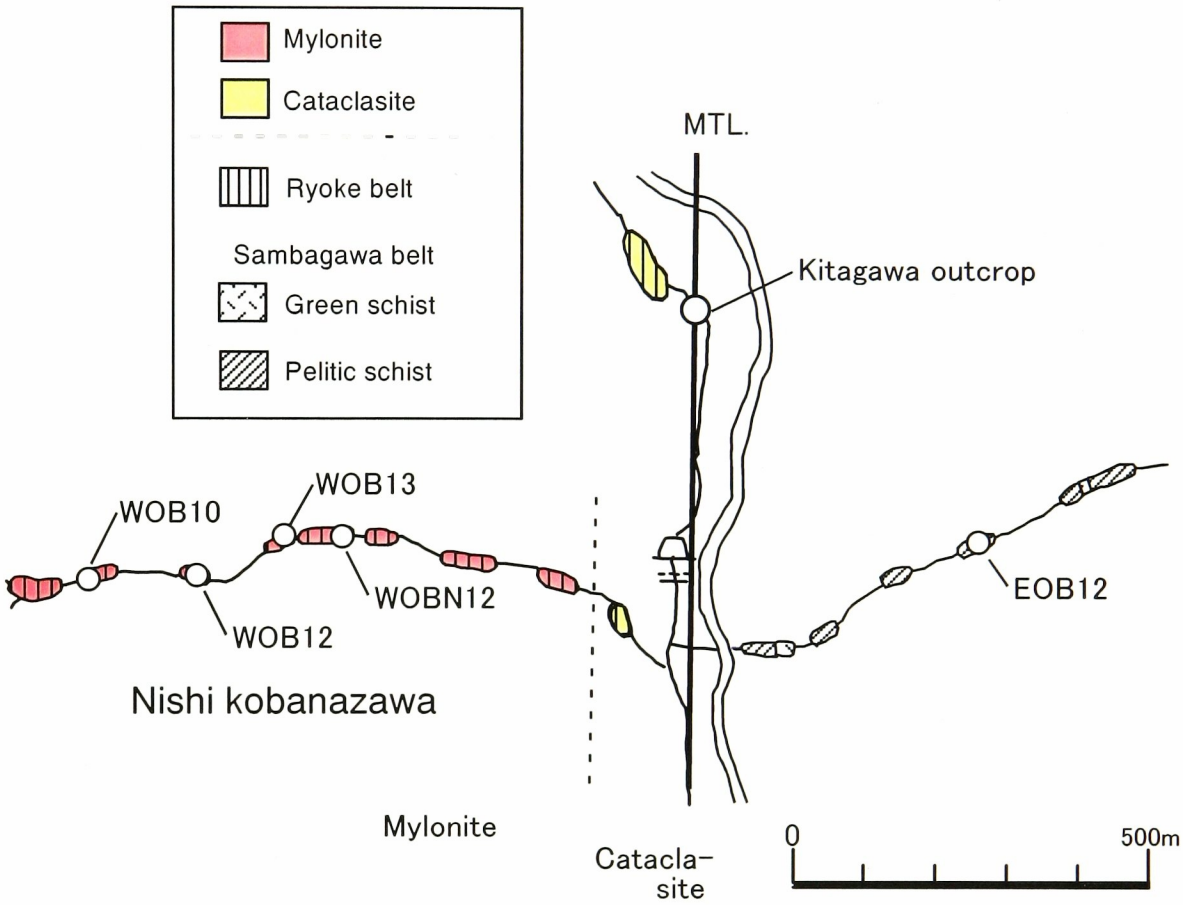

Fig. 2.2. Distribution of fault rocks in the vicinity of the Kitagawa outcrop, showing sampling locations (open circles).

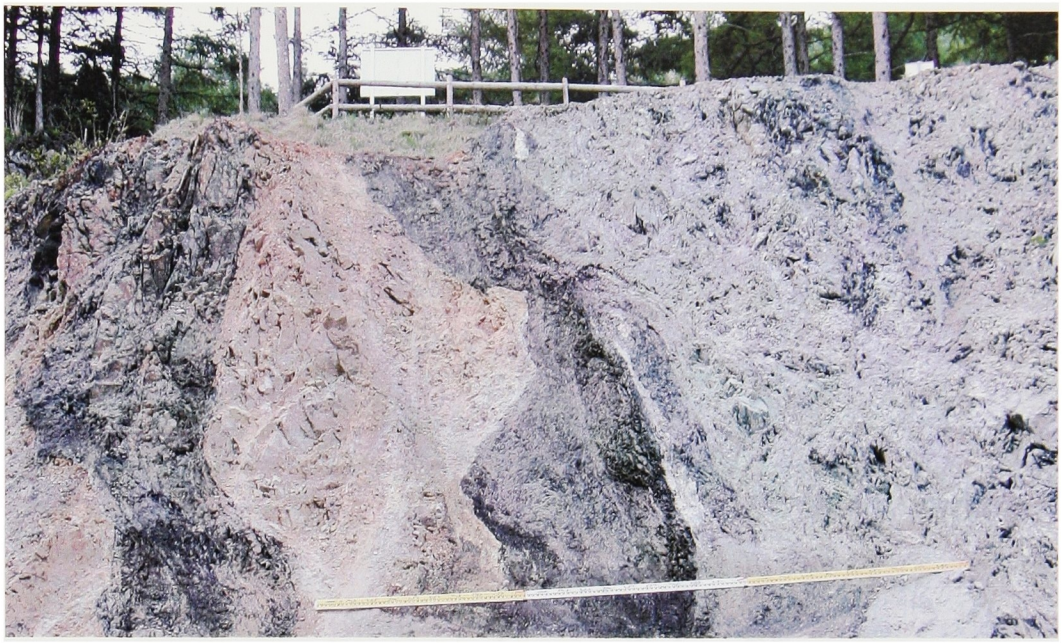

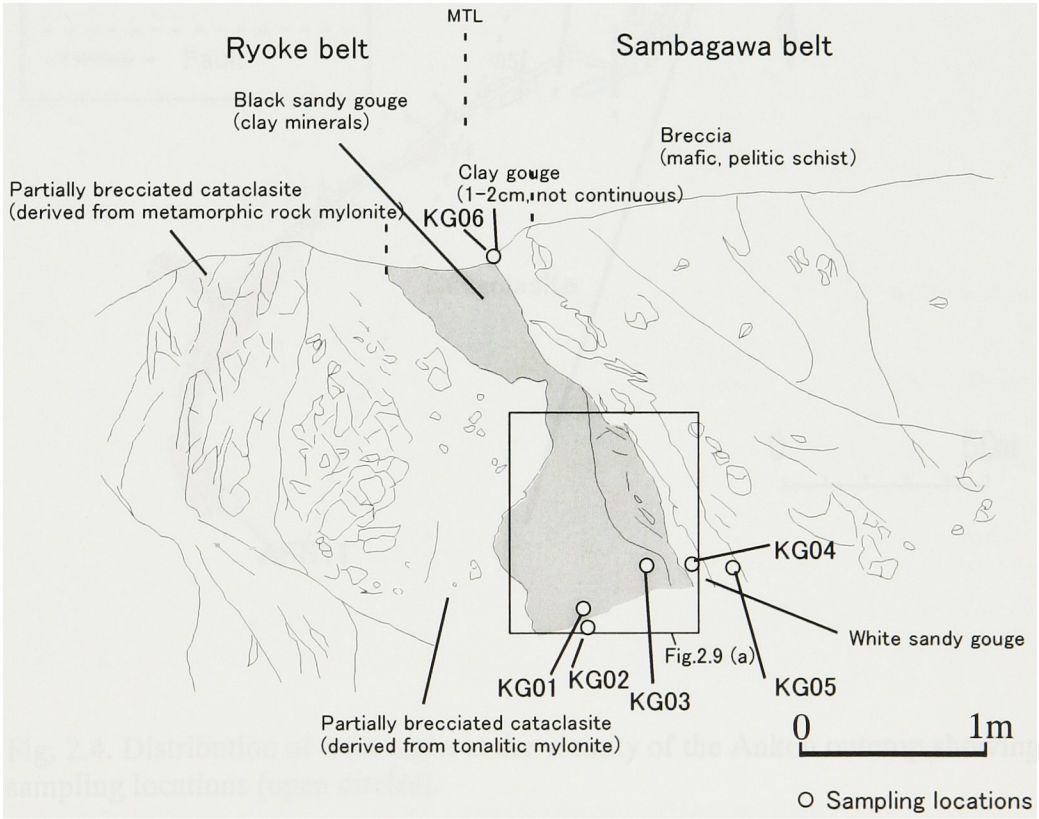

Fig. 2.3. Photograph and sketch of the Kitagawa outcrop of the Median Tectonic Line, showing sampling locations (open circles), located in Fig. 2.2.

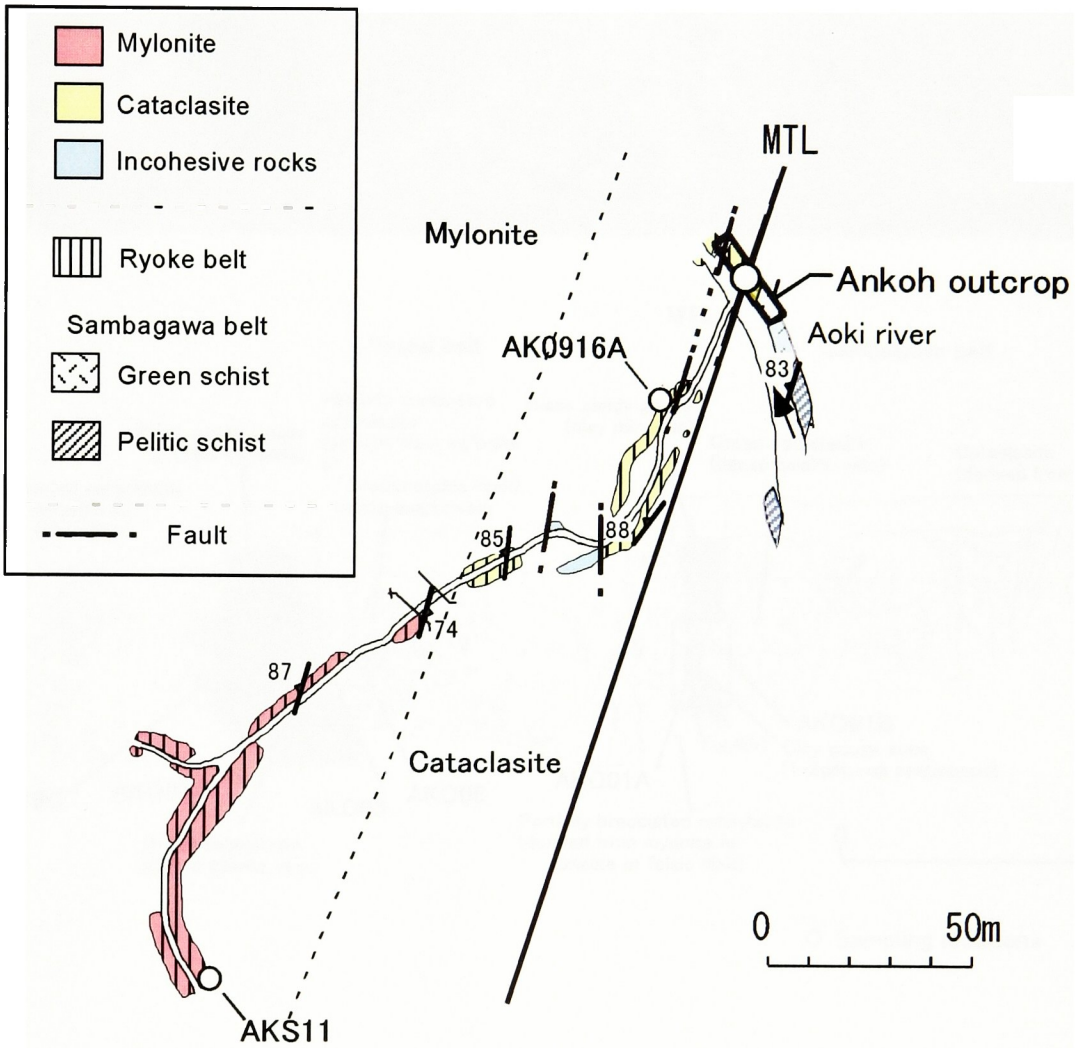

Fig. 2.4. Distribution of fault rocks at the vicinity of the Ankoh outcrop showing, sampling locations (open circles).

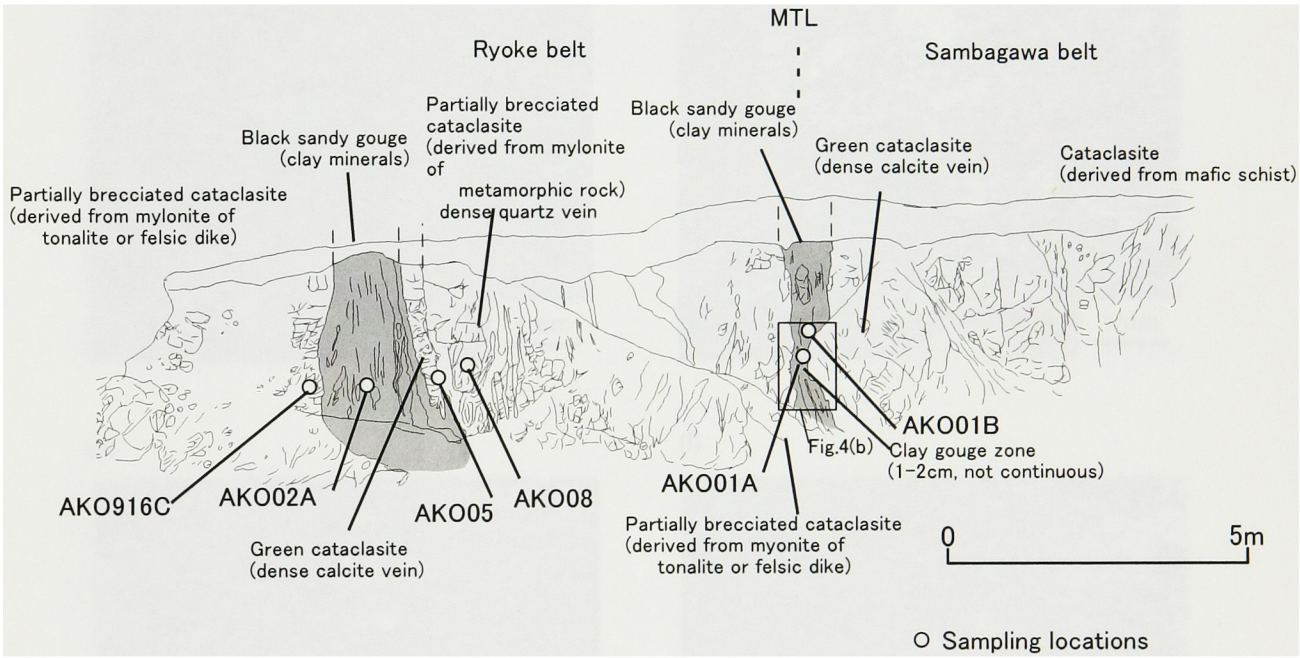

Fig. 2.5. Photograph and sketch of the Ankoh outcrop of the Median Tectonic Line, showing sampling locations (open circles), located in Fig. 2.4.

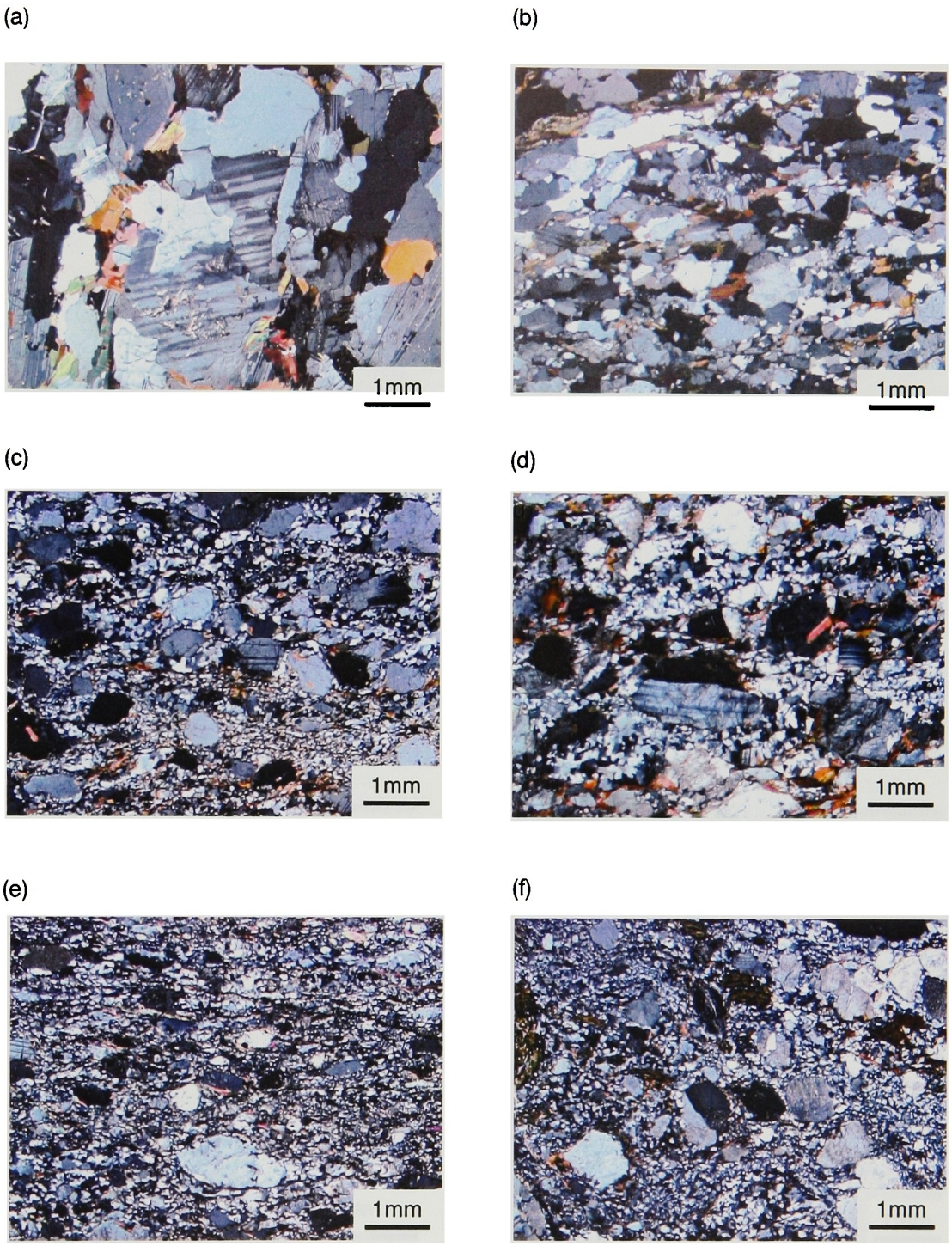

Fig. 2.6. Optical photomicrographs taken under crossed-polar of rocks collected from the Nishi Kobanazawa stream transect except for (a). (a) Tonalite (SR1), taken 3400m west of the MTL. (b) Gniess 1060m west of the MTL. (c)~(f) Mylonites (c) 850m (WOB10), (d) 750m (WOB12), (e) 600m (WOB13), (f) 500m (WOBN12) west of the MTL.

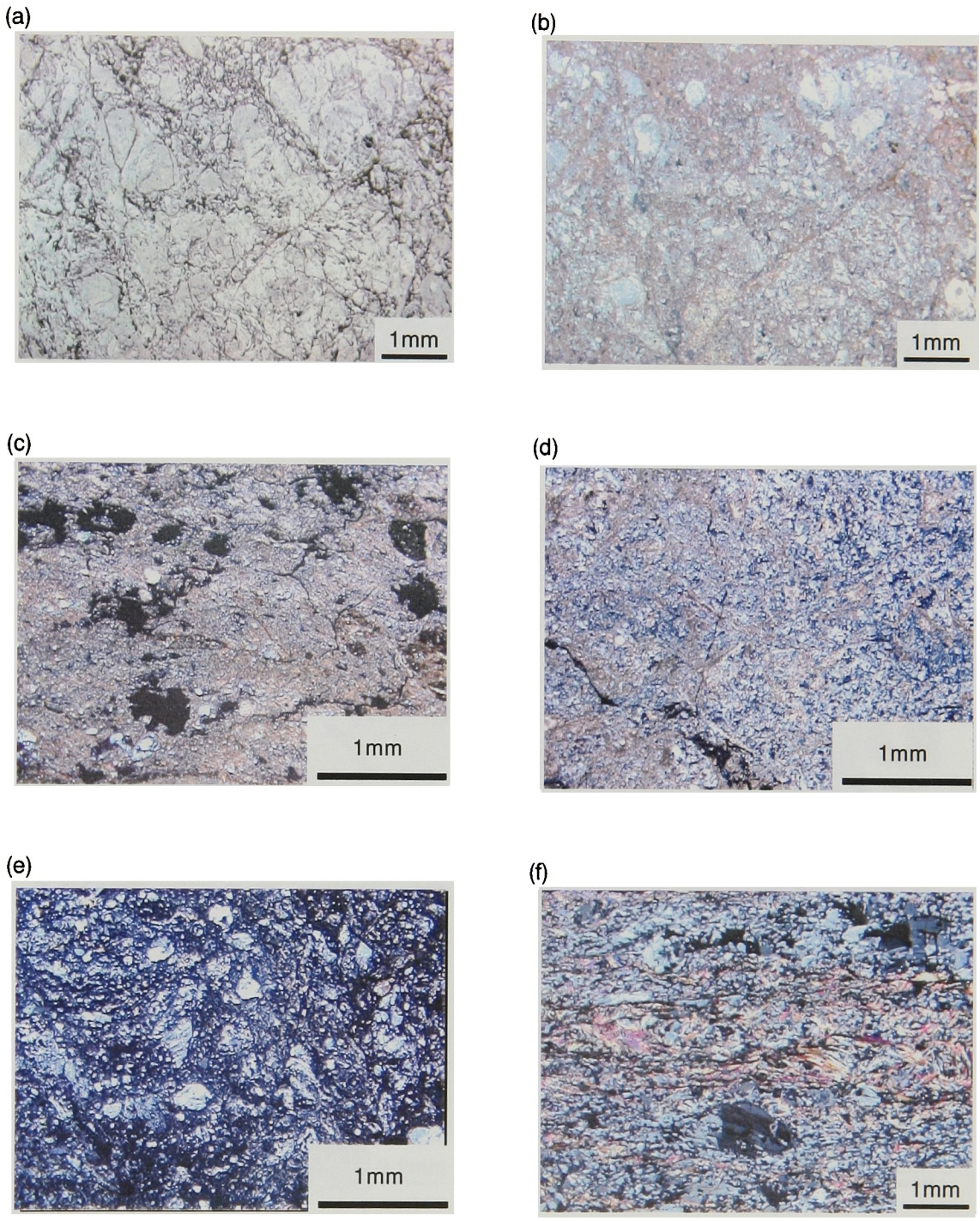

Fig. 2.7. Optical photomicrographs of rocks collected from the Kitagawa outcrop except for (f), taken under crossed-polar except for (a). (a),(b) Ryoke cemented cataclasite just next to black sandy gouge zone, taken under (a) plane-polar and (b)crossed-polar. (c) Black sandy gouge. (d) White sandy gouge. (e) Sandy gouge derived from green schist. (f) Pelitic schist 370m east of the MTL (EOB11).

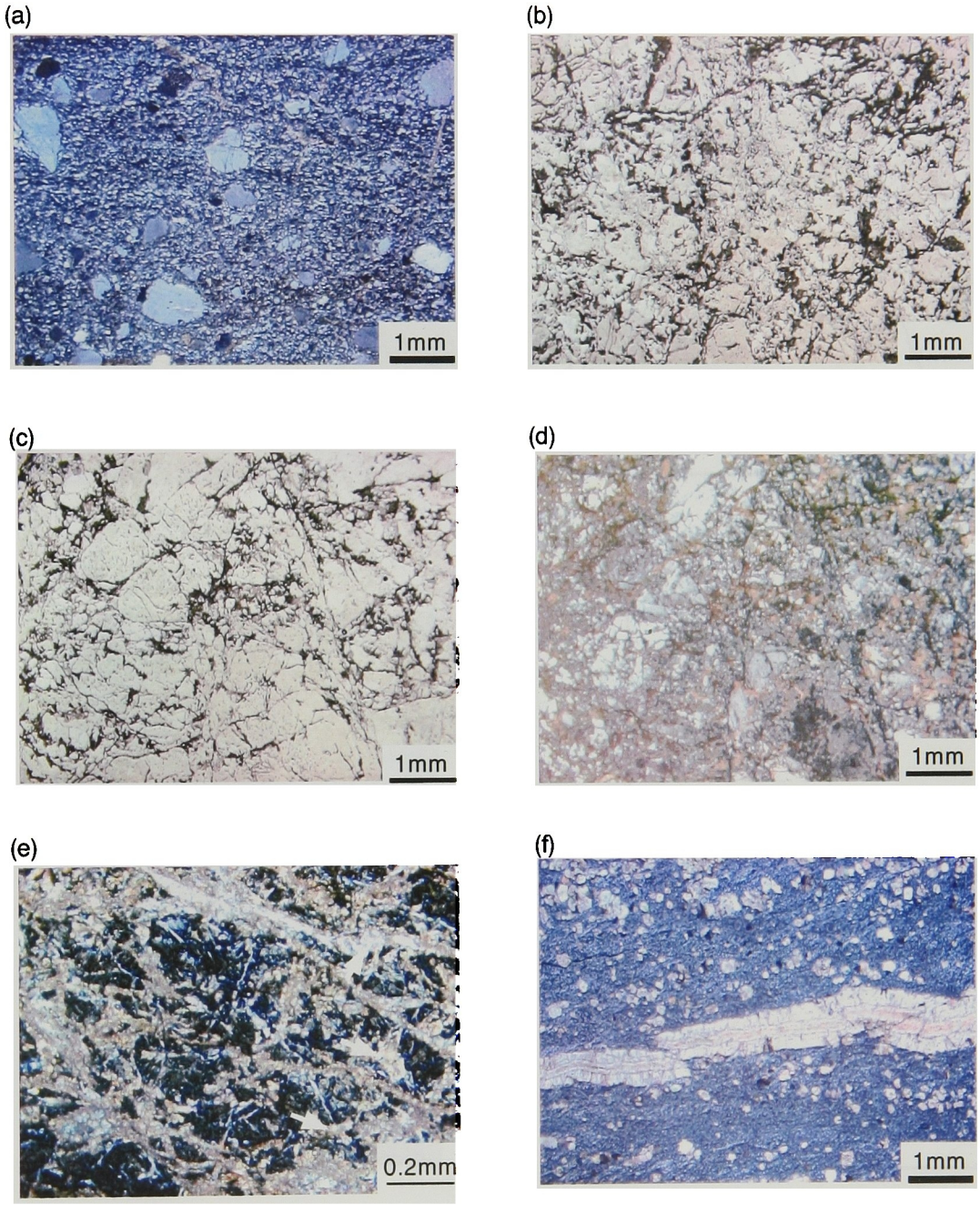

Fig. 2.8. Optical photomicrographs of rocks collected from the Ankoh outcrop and its visinity, taken under crossed-polar except for (b) and (c). (a) Ryoke mylonite (AKS11) 70m west of the MTL (b) ~ (d) Ryoke cemented cataclasite just next to black sandy gouge, taken under (b), (c) plane-polars and (d) crossed-polars; (b) AK0916A, (c),(d) AK0916C. (e) Black sandy gouge. White arrows indicate calcite or dolomite veins. (f) Sambagawa cataclasite just next to the black gouge zone.

(a)

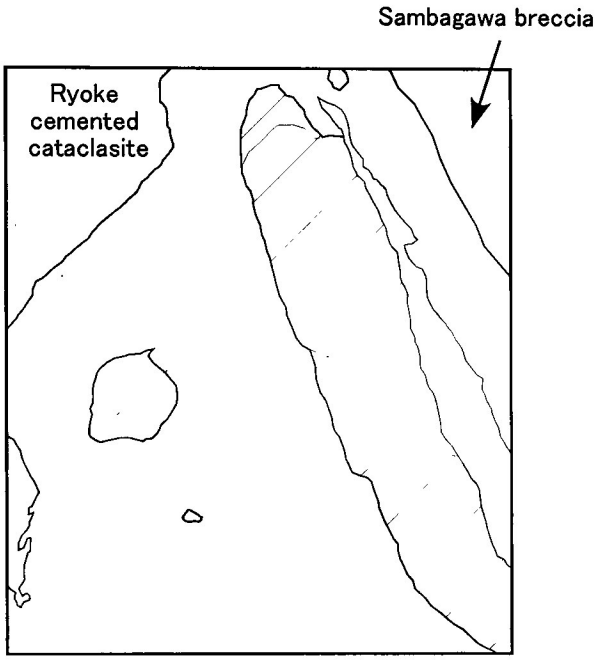

(b)

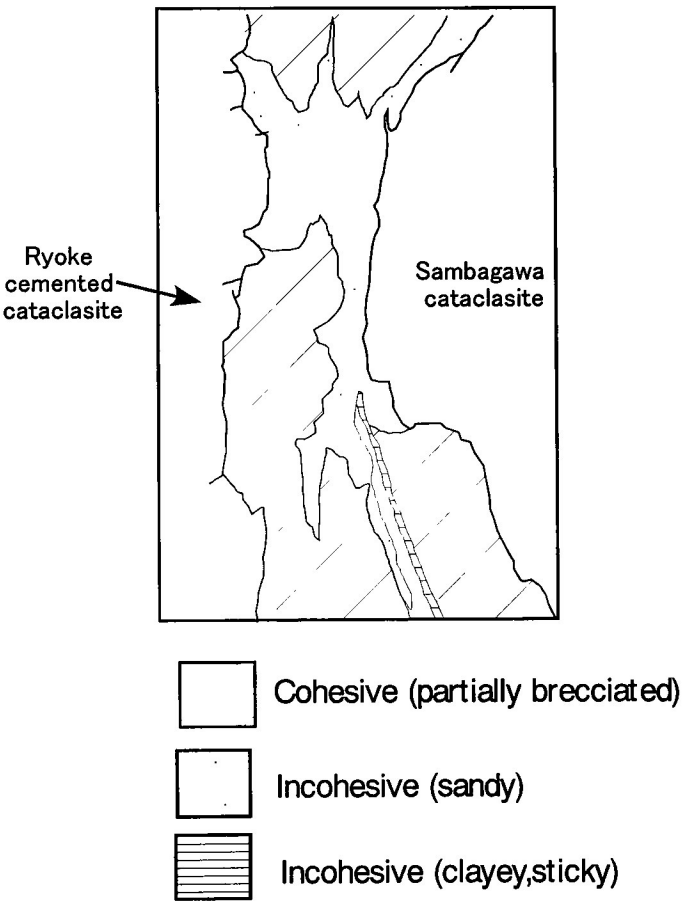

Fig. 2.9. Example of the distribution of cohesive and incohesive portions of the black gouge zone at (a) the Kitagawa and (b) the Ankoh outcrop.

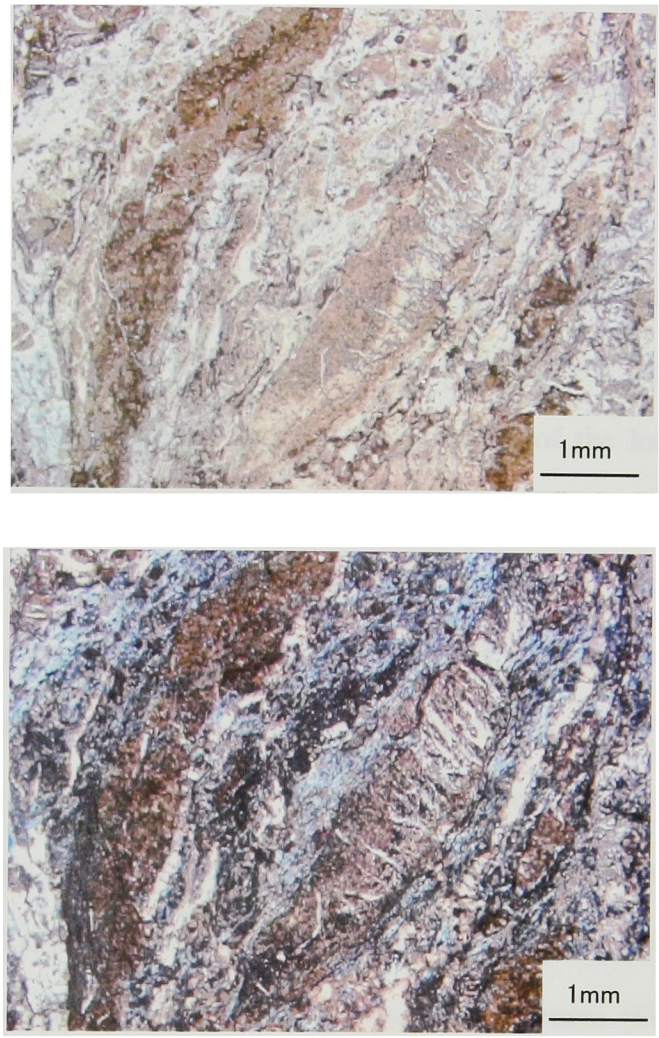

Fig. 2.10. Optical photomicrographs of black gouge at the Ankoh outcrop taken under plane-polars (up) and crossed-polars (down) (see text).

3. EXPERIMENTAL PROCEDURES

3.1 A High-pressure Gas Apparatus

The experimental gas-medium apparatus used to measure permeability is illustrated schematically in Fig. 3.1. In the upper part of pressure vessel (Fig. 3.2(c)), there is the space in which gas pressure is the same as the radial confining pressure (Fig. 3.1(b)), allowing the force acting downward on the piston from the gas in this space to equal that upward from the confining pressure so that pressure is applied equally to sample ends and sides. Therefore the piston loading the pressure vessel doesn't support the force derived from confining pressure, which is very important to make the most of the potential of the loading piston. The gas pressure increasing system mainly consists of generator and intensifier (Fig. 3.2(d)). The generator is usually used to increase pressure up to 110MPa, and the intensifier is then used up to 200MPa. One of the important features of this system is the oil actuators controlled by the servo system. The loading piston and pore pressure control piston (Fig. 3.2 (e)) can move speedy in various manners with the servo system which controls the flow rate of oil into or out from the actuators. This system is very useful for the tests such as controlling pore pressure, confining pressure and axial load according to each other, and pore pressure oscillation method, which is explained in section 3.2. The flow measurement system (Fig. 3.2(f)) is used for gas-flow method also explained in section 3.2. There are five flow meters in this system of which the upper limit of flow rate measured is 30*l*/min, 5*l*/min, 500m*l*/min, 50m*l*/min and 5m*l*/min.

When the length changes of specimens during deformation can not be measured directly, as with the experimental system used in this study, measuring the stiffness of the piston of the experimental machine was necessary for deformational tests. Fig. 3.3 shows the relations between the axial load and the deformation of the piston from the results of the deformational

experiments of cataclasite described precisely in Chapter 5. The deformation of the piston is the difference between the axial displacement of the loading piston (measured externally) and the axial shortening of the sample estimated with the strain gauges put on the sample. In the case when the effective pressure is 10.2MPa, the axial load is almost in proportional to the deformation of the piston during the measurement range of the strain gauge. Although such linear relation are not found for the other tests, the slopes of the axial load do not differ from that of Pe = 10.2MPa during the range of the gauges Therefore the stiffness of the piston is estimated here as 1.4×10^8 N/m from those results and this value was used for the analyses in Chapter 5.

3.2 Methods of Permeability Measurements

Sample preparation

Samples of incohesive rocks were collected by pushing a stainless steel tube of 25 mm in diameter or a copper tube of 20 mm in diameter with a wall thickness of 0.5 mm into the outcrop (Fig. 3.4(a)). Samples of cohesive rocks were made by laboratory coring from blocks using a 20mm diamond core (Fig. 3.4(b)). The length of samples is approximately 40mm or less. Cores were taken nearly parallel to their foliation and/or the MTL fault plane, with a few additional cores perpendicular to foliation. Samples were dried at a temperature of 80℃ for several days prior to permeability measurements to eliminate any pore water. Then samples were jacketed in polyolefin heat-shrink tubing and set in the pressure vessel (Fig. 3.5).

Experimental conditions

Measurements were made with nitrogen as a pore fluid at room temperature. Although there are some problems for using nitrogen as a pore fluid instead of water, for example as discussed in Falkner and Rutter (2000), there are also some advantages. One of them is that we can complete the experiment dramatically faster than using water, because nitrogen is less

viscous than water.

These methods to measure permeability of rock samples in laboratories, constant-pressure difference method, transient step method (Brace et al., 1968), and pore pressure oscillation method (Krantz et al., 1990; Fischer and Paterson, 1992) have been mainly been used in the past. In this study, permeability was measured with the pore pressure oscillation method and gas-flow method with constant pressure gradient.

Pore pressure oscillation method

In this method, pore pressure on one side of the sample is oscillated sinusoidally, by means of the servo-controlled piston in this study, and pore pressure on the other side is recorded. Fig. 3.6 shows an example of pore pressure measurement.

When pore pressure *Pup* on one side of the sample, which is called the "upstream" side in the following, is oscillated sinusoidally such as

$$Pup = A_{up}\sin(\omega t + \delta_0),$$

the pore pressure *Pdown* of the other side, that is, the "downstream" side, can be shown theoretically by

$$Pdown = A_{down}\sin(\omega t + \delta_0 + \delta) + tr$$

where *tr* is transient part, which can be ignored when the oscillation has continued for enough time.

From the amplitude ratio A_{down} / A_{up} and the phase difference δ, permeability can be calculated theoretically using equations in Krantz et al. (1990) and Fischer and Paterson (1992). One of the good points for this method as compared with other methods is that it is relatively easy to avoid the effects of any external pore pressure change (ex. caused by thermal change or leak of pore fluid). Because the time period of the response is known, it is easy to measure the amplitude and phase of the corresponding downstream pore-pressure oscillation. In this study, Pp was set to be 20MPa, and at this pore pressure the downstream storage capacity of our

system is $2.5 \times 10^{-13} m^3$/ Pa.

Error bars which put on the results of some samples in this study show the range of permeability calculated from amplitude ratios and phase differences between the average minus 2σ to the average plus 2σ of the distribution of measured data. Generally, the error bars are large at low confining pressure (high permeability) because only a sinusoidal oscillation of high frequency is suitable for measurements of high permeability, and the oscillation tends to become disrupted at much high frequency. The permeability also depends on he frequency of oscillation Some of the results in this study show the error from this.

Gas-flow with constant pressure gradient method

The theory of this method is much simpler than pore pressure oscillation method. When the flow is laminar, the relationship between fluid flux q in porous material and the pressure gradient dP/dl can be given by

$$q = -\frac{kA}{\mu}\frac{dP}{dl} \quad \text{..... (3-1)} \quad \text{(Darcy's law)}$$

where k is permeability of the material, A is its cross section perpendicular to the flow and μ is viscosity of fluid flow. The direction l is parallel to flow. When the difference between pore pressures at both sides of sample is set to be constant, permeability k can be given from the fluid flux q.

This equation is derived on the assumption that the fluid is incompressible. For the case of the system used in this study, however, the pore fluid is nitrogen gas and the downstream pore pressure is almost 0 MPa (1 bar), so the density of pore fluid at the upstream and downstream sides of the sample may be different from each other. Thus the relationship between the pressure difference, q and k has to be calculated.

Conservation of mass in an infinitesimal volume in the sample requires,

$$\frac{d(v\rho)}{dl} = 0 \quad \text{..... (3-2)}$$

where v is fluid velocity and ρ is fluid density. If the fluid is an ideal gas, from Boyle's law we get

$$\rho = \alpha P \quad \ldots\ldots (3\text{-}3)$$

where α is constant and P is the fluid pressure. Actually this relationship is satisfied during pressure range used for measurements in this study. The combination of equations (3-2) and (3-3) gives

$$\frac{d(v\alpha P)}{dl} = 0 \quad \ldots\ldots (3\text{-}4)$$

so that

$$\frac{d(vP)}{dl} = 0 \quad \ldots\ldots (3\text{-}5)$$

If equation (3-1) can be assumed to be suitable for infinitesimal volume, v can be given by

$$v = -\frac{k}{\mu}\frac{dP}{dl} \quad \ldots\ldots\ldots (3\text{-}6)$$

Substitution of equation (3-6) into equation (3-5) gives

$$\frac{d}{dl}\left(-\frac{k}{\mu}\frac{dP}{dl}P\right) = 0$$

so that

$$\frac{d}{dl}\left(P\frac{dP}{dl}\right) = 0 \quad \ldots\ldots (3\text{-}7)$$

The boundary conditions of P for both sides of sample are

$P=Pup$ on $l = 0$

$P=Pdown$ on l = L, where L is the length of sample.

Application of these conditions leads to the following expression for P

$$P = \sqrt{Pup^2 - \frac{Pup^2 - Pdown^2}{L}l}$$

so that

$$\frac{dP}{dx} = \frac{\frac{1}{2}\left(-\frac{Pup^2 - Pdown^2}{L}\right)}{\sqrt{Pup^2 - \frac{Pup^2 - Pdown^2}{L}x}} \quad \cdots\cdots (3\text{-}8)$$

Substitution of equation (3-8) into equation (3-6) gives

$$v = \frac{k}{\mu}\frac{\frac{1}{2}\left(\frac{Pup^2 - Pdown^2}{L}\right)}{\sqrt{Pup^2 - \frac{Pup^2 - Pdown^2}{L}l}} \quad \cdots\cdots (3\text{-}9)$$

so that

$$v(l = L) = \frac{k}{\mu}\frac{\frac{1}{2}\left(\frac{Pup^2 - Pdown^2}{L}\right)}{\sqrt{Pup^2 - \frac{Pup^2 - Pdown^2}{L}L}}$$

$$= \frac{k}{\mu}\frac{\frac{1}{2}\left(\frac{Pup^2 - Pdown^2}{L}\right)}{\sqrt{Pdown^2}}$$

$$= \frac{k}{\mu}\frac{1}{2L}\frac{Pup^2 - Pdown^2}{Pdown}$$

Thus we obtain

$$q(l = L) = v(l = L)A = \frac{kA}{\mu}\frac{1}{2L}\frac{Pup^2 - Pdown^2}{Pdown}$$

or

$$k = \frac{2\mu Lq(l = L)}{A}\frac{1}{\frac{Pup^2 - Pdown^2}{Pdown}}$$

At actual calculations of permeability, *Pdown* was set to be 0.1MPa, and *Pup* was the sum of 0.1MPa and the value from pressure gage at upstream side.

Fig. 3.7 shows examples of flow rate measurements. In general, flow rate q is proportional to (Pup^2 $Pdown^2$)/ *Pdown* when it is comparatively small (Fig. 3.7(a)). However, when q becomes comparatively large (more than about 100m*l*), the gradients of q decrease (Fig. 3.7 (b)). The reason of this has not been clear yet, however this possibly reflects the limitation for the application of Darcy's law, or the friction between fluid flow and the system may

become too large to be ignored.

One of the good points of this method is that the system for measurement can be simple. However, because it is difficult to measure small flow rates precisely, this method is not suitable for impermeable rocks, although the limitation depends on the flow rate meter. The range of flow rates that can be measured with our measurement system are from around 1m*l*/min to 30*l*/min.

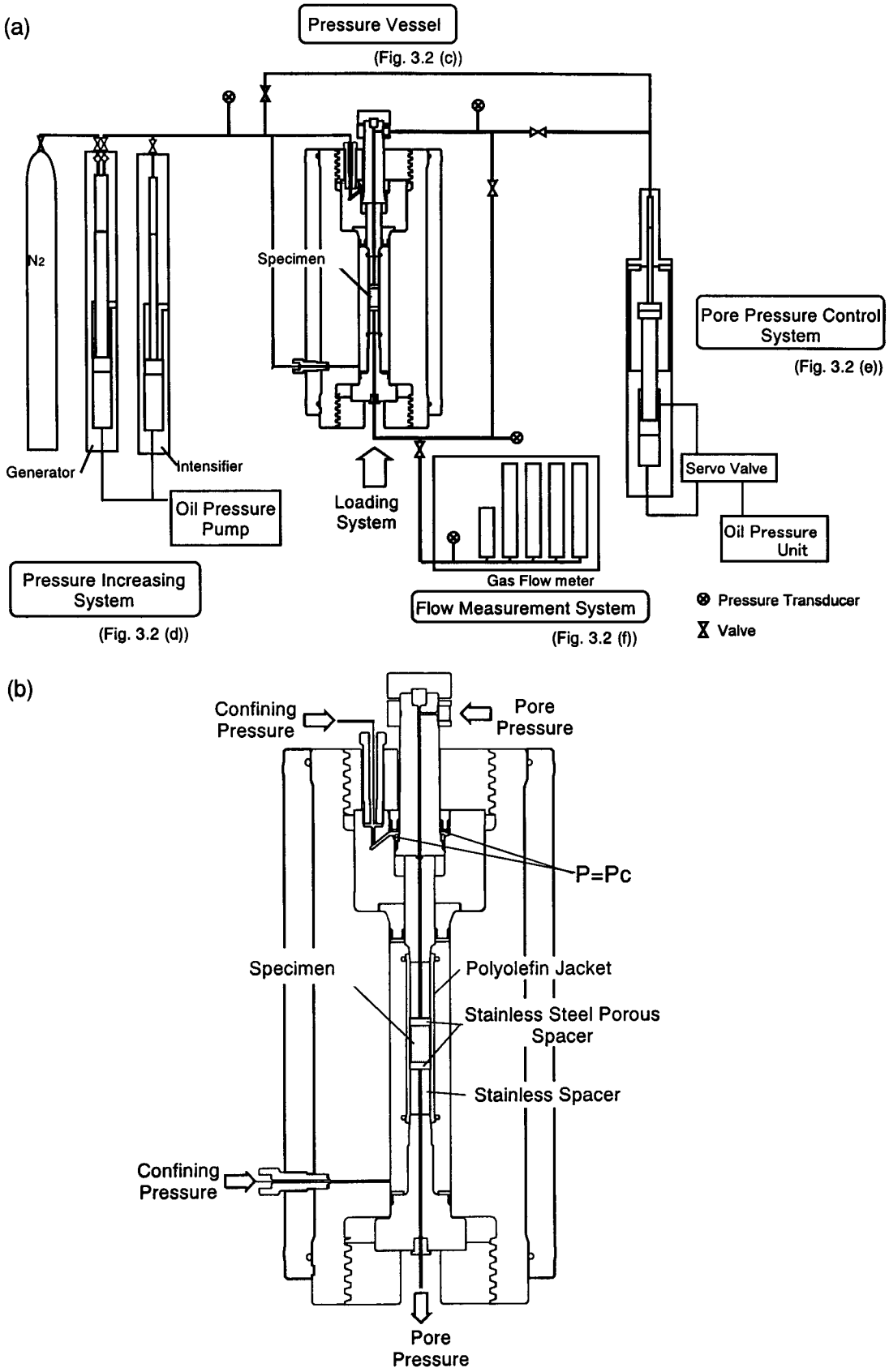

Fig. 3.1. (a) Experimental set-up used for this study. (b) Pressure vessel with sample assembly.

(a)

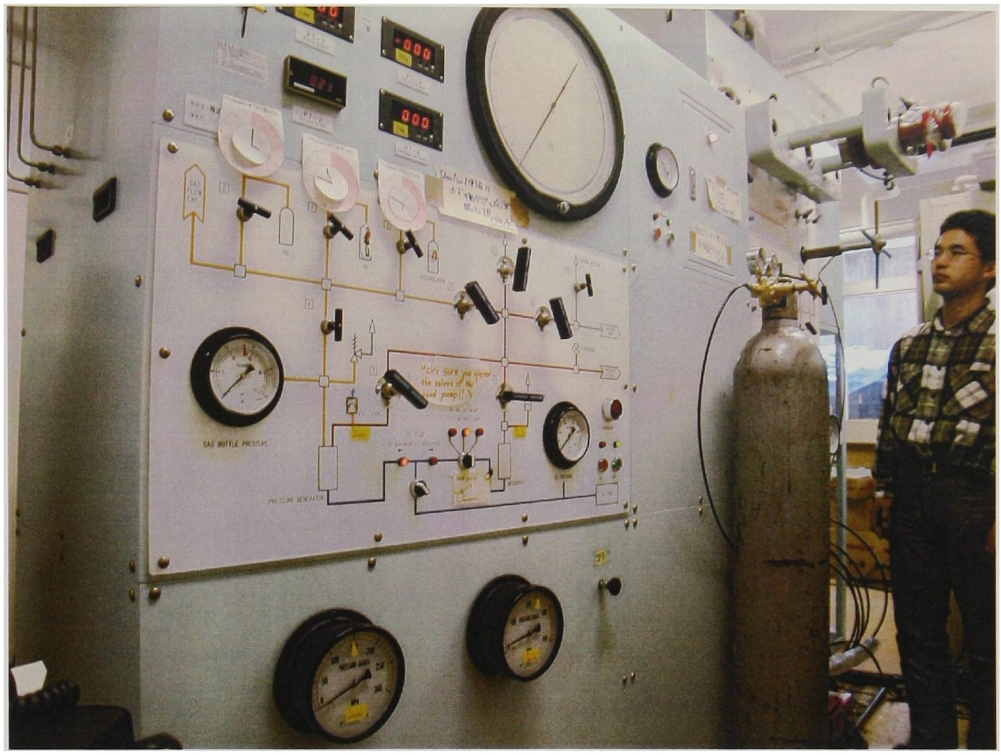

(b)

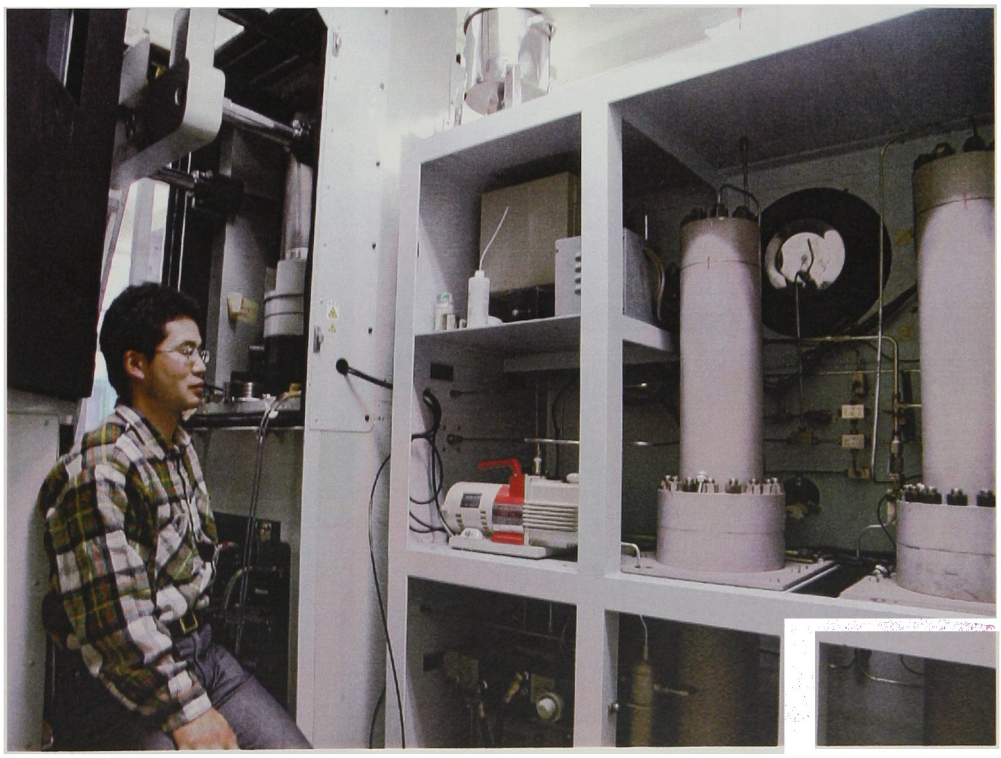

Fig. 3.2. Photographs of the experimental system. (a) The front side and (b) back side of the whole system.

(c)

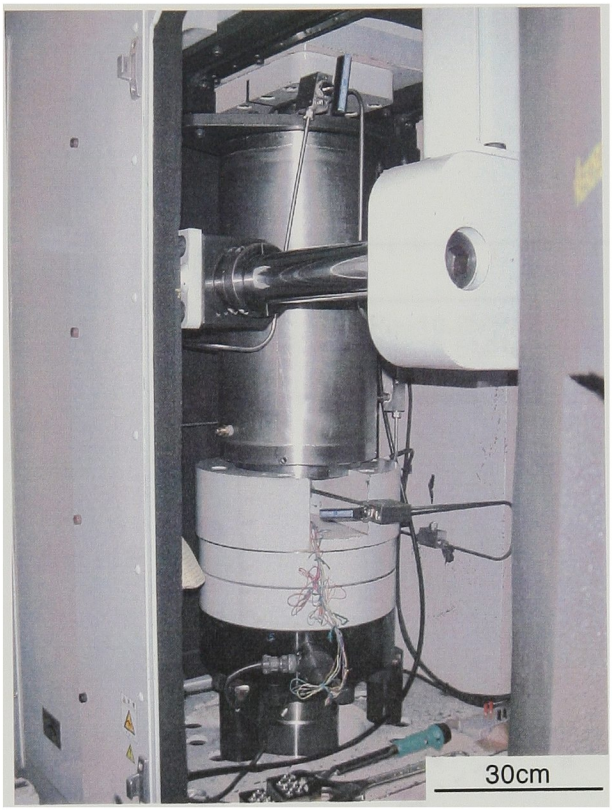

(d)

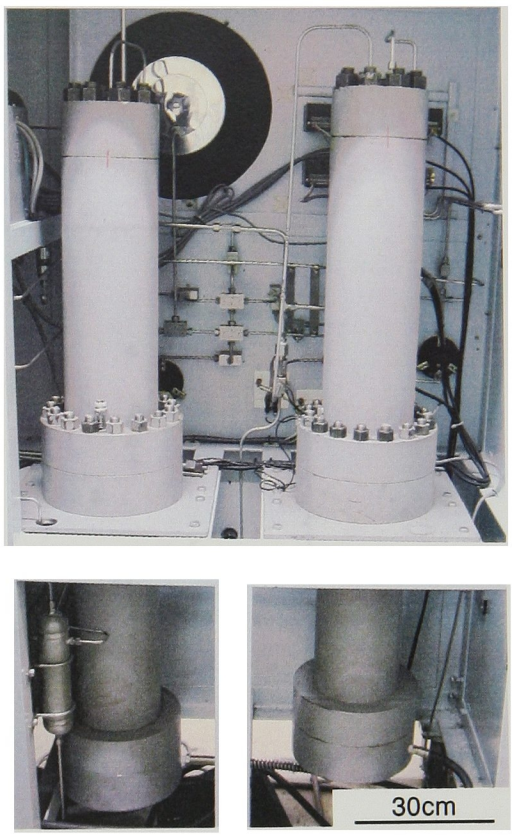

(e)

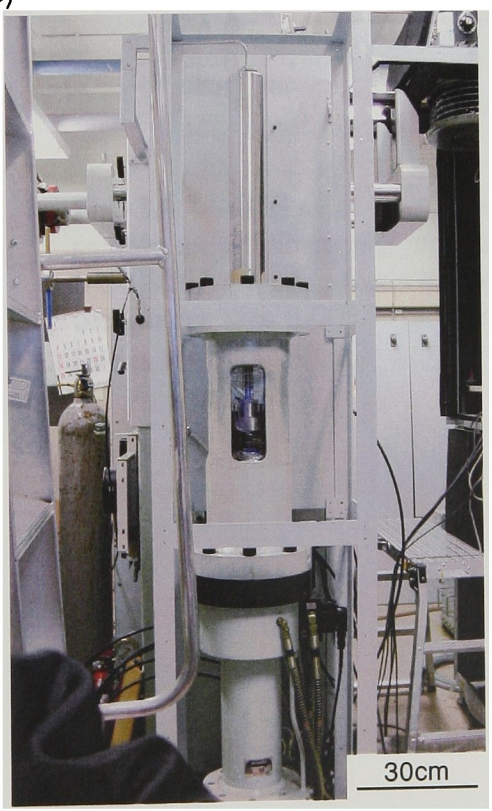

(f)

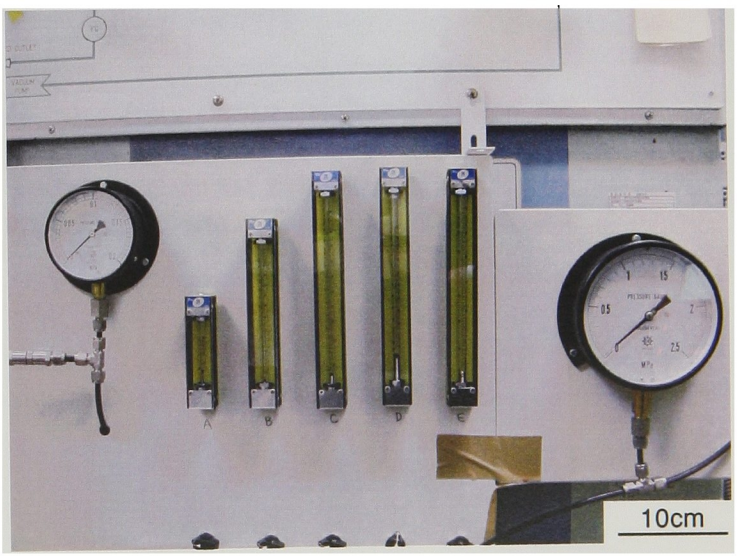

Fig. 3.2. (c) Pressure vessel. (d) Pressure generator (right) and intensifier (left). (e) Pore pressure control piston. (f) Flow rate measurement system.

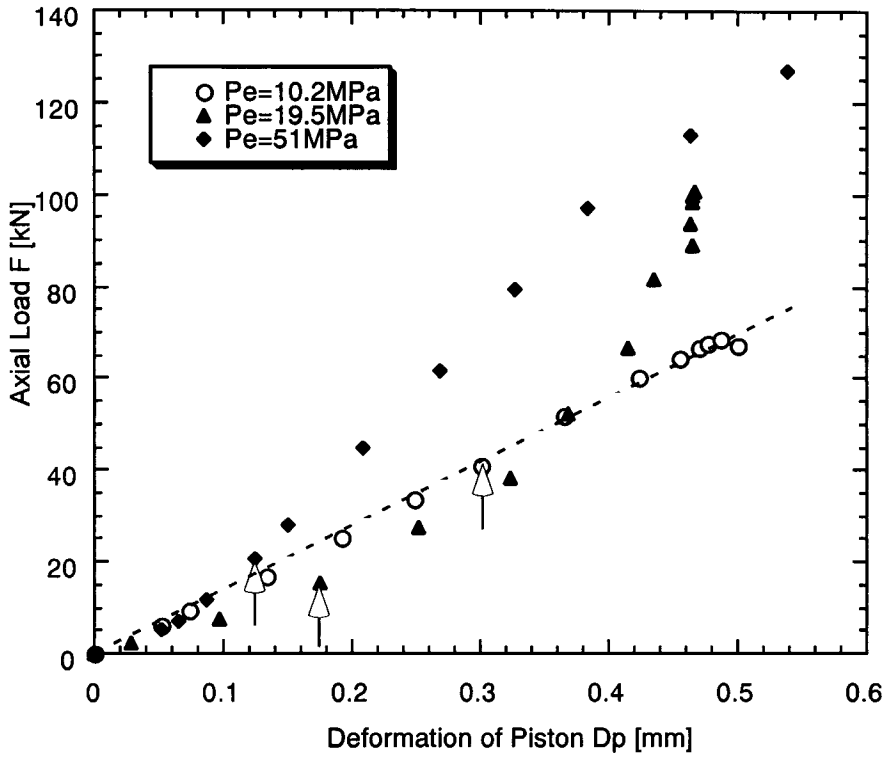

Fig. 3.3. Stiffness of the piston calculated from piston displacement and the sample axial shortening measured by strain gauges on samples of cataclasite (AK0916A). Open arrows show the points at which the axial strain recorded by the gauges was 0.002, which is its measurement limit. The slope of the dotted line is 1.4×10^8 N/m.

(a)

(b)

Fig. 3.4. Photograph of collecting (a) incohesive samples with a stainless steel tube of 25 mm in diameter or a copper tube of 20 mm in diameter with a wall thickness of 0.5 mm and (b) samples of cohesive rocks with coring machine.

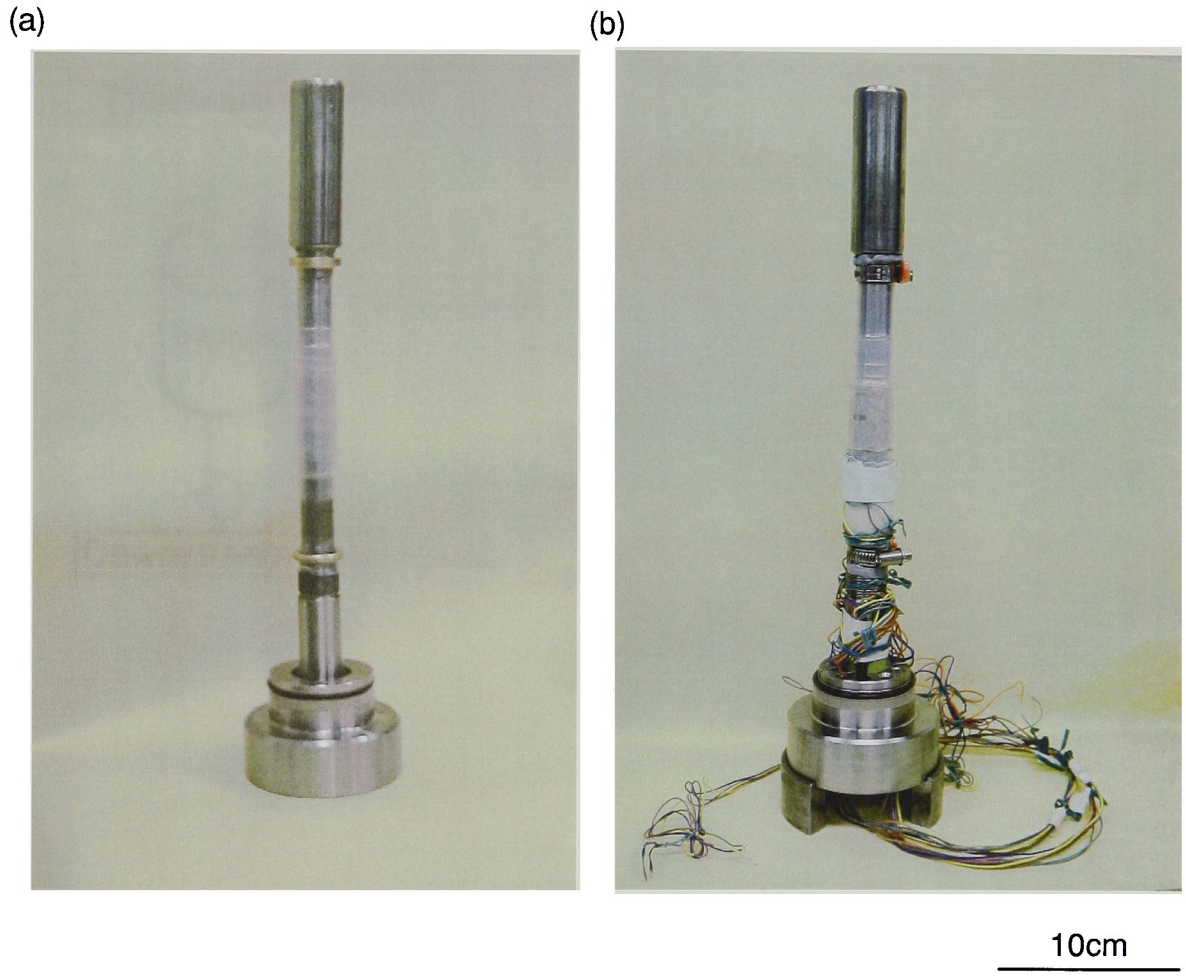

Fig. 3.5. Photographs of sample assembly. (a) Initial assembly for permeability measurement without strain gauges. (b) Assembly for deformation experiment in which the strain gauge are put on the sample.

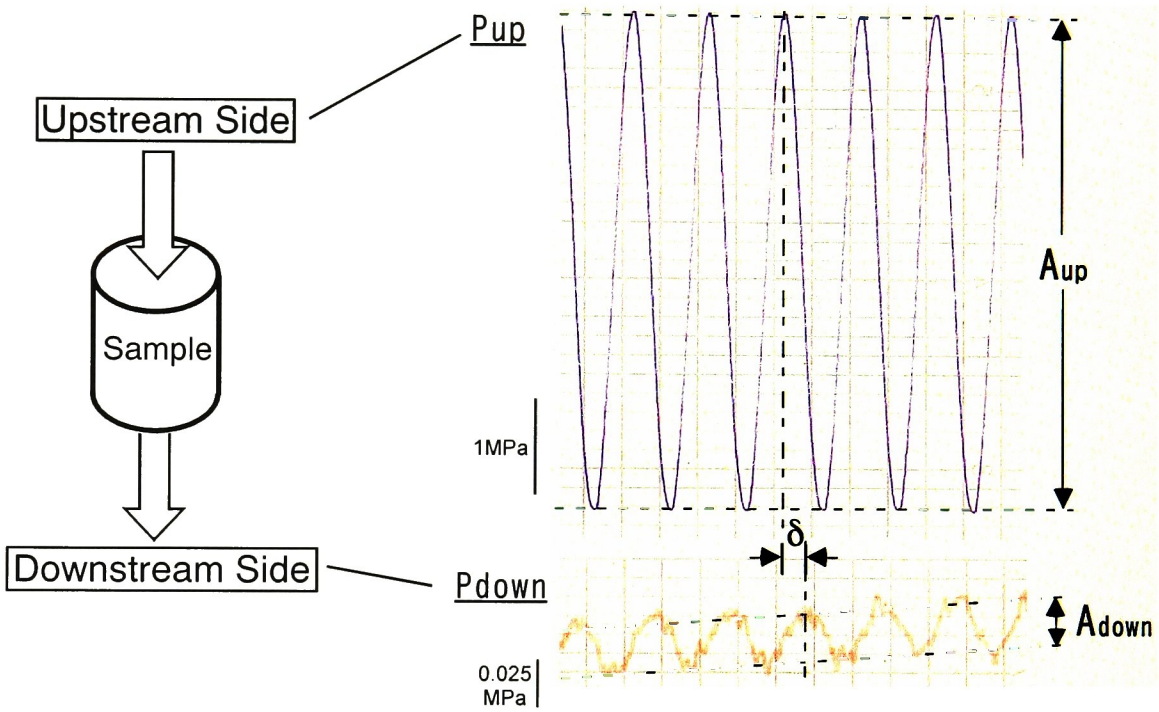

Fig. 3.6. Example of measured pore pressure on both sides of a sample for pore pressure oscillation method.

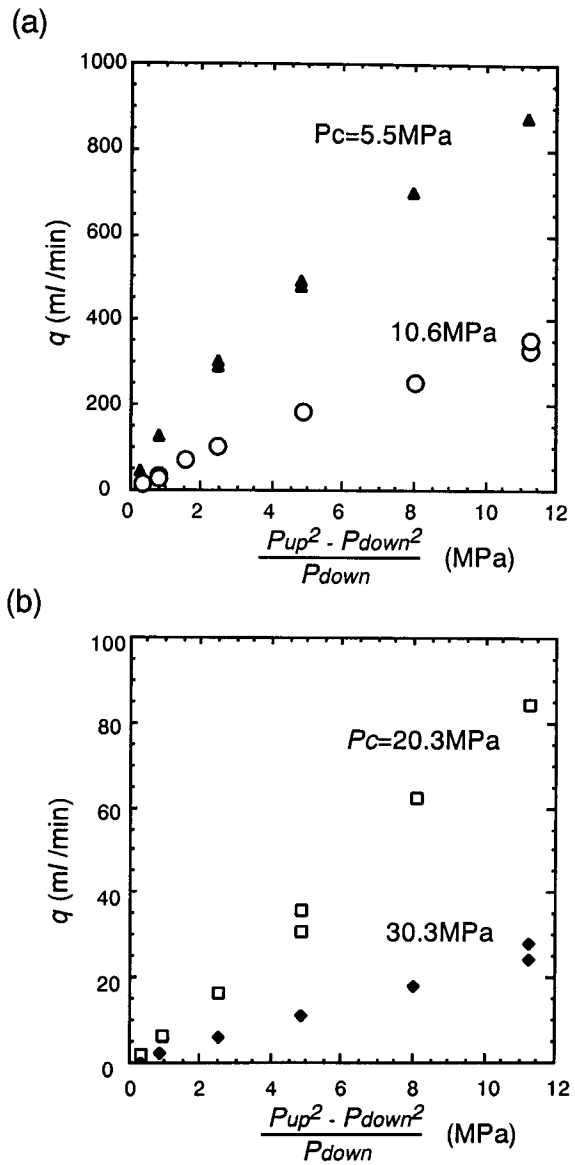

Fig. 3.7. Examples of flow rate measurements. For all results the sample is same, but confining pressure *Pc* is different from each other.

4. PERMEABILITY STRUCURES OF MTL AS STUDIED BY PRESSURE-CYCLING TESTS

4.1 Samples and Measurement Conditions

In this chapter present permeability measurements under hydrostatic stress of faults rocks from the Median Tectonic Line (MTL) in central Japan are presented. Various types of fault rocks, such as fault gouge, cataclasite, mylonite and their host rock tonalite, are found along the MTL in central Japan as described in Chapter 2 (e.g. Hara et al., 1980; Takagi, 1983, 1984; Michibayashi & Masuda, 1993; Michibayashi, 1993), indicative of deformation processes during MTL activity at different levels in the Earth's crust. The MTL is therefore a good example for considering the permeability structure of fault zones from shallow to deep parts of the crust.

Compared with incohesive rocks, it is difficult to evaluate adequately the permeability of cohesive rocks, because the permeability of them would be influenced enormously by fractures in them. This problem is addressed in Chapter 6 by measuring the permeability of single fractures under normal stress.

Permeability was measured using the pore-pressure oscillation method. With the pore pressure Pp fixed at 20MPa, the confining pressure was incrementally increased from 30MPa to a peak value, after which it was decreased incrementally to the initial. Permeability was measured at each stage in the confining pressure cycle. The peak value of Pc was either 110MPa or 200MPa.

4.2 Results of Permeability Measurements

Fault gouge

Fig. 4.1 shows permeability as a function of effective pressure Pe (Pe = Pc – Pp) for

incohesive samples from the Kitagawa and Ankoh areas. Both loading and unloading portions of each test cycle are shown. I found that permeability k tends to decrease when Pe increases as noted in many previous works on laboratory permeability variation with pressure (e.g. Brace et al., 1968; Morrows et al., 1986; Bernabe, 1987; Huenges et al., 1989). There is a large difference in the permeability variance between the confining and deconfining parts of the pressure cycle; that is, the slope of permeability with Pe change on the deconfining portion is much smaller than that on the confining portion except for that in the lower Pe range (<30MPa). Figs. 4.2 and 4.3 show that the difference between the slopes of permeability change between the confining and deconfining parts of the pressure cycle of cohesive rocks is smaller than that of incohesive rocks.

The permeability normalized to that at Pe = 10MPa on confining path vs effective pressure plots in Fig. 4.4 show the characteristics of permeability responses to Pe clearly. To compare the slope of permeability changes, the normalized permeability in Fig. 4.4(a) are approximated by the function:

$$k = k_0 \exp(-\gamma P_e).$$

γ of the plots are shown in Table 1. For comparison, the parameters of several cohesive rocks are also shown. In the case of incohesive rocks, γ of the loading paths (0.039 – 0.09) are generally larger than those of the unloading paths above Pe = 30MPa (0-0.017), and, on the other hand, γ below Pe = 30MPa (0.004-0.08) tend to be closer to those of the loading paths than those above Pe = 30MPa. The differences of γ between loading and unloading portions are larger for incohesive rocks than those in the case of cohesive rocks (0.03-0.043 for the loading paths and 0.02-0.029 for the loading paths).

We can see the steep change of permeability at the portion where Pe is less than 30MPa in several results from incohesive rocks. This shows that, at low Pe (<30MPa), the permeability changes of some incohesive rocks are effected strongly by elastic deformation, however the

effects vanish or are very small at high Pe (>30MPa).

Ryoke and Sambagawa metamorphic rocks, and mylonites and cataclasites

Figures 4.2 and 4.3 show permeability as a function of effective pressure Pe (Pe = Pc – Pp) for each sample of cohesive fault rocks from the Kitagawa and Ankoh areas. The results of two mylonites (WOB10 and WOB12) show the anisotropy such as the permeability parallel to the foliation is larger than that perpendicular to the foliation.

Fig. 4.1 shows that, in general, the slopes of permeability of incohesive samples are almost constant during the loading path. While, those of cohesive samples are not constant. The normalized permeability in Fig. 4.4 shows the difference clearly. The slopes of cohesive rocks are comparatively steep at low Pe, but those reduce at high Pe. Such features can also be observed in the permeability of a single fracture, and those may be able to be explained by the closure of fractures under pressure as discussed later in Chapter 6.

As mentioned before, it is difficult to discuss the permeability of whole cohesive rocks from the results shown here. The permeability measured in this study is that of the matrix on the scale larger than the sample. Because the cohesive rocks measured are generally impermeable, the permeability of whole rocks may be influenced from the distribution of fractures in it. The permeability of a single fracture is discussed in Chapter 6.

Comparison between permeability responses on Pe of incohesive and cohesive rocks

The results show that, as compared with cohesive rocks, the pore structure of incohesive rock relating to the permeability deforms inelastically during the loading-unloading cycle. Such inelastic deformation is probably caused by the rearrangement of grains and their plastic deformation. However, at the unloading portion below 30MPa, the permeability change is generally close to that of the loading portion, which may reflect the elastic deformation of pore structure. Because of such inelasticity of the pore structure, the permeability of incohesive rock during deconfinement is influenced by the peak value of Pe to which the samples have been

subjected. The fault zone of the MTL has evolved during uplifting and exhumation, and the depth at which incohesive rock was formed might influence permeability structure, although, needless to say, the evolution of fault activity must be borne in mind.

4.3 Permeability Structure of the MTL

In order to compare permeability of various fault rocks and to estimate permeability structure across the MTL, the permeabilities of samples at Pe = 80MPa from the confining part of the pressure cycle are plotted for permeability as a function of distance from the MTL for the Kitagawa and Ankoh areas (Figs. 4.5 (a) and (b)).

Kitagawa outcrop and its vicinity

Fig. 4.5(a) shows that host rocks and Ryoke mylonite are more than two orders of magnitude less permeable that fault gouge at Pe = 80 MPa. The permeability of mylonite is equal to or less than that of tonalite. In the black sandy gouge zone clayey gouge is present, which is more impermeable than sandy gouge, but it does not maintain good structural continuity.

Ankoh outcrop and its vicinity

The results from the Ankoh area also show that the permeability of fault sandy gouge is more permeable than that of the fault rocks around it. Clayey gouge in the black sandy gouge is less permeable than the sandy gouge, but it is not continuous. Cemented cataclasite is impermeable, although the difference between samples may be large. Needless to say, the permeability of the cataclasite might be dramatically different from that shown here. The permeability of the cataclasite under deformation is discussed in Chapter 5.

Table 4.1. Effective pressure sensitivity coefficient for the permeability.

	$k = k_0 \exp(-\gamma Pe)$						
	loading		unloading		unloading (>30MPa)		unloading (<30MPa)
	γ [MPa^{-1}]	R	γ [MPa^{-1}]	R	γ [MPa^{-1}]	R	γ [MPa^{-1}]
Fault Gouge							
KG01A	0.061	0.98	0.011	0.84	-0.0090	0.78	0.042
KG01B	0.050	0.99	0.013	0.95	0.0064	0.99	0.024
KG01C	0.072	0.99	0.0063	0.61	0.0023	0.18	0.0040
KG02	0.063	0.72	0.0039	0.68	0.0023	0.46	0.02
KG03	0.039	0.94	0.0074	0.85	0.0047	0.99	0.025
KG04	0.065	0.95	0.014	0.67	0.0049	0.89	0.082
AKO1A	0.041	0.95	0.021	0.96	0.017	0.91	0.02
AKO1B	0.049	0.95	0.018	0.82	0.0098	0.93	0.025
AKO2A	0.053	0.97	0.018	0.79	0.0079	0.91	0.082
Cohesive rocks							
SR1x	0.033	0.997	0.029	0.94			
WOB10x	0.030	0.99	0.019	0.99			
EOB12x	0.043	0.95	0.025	0.97			

R:correlation coefficient; they for 'unloading (<30MPa)' are not shown, because there are only a few data points.

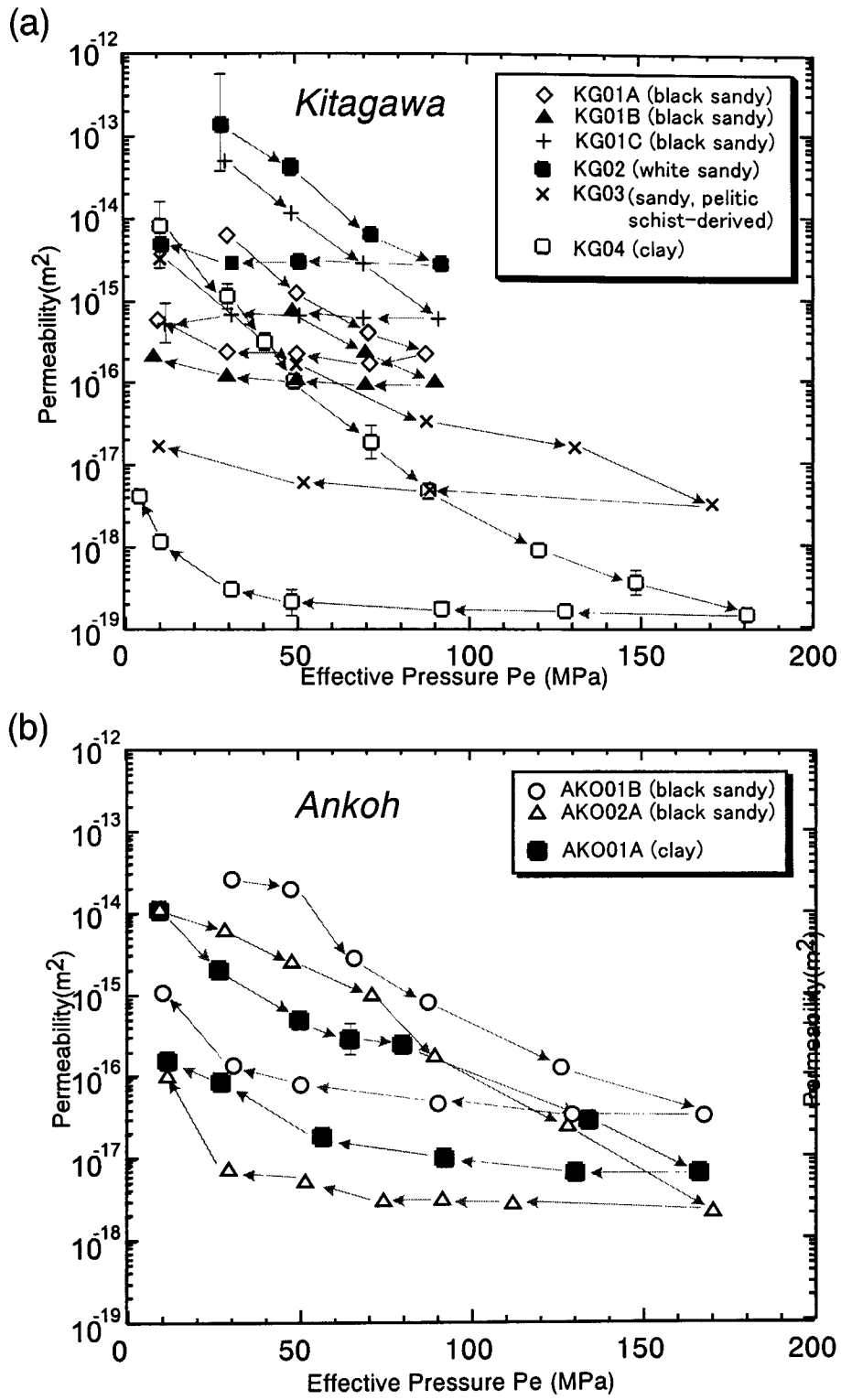

Fig. 4.1. Permeability data of incohesive fault rock samples taken from (a) the Kitagawa outcrop, and (b) the Ankoh outcrop, as a function of effective pressure Pe (Pe = Pc - Pp). The sampling locations are shown in Figs. 2.3 and 2.5.

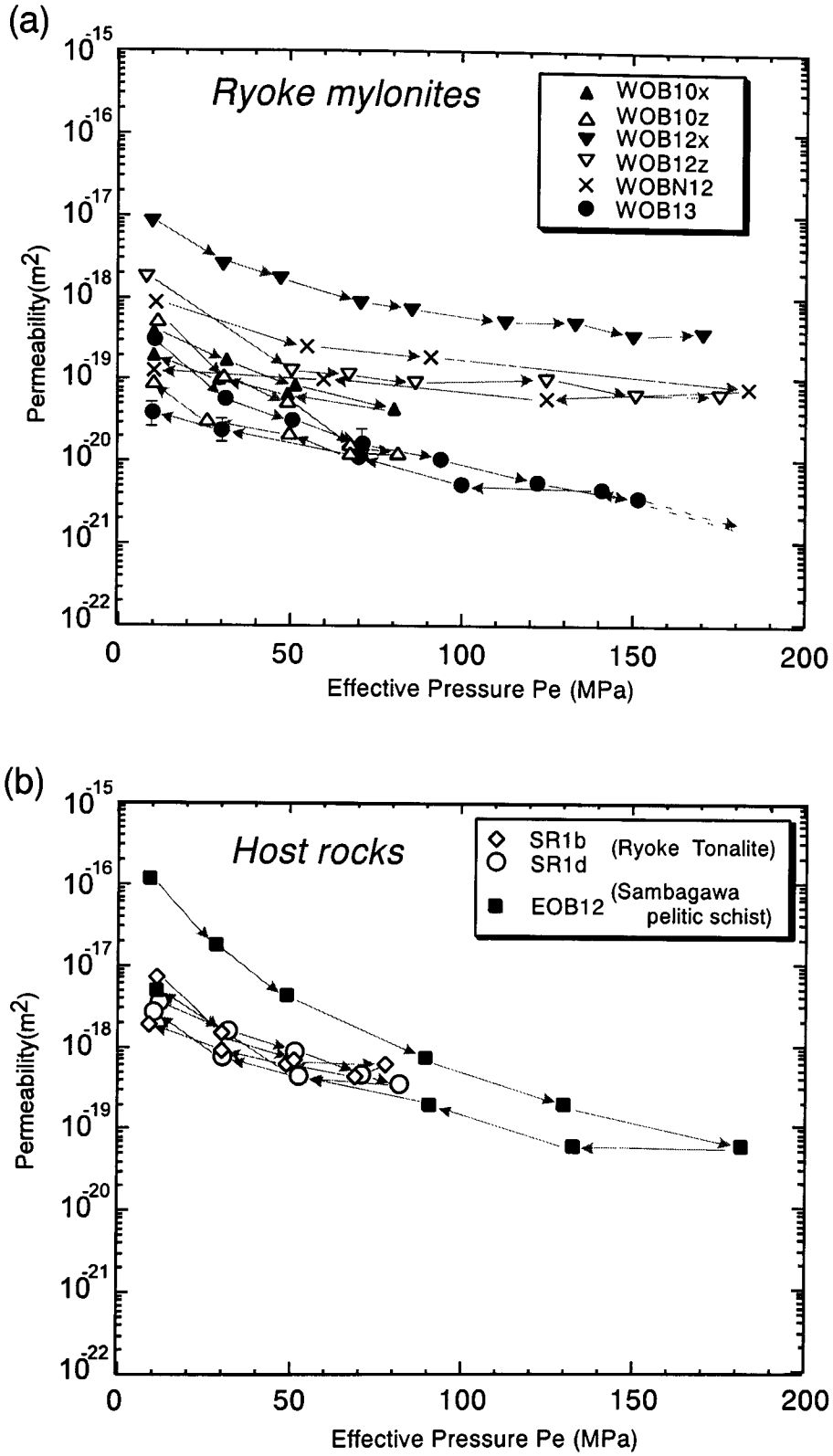

Fig. 4.2. Permeability data of (a) cohesive Ryoke fault rocks and (b) Ryoke and Sambagawa host rocks from the Kitagawa area as a function of effective pressure Pe. The sampling locations are shown in Figs. 2.2 except for that of SR1 (Tonalite), which was taken from about 3.4 kilometers West of the MTL. The permeability of WOB13b could not be measured when Pe was 180MPa because the amplitude of downstream side pore pressure could not be detected.

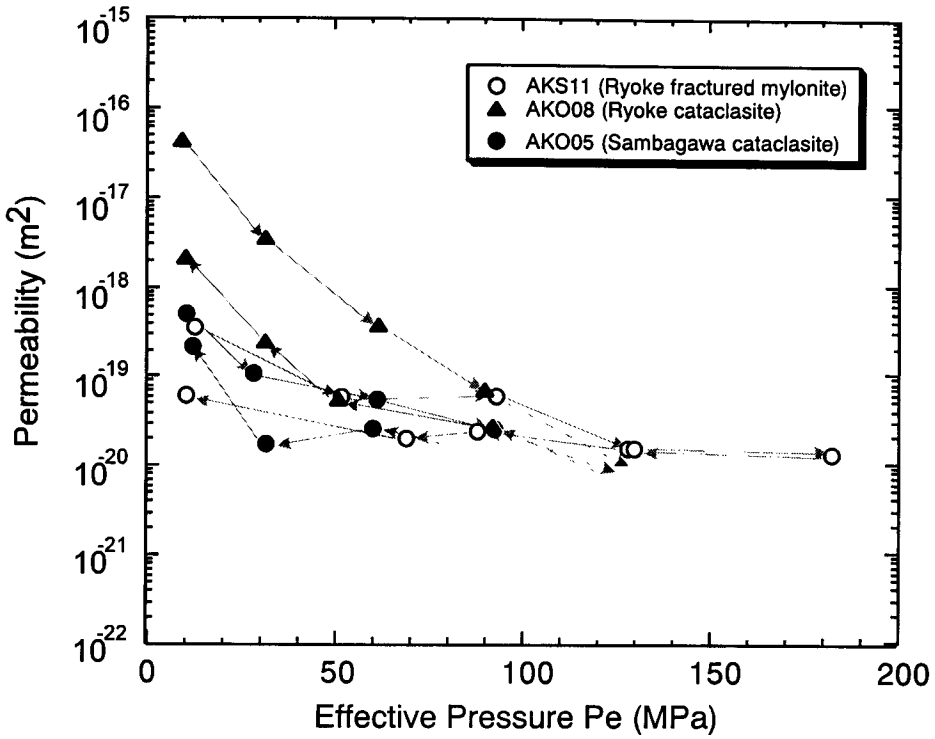

Fig. 4.3. Permeability data of host rocks and cohesive fault rocks from the Ankoh area as a function of effective pressure Pe. The sampling locations are shown in Figs. 2.4 and 2.5. The permeability of AK05 and AKO08 could not be measured when Pe was over 100MPa because the amplitude of downstream side pore pressure could not be detected. Therefore, after Pe was increased up to 180MPa and decreased down to 100MPa, the measurements were continued.

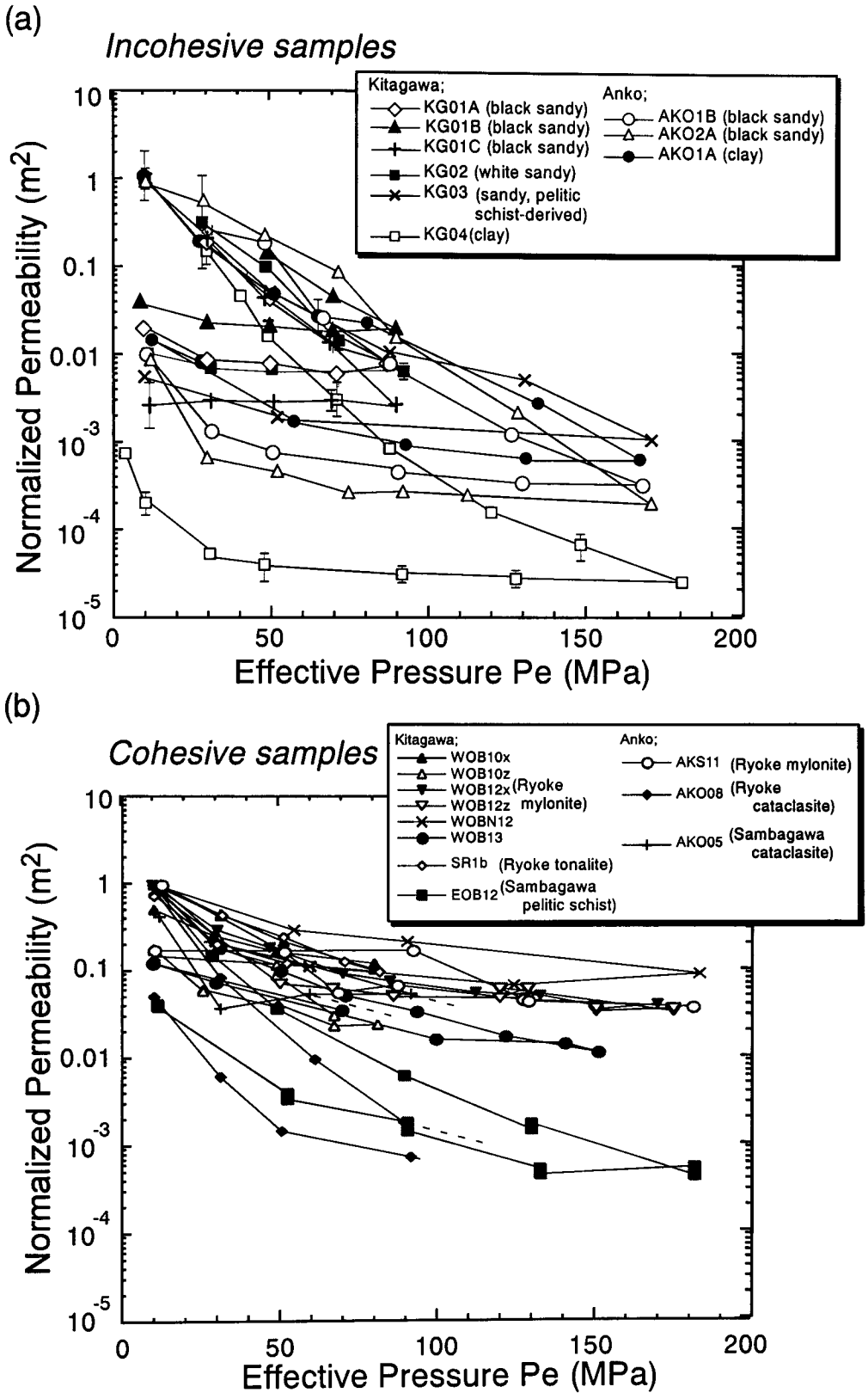

Fig. 4.4. Normalized permeability of (a) incohesive rock and (b) cohesive rock samples as a function of effective pressure Pe.

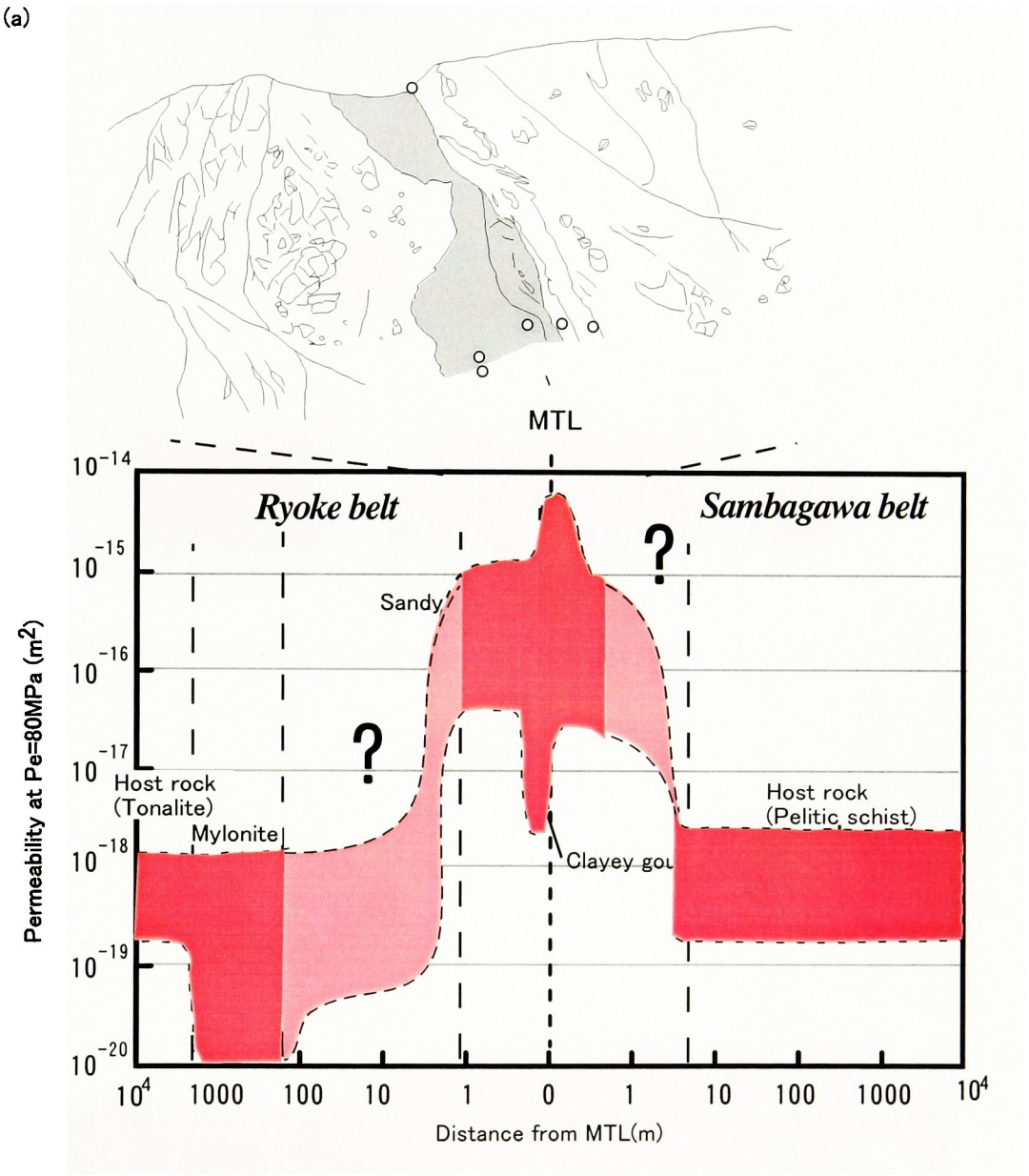

Fig. 4.5. (a) Permeability data of fault rocks from the Kitagawa area at the Pe = 80MPa on the Pc confining path as a function of distance from the MTL. X: direction parallel to the MTL fault plane and horizontal plane, Z: direction perpendicular to the MTL fault plane.

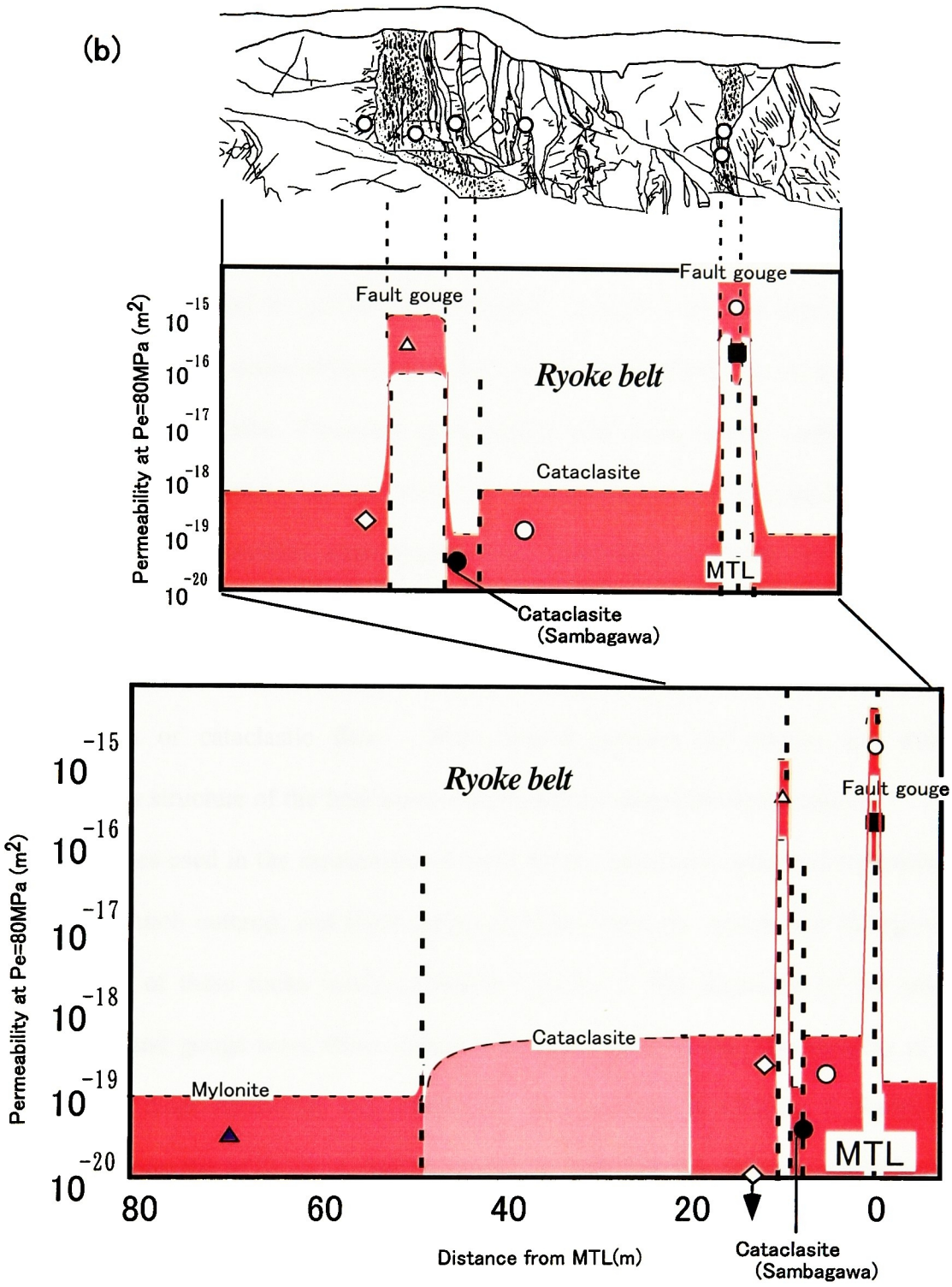

Fig. 4.5. (b) Permeability data of fault rocks from the Ankoh area at the Pe = 80MPa on the Pc confining path as a function of distance from the MTL.

5. PERMEABILITY OF MTL FAULT ROCKS DURING TRIAXIAL DEFORMATION

5.1 Samples and Experimental Procedures

In the previous chapter, permeability data were presented for fault rocks under hydrostatic stress and he permeability structure of fault zone was discussed. However, the actual fault zone is under differential stress and the stress field may be changing through the cycle of fault activity. Therefore permeability evolution during deformation should be investigated to construct a realistic model for permeability structure of fault zones.

Triaxial compression experiments were performed to study the axial permeability evolution during deformation of the Ryoke cataclasite cemented by calcite and the black sandy gouge consisting of clay minerals, which were typical fault rocks experiencing the brittle deformation or cataclastic flow. This chapter presents the results and discusses the permeability structure of the fault zone under brittle or cataclastic deformation.

Samples used in the measurements were Ryoke cataclasite cemented by calcite collected from the Ankoh outcrop, and black gouge collected from the Ankoh and Kitagawa outcrops. Description of these rocks was provided in Chapter 2. The diameters of the samples from cataclasite and gouge were about 20mm and 25mm respectively. The samples of cataclasite were cored from AK0916A and AK0916C. As explained in Chapter 2, Ryoke cataclasite observed along the MTL are partially brecciated. Although the difference between AK0916A and AK0916C is not so clear, thin section observation showed that the content of fine grain area is a little higher in AK0916A than that in AK0916C (Fig. 2.8), and AK0916A is a little more fractured than AK0916C on a sample scale. I could not prepare samples long enough for deformation tests from cataclasites by coring because of such fractures in them.

Table 5.1 shows the conditions for each experiment. The permeability of cataclasite was measured by the sinusoidal pore pressure oscillation method, which was made at 20MPa pore

pressure, and that of black gouge was measured by the constant gas flow rate method, which was made at 0 to 1MPa pore pressure. The samples were deformed with constant axial velocity and with constant Pc. The axial velocity was 0.001mm/s for all experiments of the samples from AK0916C and black gouge, but that of each sample from AK0916A was different from each other. Effective pressure Pe was around 20, 50, and 80MPa for the samples from AK0916C and black gouge, and it was around 10, 20, and 50MPa for them from AK0916A. As explained in Chapter 3, the axial displacement and the axial load were measured out of pressure vessel. Axial and circumferential strains were measured during deformations for the samples from AK0916A by putting strain gauges on them in the direction parallel and perpendicular to the sample cylinder axis. The measurement limitation of the strain gauge was ± 0.002. The electrical lines from the gauges passed through the jacket and epoxy paste was put in and around the hole and a polyolefin tube covered them. In order to prevent the stress concentrations at the ends of the specimen, I put epoxy paste on the samples from AK0916A on trial as Mogi (1967) (Fig. 5.1), but it did not seem to work well. One of the possible reasons of this is that the samples were not long enough.

5.2 Permeability of Cataclastic Rocks during Deformation

The differential stress and permeability as functions of the axial strain for each measurement are shown in Figs. 5.2 (a) and (b). The bulk axial shortening of each sample was estimated from the difference between the detected axial displacement and shortening of piston of the experimental machine which was derived from the axial load and the stiffness of the piston evaluated in Chapter 3.

Although the absolute values of permeability of AK0916A and AK0916C were very different from each other, the relations of the permeability to the differential stress and the axial strain were similar. Fig. 5.2 (a) and (b) show that, as the axial strain increases, the permeability

of cataclasite samples decreases initially down to 0.1 0.2 of their initial values in general when the differential stress is around 0.3 0.4 of the maximum, and then starts to increase up to 30 200 times the initial value when the stress is around 0.7 – 0.95 of the maximum stress, and becomes stable after the sudden decrease of the differential stress. One or a few major fractures (or faults) could be observed intersecting specimen faces after the experiments, which might be produced at the sudden decrease of the differential stress. Figs. 5.3 (a) and (b) show that the relations between the permeability and the differential stress under the different effective pressure were close to each other.

The permeability of the specimen from AK0916A when Pe = 51MPa could not be measured before the rupture happened except for the initial points, because it was below the lower limit of permeability which can be observed with the measurement system. After the deformational experiment, the permeability of the specimen from AK0916A was measured under hydrostatic stress (Fig. 5.2 (a)). The permeability was less than the "final" one during deformation when Pe is 10.2MPa and 51MPa, but, in the case that of Pe = 19.5MPa, the relation was opposite. The reason of this discrepancy is unknown, but as described in Table 5.1, there was the leak through the jacket and Pp was increasing slightly and became around 24MPa just before unloading and the permeability was around 5 x 10^{-18} m^2 at the experiment that Pe is 19.5MPa. Pp decreased back to 20MPa at the measurements under hydrostatic stress, but the effect of this Pp increasing might be left.

The decrease of the permeability as the increase of the differential stress probably reflects the closure of pre-existing cracks. In Figs 5.2 (a) and (b), as the axial strain progresses, differential stress increases, however, the gradient of differential stress becomes larger in general. Walsh (1965) explained theoretically this variance of the differential stress by the closure of pre-existing cracks.

On the other hand, the increase of the permeability just before the failure probably

reflects the production of new cracks. Fig. 5.4 shows the volumetric strain of the samples from AK0916A under Pe = 10.2MPa which computed by summing the axial strain with twice the circumferential strain as described by Brace et al. (1966). Although the strain gauges were also used other experiments of AK0916A samples under different Pe, the output showed that the strain exceeded its limit just after loading. Here the strain on the Pe increasing paths was ignored, although it was not clear if it was small enough or not to justify doing this. The volumetric strain in Fig 5.4 decreased initially, but increased suddenly when the differential stress was around 0.8 – 0.9 of the maximum. The relation between the increase of permeability and the dilatancy of fractured rock has been reported by Zoback and Byerlee (1975). Thin section observation showed that there are many small fractures in the specimen after deformation (Fig. 5.5).

5.3 Permeability of Fault Gouge during Deformation

The evolution of the permeability and the differential stress of black gouge were not similar to those of cataclasite (Fig. 5.2(c)), although a major fault, or the narrow zone where shear was concentrated, was observed in the deformed sample. As the axial strain was increasing, in general, the differential stress was increasing and the permeability was decreasing, and the slope of them became small when axial strain exceeded around 0.08 to 0.12. Fig. 5.3(c) shows that the relations between the permeability and the differential stress under the different effective pressure were similar to each other, although the slopes might be a little different. The permeability as functions of the effective mean stress ($(\sigma 1 + 2\sigma 3)$ Pp) for the samples of black gouge are shown in Fig. 5.6(a). The relations of the permeability to the effective mean stress are close to those between the permeability under hydrostatic and effective pressure Pe during the confining path (Fig. 5.6(b)), but the slopes of the permeability change increase as the deformation progresses.

5.4 Strength of Cataclasite and Fault Gouge under Confining Pressures

When the relation between the differential stress and the axial strain were compared between cataclasite and black gouge samples, the difference could be found at its dependencies on effective pressure. Figs. 5.2(a) and (b) show that the gradients of differential stress did not vary with effective pressure for the cataclasite samples prior to rupture. However, the gradients of gouge samples were clearly dependant on effective pressure until the deformation became stable. Nevertheless, the axial strains where deformation became stable were close to each other.

Fig. 5.7 shows the relation between the maximum of the differential stress, the residual stress after rupture, and Pe for the samples of cataclasite. These relations of the specimen from AK0916A and AK0916C were close to each other, although the axial strain at which rupture occurred were different. When the axial strain was around 0.2, the differential stress of the samples of gouge did not change so much, and the differential stresses are also plotted in Fig. 5.7. From these results, Coulomb-Navier failure criterion of cataclasites were calculated (Fig. 5.8). The relations between the shear stress and the normal stress of cataclasite after the rupture and those of gouge at almost stable deformation were also estimated. The results show that fault gouge and cataclasite have internal angle of friction of about 36 and 45 degrees, respectively, as typical of brittle rocks.

5.5 Contrasting Behavior in Permeability of Cataclasite and Fault Gouge

The results of the permeability measurements under deviatoric stress at constant deformation rate determined the characteristic permeability evolution under effective pressure between 10 and 80 MPa of the specimens from the Ryoke cataclasite cemented by calcite and the black gouge consisting of clay minerals collected from the MTL outcrop. When the

deviatoric stress increases and becomes close to the failure stress, the permeability of the cataclasite increases, probably because of the production of cracks and increase in their connectivity. After failure occurs and the differential stress decreases suddenly, the permeability becomes higher than that before deformation. Nevertheless the permeability of the gouge decreases gradually and becomes almost constant as the deformation evolves. These results suggest the possibility that the permeability structure of the fault zone along the MTL evolves dramatically during the cycle of fault activity.

Table 5.1. Specimens and conditions for experiments.

Sample	Locality	Pc[MPa]	Pp[MPa]	Length[mm]	Diameter[mm]	Velocity of Axial Displacement[mm/s]	Comments
AK0916A(cataclasite)	Anko	30.2	20	43.8	20.5	0.001	Strain gauge used
AK0916A	Anko	39.5	20	41.3	20.4	0.0005	Strain gauge used
AK0916A	Anko	71	20	40	20.2	0.0001	Strain gauge used
AK0916C(cataclasite)	Anko	40.2	20	24.2	20.4	0.001	
AK0916C	Anko	71.5	20	22.4	20.5	0.001	
AK0916C	Anko	98.5	20	24.9	20.6	0.001	
KG1203B (gouge)	Kitagawa	20.3	0 – 0.6	43.5	24.1	0.001	
AK02A8 (gouge)	Anko	49.8	0 – 0.74	37.3	24.3	0.001	
KG1102 (gouge)	Kitagawa	80.7	0 – 0.62	37.2	24.4	0.001	

※1 Pc increased up to 100MPa, and then Pc and Pp were kept at 0MPa for about 6 hours before the measurement.
※2 Pc increased up to 80MPa before the measurement.
※3 Pp started to increase gradually up to 24MPa (when the axial strain was 0.05) just after the differential stress decreased suddenly because of the gas leak through the jacket.

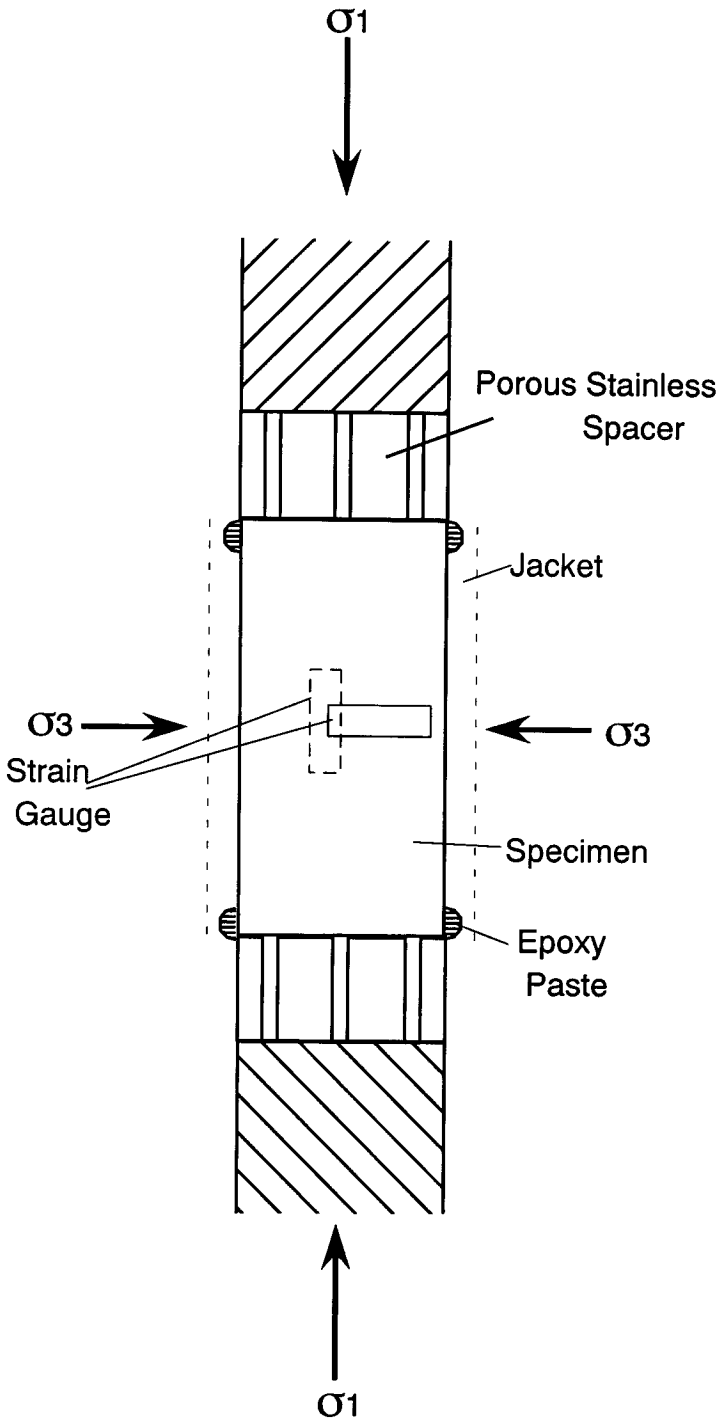

Fig. 5.1. Specimen assembly for AK0916A (cataclasite) for deformation experiments. Strain gauges and epoxy pate were not put on the other samples.

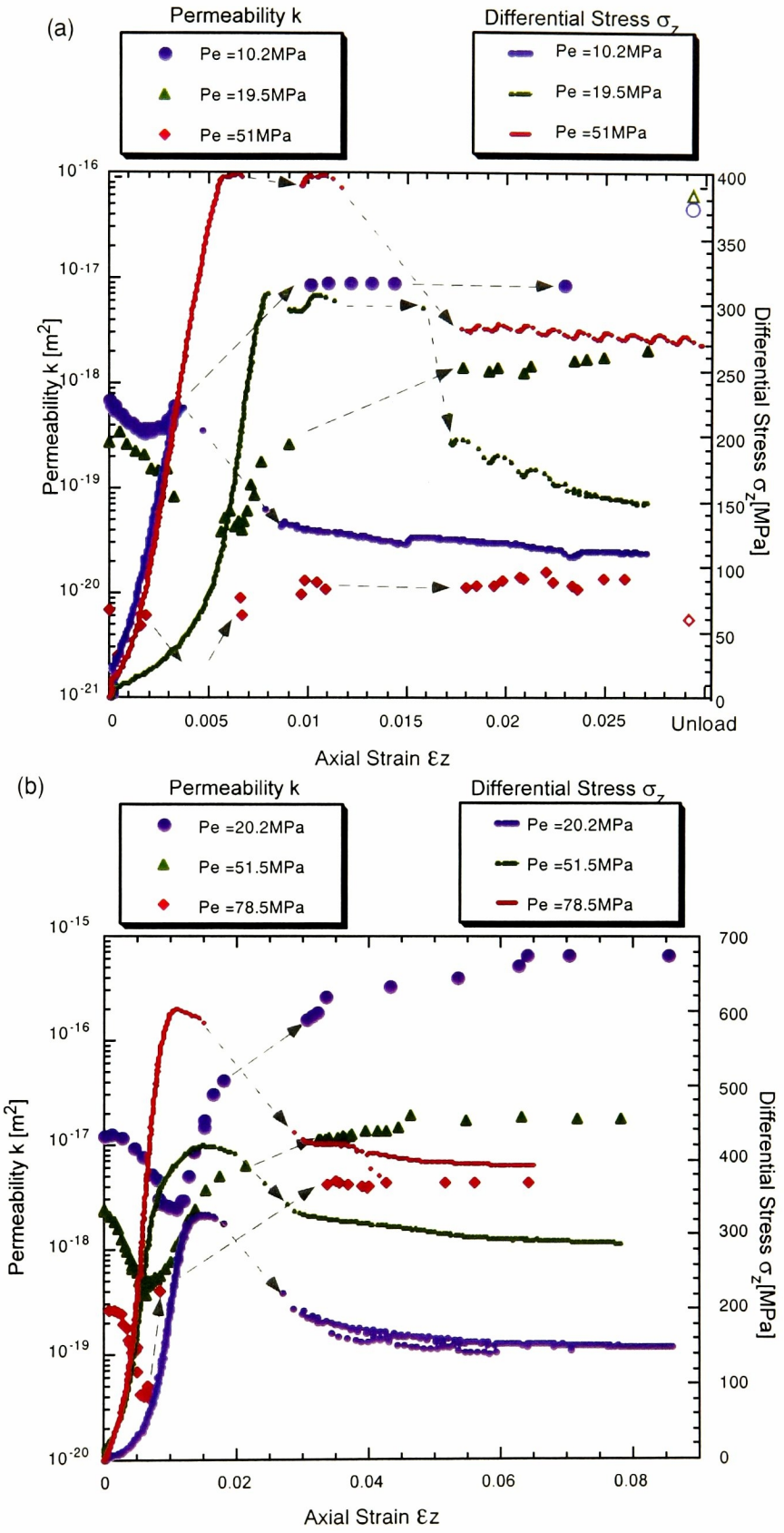

Fig. 5.2. Permeability and differential stress of specimens from (a) AK0916A and (b) AK0916C as functions of the axial strain. Open marks in (a) are the permeability measured under hydrostatic stress after deformation.

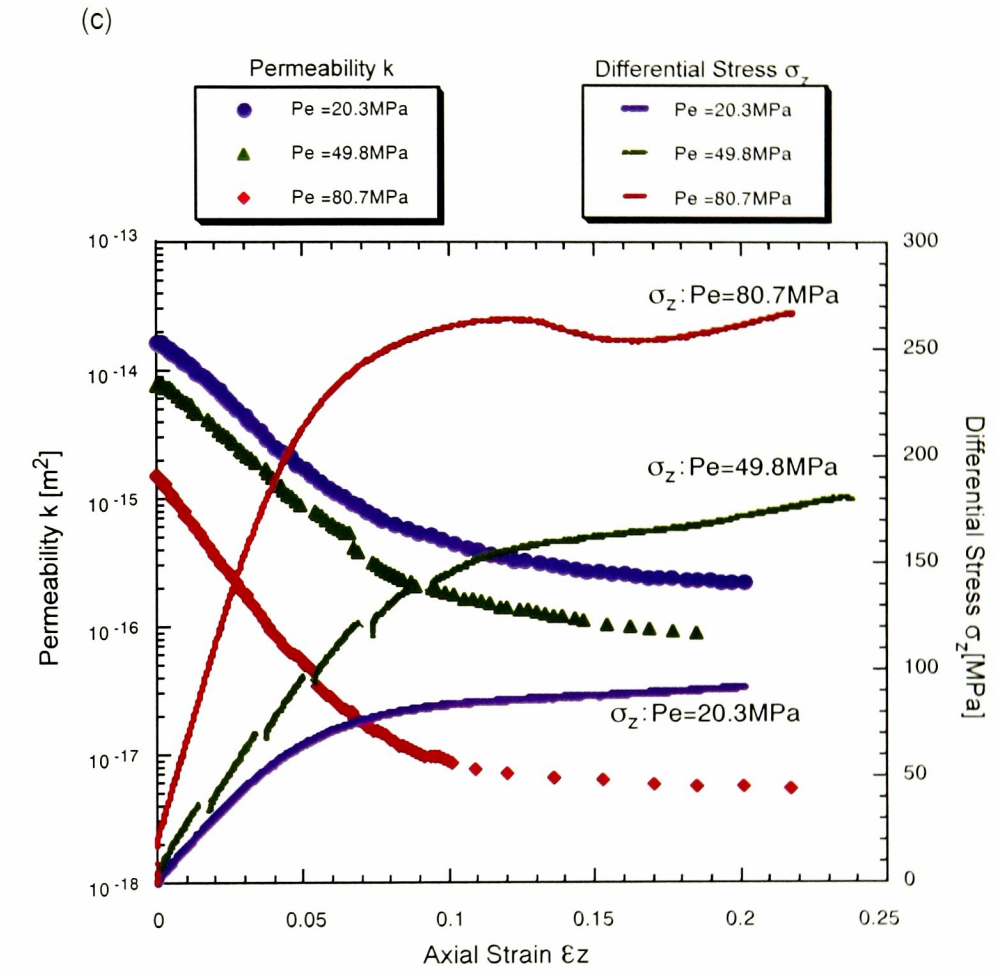

Fig. 5.2. (c) Permeability and differential stress of specimens from black sandy gouge as functions of the axial strain.

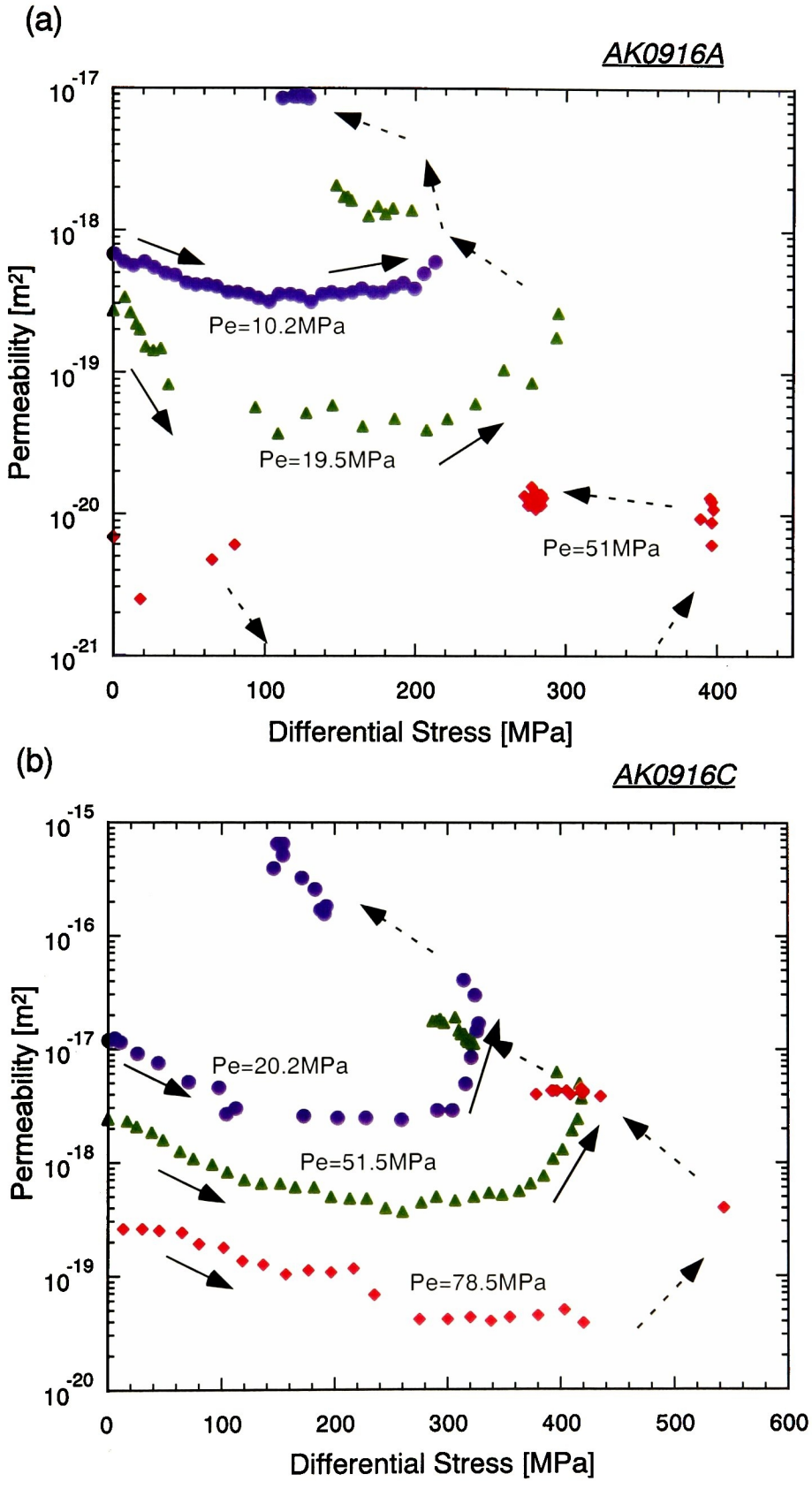

Fig. 5.3. Permeability of specimens from (a) AK0916A and (b) AK0916C as functions of the differential stress.

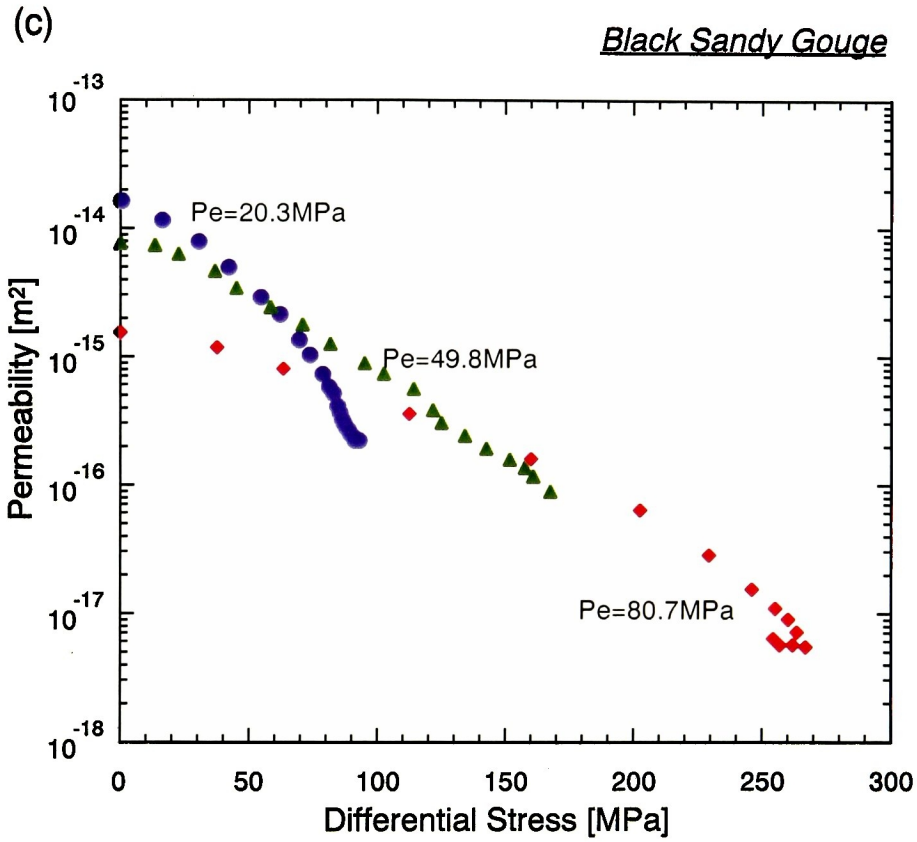

Fig. 5.3. (c) Permeability of specimens from black sandy gouge as functions of the differential stress.

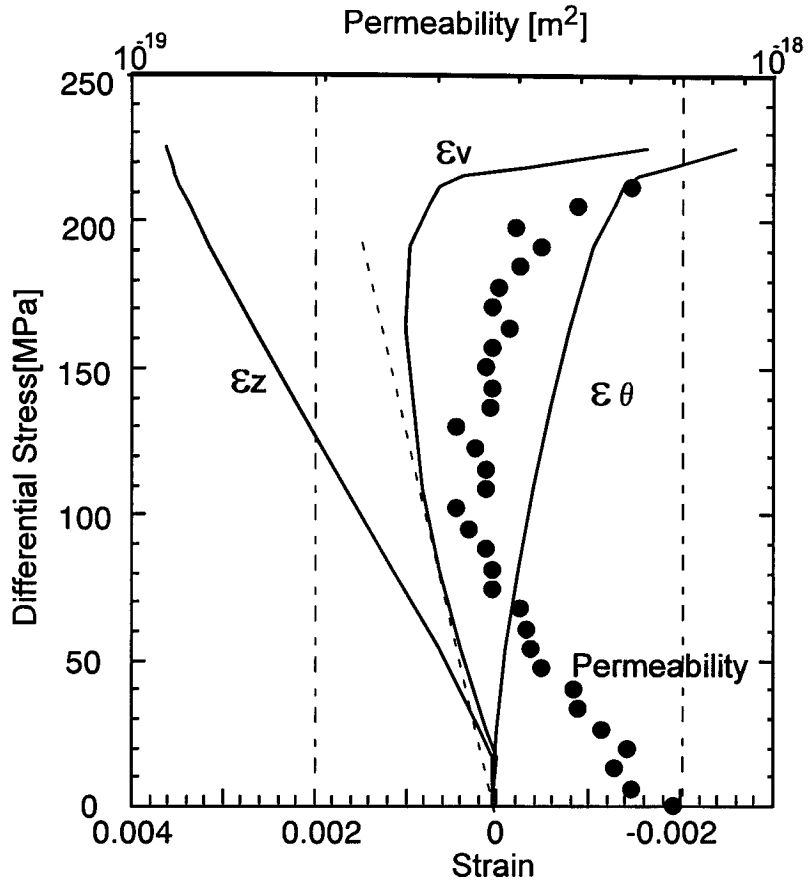

Fig. 5.4. Permeability and strains of specimens from AK0916A as functions of the differential stress when Pe = 10.2MPa. The axial and circumferential strains were measured by strain gauges, and the volumetric strain was calculated from them. εz, ε_θ and εv are the axial strain, the circumferential strain and the volumetric strain respectively. Dotted vertical lines show the measurement limit of the strain gauges, although the strain gauge output was continued to be monitored beyond these limit.

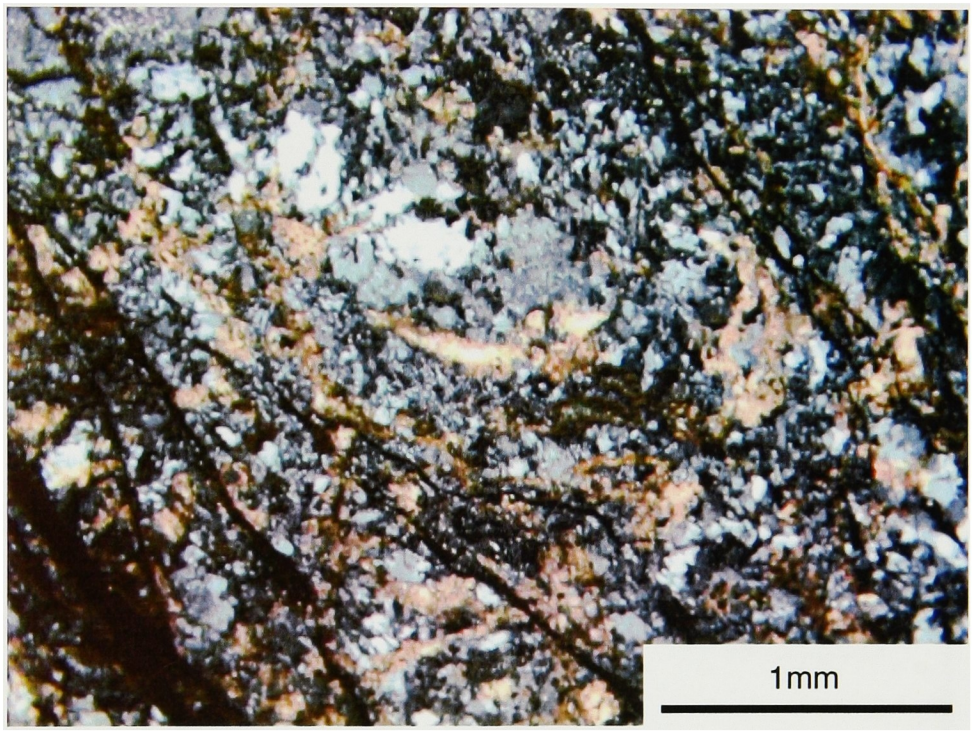

Fig. 5.5. Optical photomicrograph of the deformed specimen from AK0619C, taken under crossed-polars.

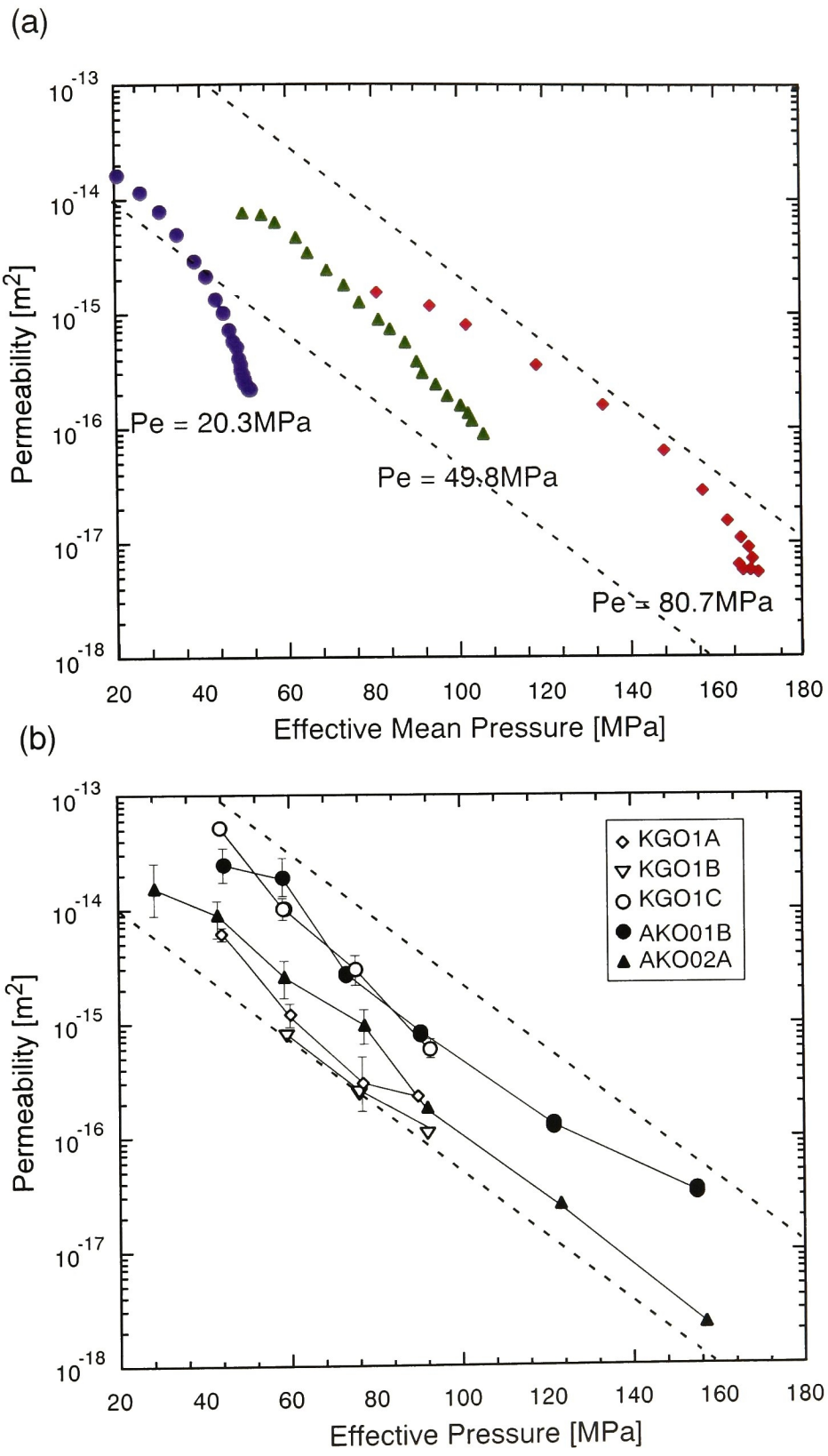

Fig. 5.6. (a) Relation between permeability of black sandy gouge samples and effective mean stress ($(\sigma_{1+2}\ \sigma_3)/3$ Pp). (b) Permeability of black sandy gouge collected from the Kitagawa and Ankoh outcrops under hydrostatic stress as a function of effective pressure. Only the permeability data measured on the Pe increasing path are shown. The area bounded by dotted lines in (a) is decided by (b).

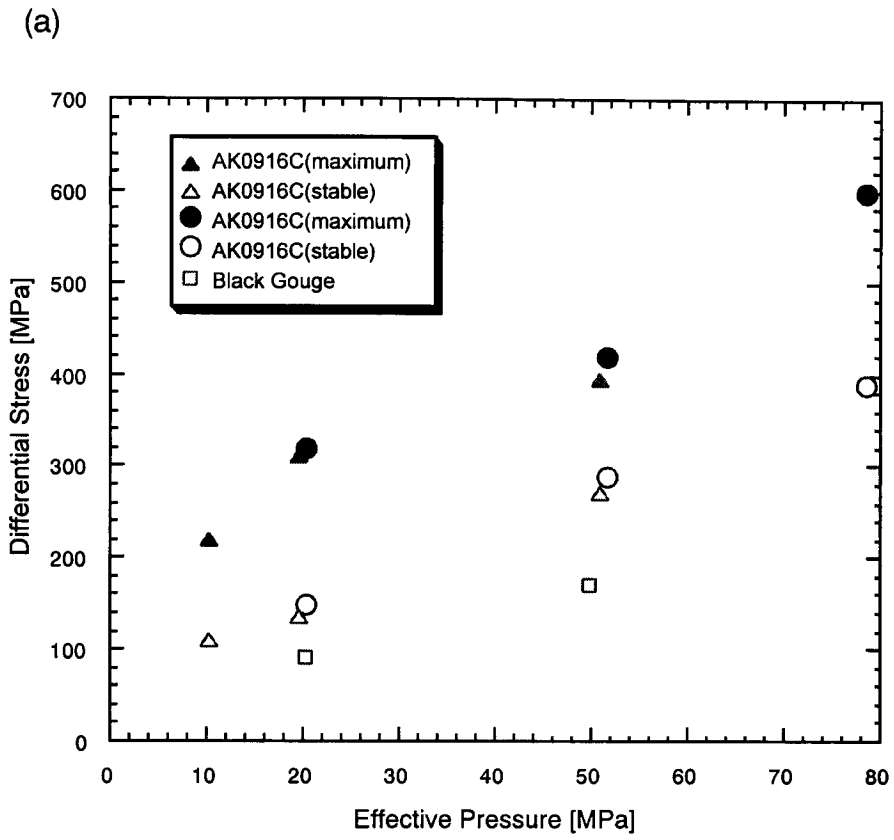

Fig. 5.7. Maximum differential stress of specimens from cataclasite and the differential stress at stable deformation of the samples, as functions of effective pressure. The differential stress of sandy gouge samples is that when the axial strain is around 0.2.

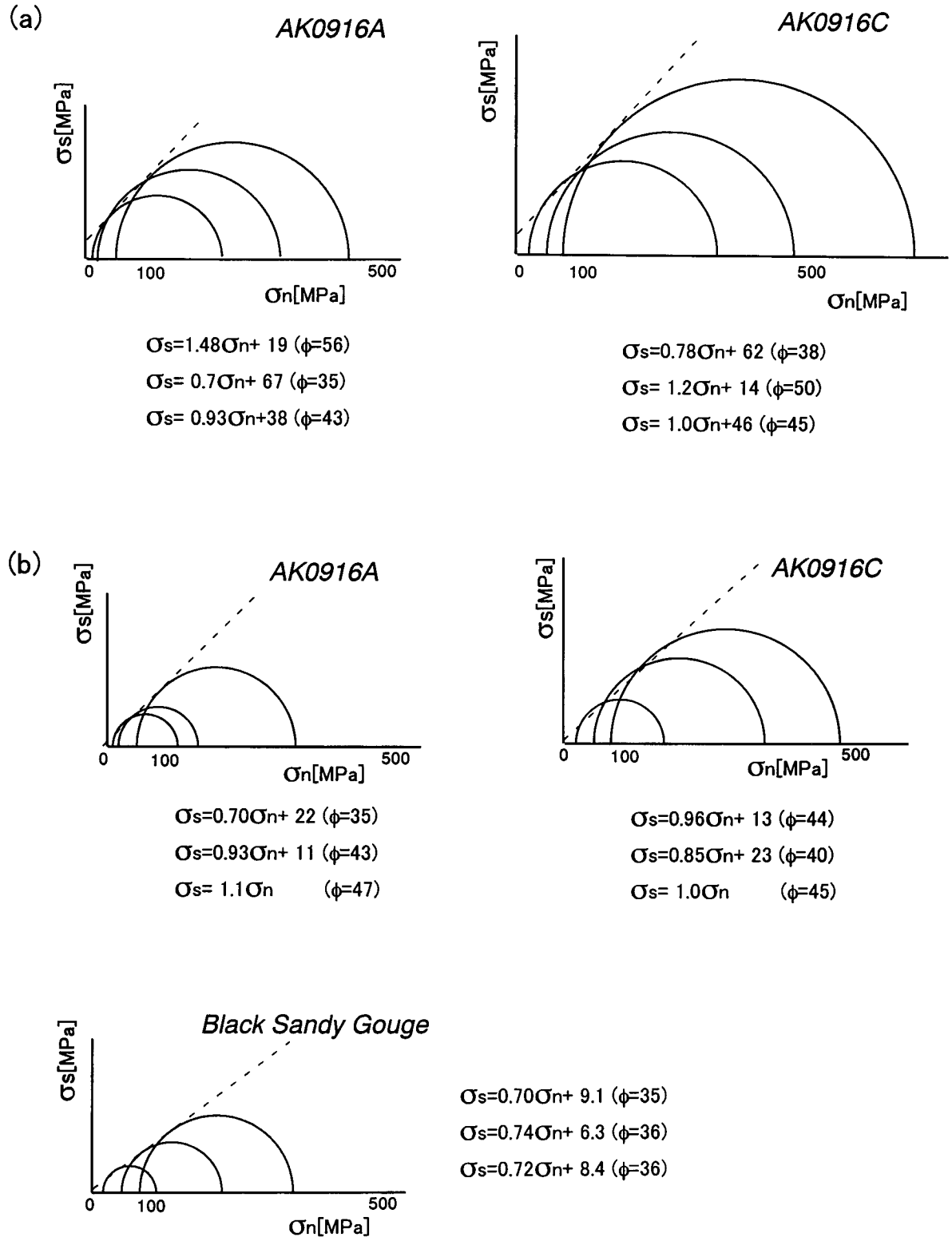

Fig 5.8. Mohr circles for (a) the failures of cataclasite samples and (b) the stable deformation, and Coulomb-Navier failure criterions of cataclasites and the relations between the shear stress (σ_s) and the normal stress (σ_n) at stable deformation calculated from the circles.

6. FRACTURE PERMEABILITY OF SAMBAGAWA SCHIST AND MTL MYLONITE

6.1 Samples and Experimental Procedures

Fractures in comparatively impermeable rocks may play important roles as conduits of fluid. The permeability of a fracture is difficult to discuss directly from laboratory data, because it may depend on its size. Therefore it is strongly important to develop a method to estimate fracture permeability under normal stress indirectly.

It may be possible to evaluate permeability of a single fracture from its surface topography. In this chapter, as a first step to evaluate permeability of fractures on various scales, fracture apertures were estimated under loading from measured permeabilities and also calculated from contact analyses of fracture surface topography. The two results were then compared them so as to investigate the possibility to estimate fracture permeability from surface topography. For the measurements, I used samples which have a natural fracture or an "artificial fracture" of which surfaces were ground.

Host rocks of samples with ground surface fractures are Sambagawa pelitic schist and Ryoke tonalitic mylonite, and that of natural fracture is the mylonite. It was not clear if the natural fracture has slid or not but opposite wall rock surfaces fitted to each other on the sample scale. The samples for measurements were cored by a laboratory coring machine using a 20mm diamond core and were shaped into cylinders. The axis of the samples with ground surface fracture were nearly parallel to the slip direction of the MTL. I cut the samples for ground surface fractures parallel to the coring direction (Fig. 6.1) and the cut surfaces were polished with Carborundum to the roughness of #400, 1200 and 6000. Table 6.1 shows information about measured samples with ground surfaces.

6.2 Measurement of Fracture Permeability

Fracture permeability

I measured permeabilities using the pore-pressure oscillation method with the pore pressure Pp fixed at 20MPa, and the confining pressure Pc was incrementally increased from 30MPa to 200MPa (Figs. 6.2 (a) and 6.3 (a)). Permeabilities of rocks with no fracture are much less than these with a fracture for both the samples with ground surfaces and natural fractures, therefore matrix permeability was ignored in the following analyses. Figures 6.2 (a) and 6.3 (a) show that ,in general, the slopes indicating permeability change decrease as the effective pressure increases.

Estimation of aperture from permeability

From the results of measured gas permeability I calculated apertures of cracks on the assumption that they consist of parallel and smooth walls. The fluid flow rate through smooth, parallel plates is given by

$$Q = -\frac{La^3}{12\mu}\frac{dP}{dx} \qquad (6\text{-}1)$$ (often called the "cubic law")

where L is the width of the fracture perpendicular to flow direction, a is the aperture, μ is the viscosity of the fluid and dP/dx is the pressure gradient. The flow rate through the measured sample is given from Darcy's law by

$$Q' = -\frac{kA}{\mu}\frac{dP}{dx} \qquad (6\text{-}2)$$

where A is the area of cross section perpendicular to the flow direction and k is permeability. From equations (6-1) and (6-2), I calculated the aperture a.

Figures 6.2(b) and 6.3(b) show the results of estimated apertures. The tendency for fractures polished with the finer Carborundum to have smaller apertures becomes more pronounced as confining pressure (Pc) increases. Permeability of samples PS#1200 and TM#1200 are almost same, although these host rocks are different to each other.

6.3 Surface Profile Measurements

The topography of fracture surfaces was measured by surface stylus profilometer (Surfcorder SE1200, Kosaka Laboratory Ltd.). The vertical resolution is at most on order of $10^{-2}\mu m$, and the range of vertical movements is about 300μm. The profiled paths were set to be perpendicular to the axes of cylindrical samples at 2mm intervals. The topography along a few lines parallel to the axis was also measured. Examples of measured surface profiles are shown in Fig. 6.4.

Fig. 6.5 shows the power spectral density (PSD) of the surfaces to describe their features. In the case of natural fracture, a logarithm of PSD is proportional to that of special frequency, and the result in this study is consistent with the results in Brown and Scholtz (1985) and Power et al. (1987). On the other hand, the gradients of PSD of ground surfaces become small at large wave length, which may be because the surfaces are polished. At small wave length, as the result of natural surface, PSD of ground surfaces becomes larger as wave length increases, although the gradients differ from that for PSD of natural surface.

From the profiles, the sizes of asperities were measured in the direction parallel and normal to crack surfaces (W, H) on various scales (around $10\mu m$,$100\mu m$, 2mm, in the direction parallel to the surfaces) (Figs. 6.6 and 6.7). Generally, in the case of asperities on the ground surfaces, the larger the W, the smaller the ratio of H to W. On the other hand, the ratios of H to W of asperities on the natural surfaces are around 0.1 for W between 10 and $10^3\mu m$ and do not depend on the asperity size.

Several typical pairs of W and H for each sample were then selected, and the aperture under normal stress was estimated on the assumption that the topography of fracture surfaces are composed of asperities which have these typical W and H values. One of the problems of this contact analysis model is that the results may affected how to choose the "representative asperity sizes", therefore they should be selected properly.

6.4 Contact Analyses of Ground and Natural Surfaces

To estimate the aperture of cracks under normal stress, I assumed asperities as sections of spheres, and calculated the depression of these asperities. The radius of the spheres were decided with the asperity scale H and W (Fig. 6.8(a)). In this assumption, the radius R is given by

$$R = \frac{1}{2}\frac{H^2 + (0.5W)^2}{H} \qquad (6\text{-}3)$$

The depression of the spherical elastic asperities under loading have been calculated with Hertzian theory in previous works (e.g. Johnson, 1985);

$$\delta = \sqrt[3]{\frac{9F^2}{4}\frac{1}{E^{*2}R^*}}$$

where F is the load, E^* is

$$\frac{2}{E^*} = \frac{1-\nu_1^2}{E_1} + \frac{1-\nu_2^2}{E_2}$$

where E_1 and E_2 are Young's modulus values for two asperities, ν_1 and ν_2 are Poisson's ratio. R^* is

$$\frac{1}{R^*} = \frac{1}{R_1} + \frac{1}{R_2}$$, where R_1 and R_2 are radius of each asperities.

Here the radius and other properties of asperities contacting each other are assumed to be the same, e.g. $R_1 = R_2 = R$, $E_1 = E_2 = E$, and $\nu_1 = \nu_2 = \nu$.

When the force F loading on a pair of asperities is written by

$$F = hW^2Pe$$

where Pe is effective pressure (Pe = Pc – Pp) and h is coefficient, the depression is expressed by

$$\delta = \sqrt[3]{\frac{9h^2W^4}{4E^*R^*}}Pe^{\frac{2}{3}} \qquad (6\text{-}4)$$

In the following, all calculations were done in the case that h=1, E=50GPa, ν=0.2, and it was assumed that the depression does not become larger than 2H. For asperities with comparatively

small W, when larger asperities do not finish the deformation, it is suitable to consider that h is more than 1. However, when this was considered in the calculation, it did not appear to the result much.

For typical sets of W and H of ground surfaces shown in Fig. 6.6, the depression was calculated (Fig. 6.9). The asperities of comparatively large W (17mm, 8mm) finished depressing (the depression becomes 2H) before Pe becomes more than 30MPa, while those whose W are 100μm or 20μm did not exceed 2H until when Pe = 200MPa.

When the surfaces of fractures are not perfectly flat, it is not simple to evaluate the apertures of cracks from the depression of the asperities which are suitable to be compared with those estimated from permeability. In the extreme case that most part of surface area can be assumed to be flat, the aperture a can be simply given by

$$a = a_0 - \delta$$

where a_0 is initial aperture. While, in the other extreme case that asperities contacting with the opposite surface distribute on most part of surface area, the aperture a may be more complicated. Here, as W is much lager than H in the samples, I simplified the shape of asperities as Fig. 6.8 (b) and assumed that cubic law holds in local area. Then the aperture a can be given by

$$a = 0.5(a_0 - \delta)\sqrt[3]{\frac{4}{W}\left(\frac{W}{2} - r\right)}$$

where r is the radius of contact area (Fig. 6.8 (c)), which can be given by

$$r = \sqrt{\delta R}$$

In fact, a may be between these cases. In the following, asperities were calculated with these extreme two models ("parallel plate" model and "asperity" model in the following).

6.5 Comparison between Apertures from Permeability and Contact Analyses

Ground surface

The results of apertures between ground surfaces estimated from the calculation of apertures are shown in Fig. 6.10 with those from permeability data. The agreements are not perfect, but the overall features of progressive reduction in aperture upon an increase in effective pressure were predicted. The deviation seems to be complex deformation of multiple contacting asperities.

Natural fractures

In the case of the ground surface fractures, I took into account deformations of all asperities that could be measured to estimate aperture changes. However, for natural fracture, it is not suitable to consider deformations of all asperities because the fracture surface topography may be fit well to the other for asperities of comparatively large wavelength. Therefore I calculated asperity changes for two combinations of typical asperities were calculated (Fig. 6.11): "set 1" consisted of asperities of which W are 20 and 2μm, and "set 2" consisted of asperities of which W are 2μm. The ratio of H and W was set to be 0.1 for all asperities. The results indicate, however, that the asperities and those changes under loading estimated from permeability are different from those from the calculations of asperity deformations.

Summary of comparison

In the cases of ground surface fractures, were generally close to each other. This supports the possibility to estimate permeability of a single fracture from the topography data of its surfaces. However, for natural fractures the methods gave different results when the matching of topographies of opposite fracture walls needed to be estimated. In such a case, the composite topography of both surfaces should be taken into account.

In the analysis of the deformation analyses, surface topography was assumed to be the

aggregation of parts of spheres. Hertzian theory suggests that the depression of the asperity is affected by the ratio of its vertical to horizontal size. If W^2>>H, that is, the horizontal scale W is much larger than the vertical scale H, R can be approximated from equation (6-3) as

$$R \approx \frac{1}{8}\frac{W^2}{H} \qquad (6\text{-}5).$$

Substitution of equation (6-5) into equation (6-4) gives

$$\frac{\delta}{H} = \sqrt[3]{\frac{18}{E^{*2}}t^2 Pe}^{\frac{2}{3}}, \qquad (6\text{-}6)$$

where t = W/H. Equation (6-6) indicates that the larger the ratio of W to H, the larger the ratio of depression per an unit load to H. In general, the larger the size of asperity of ground surface measured in this study, the larger the value of t. Thus, the comparatively large asperities depress suddenly during the loading path and finish the depression at lower normal stress, whereas the smaller ones depress gently. This is reflected in the changes of calculated apertures with loading such as the slope of aperture change becoming smaller as effective pressure increases.

Equation (6-6) also indicates that the ratio of the depression δ to H does not depend on the size of asperities if t is the same. t of asperities on the natural fracture surfaces measured in this study is almost constant for during the size range of the measurements. Therefore the change of calculated aperture strongly reflects the depression of the largest asperities considered in the calculations.

In the case of natural fractures, it is difficult to explain the change of the aperture from permeability and those from the asperities deformation. One of the reasons for such discrepancies may be that the fitness between the topography of fracture surfaces was less considered. As mentioned above, the fitness of natural fracture surfaces may be good on the scale of at least more than 1mm. On the analyses of aperture change under loading, not only surface topography of one side but also composite topography of both surfaces should be considered (Brown, 1995), although it is difficult to measure precisely. Fig. 6.11 shows that the

slope of aperture changes from permeability for load increasing is larger, especially at low effective pressure, than that from contact analyses. Above discussion about the relation between the ratio of aperture sizes and depression rate under loading suggests that, if the fitness of comparatively large asperities is good and the ratios of H to W composite topography are smaller than those for single fracture surfaces, the large asperities may depress much at low normal stress and the asperity change estimated from permeability can be explained from contact analyses. The dependency of permeability of natural fractures can be explained by the depression of surface topography, if suitable asperities are chosen as "set 3" in Fig.6.11. Set 3 consists of the asperities of which H are 0.2, 0.5 and 2mm, and W are 10, 100mm and 1mm respectively.

Table 6.1. Specimens with an artificial fracture

	PS#6000	PS#1200	PS#400	TM#1200
Host rock		Pelitic schist		Tonalitic ultramylonite
Roughness of the finest Carborundum (average grain size)	#6000 (2μm)	#1200 (13μm)	#400 (40μm)	#1200 (13μm)

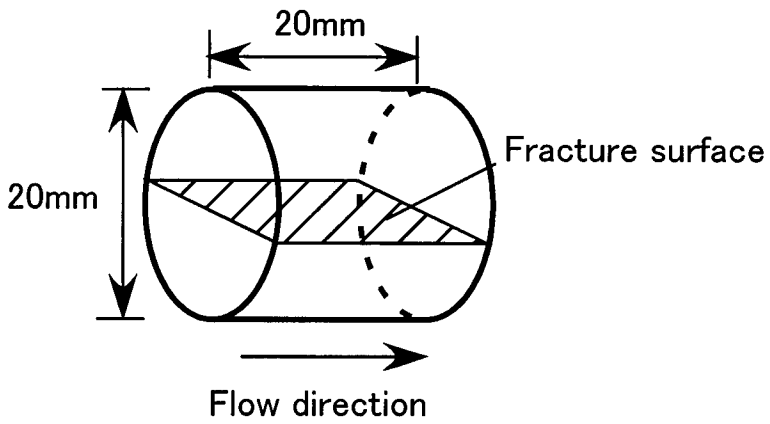

Fig. 6.1. Specimen geometry for permeability measurements.

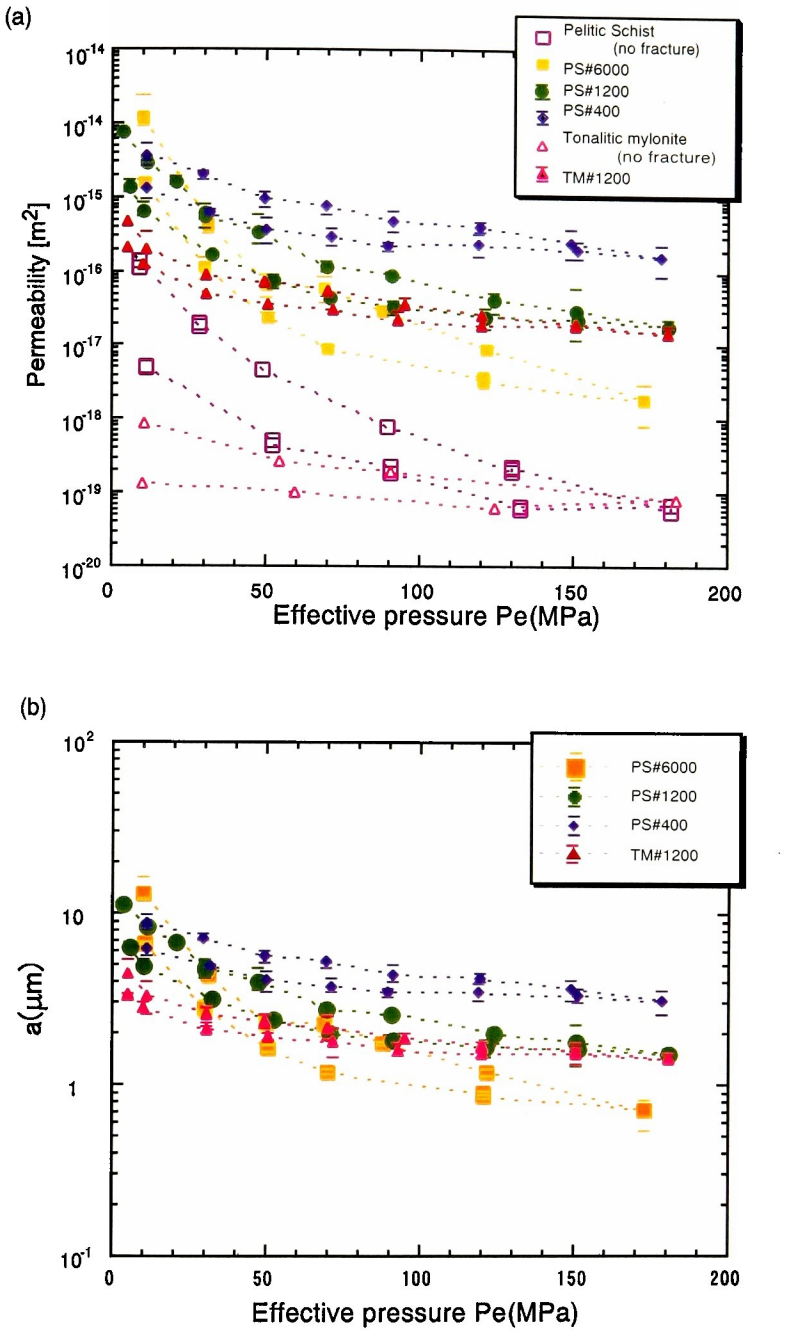

Fig. 6.2. (a) Permeability data for pelitic schist and tonalitic mylonite with and without an artificial fracture, and (b) aperture estimated from (a), as a function of effective pressure Pe.

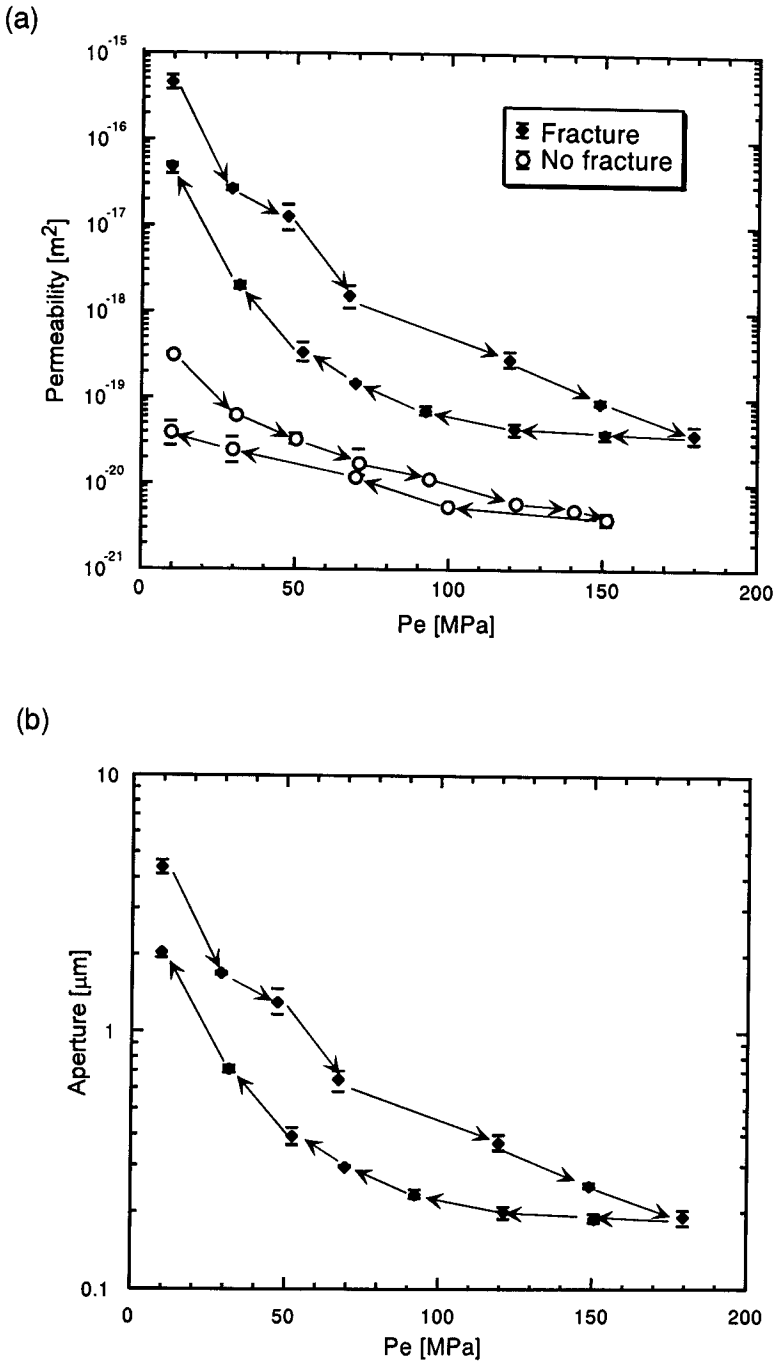

Fig. 6.3. (a) Permeability data for tonalitic mylonite with and without natural fracture, and (b) aperture estimated from (a).

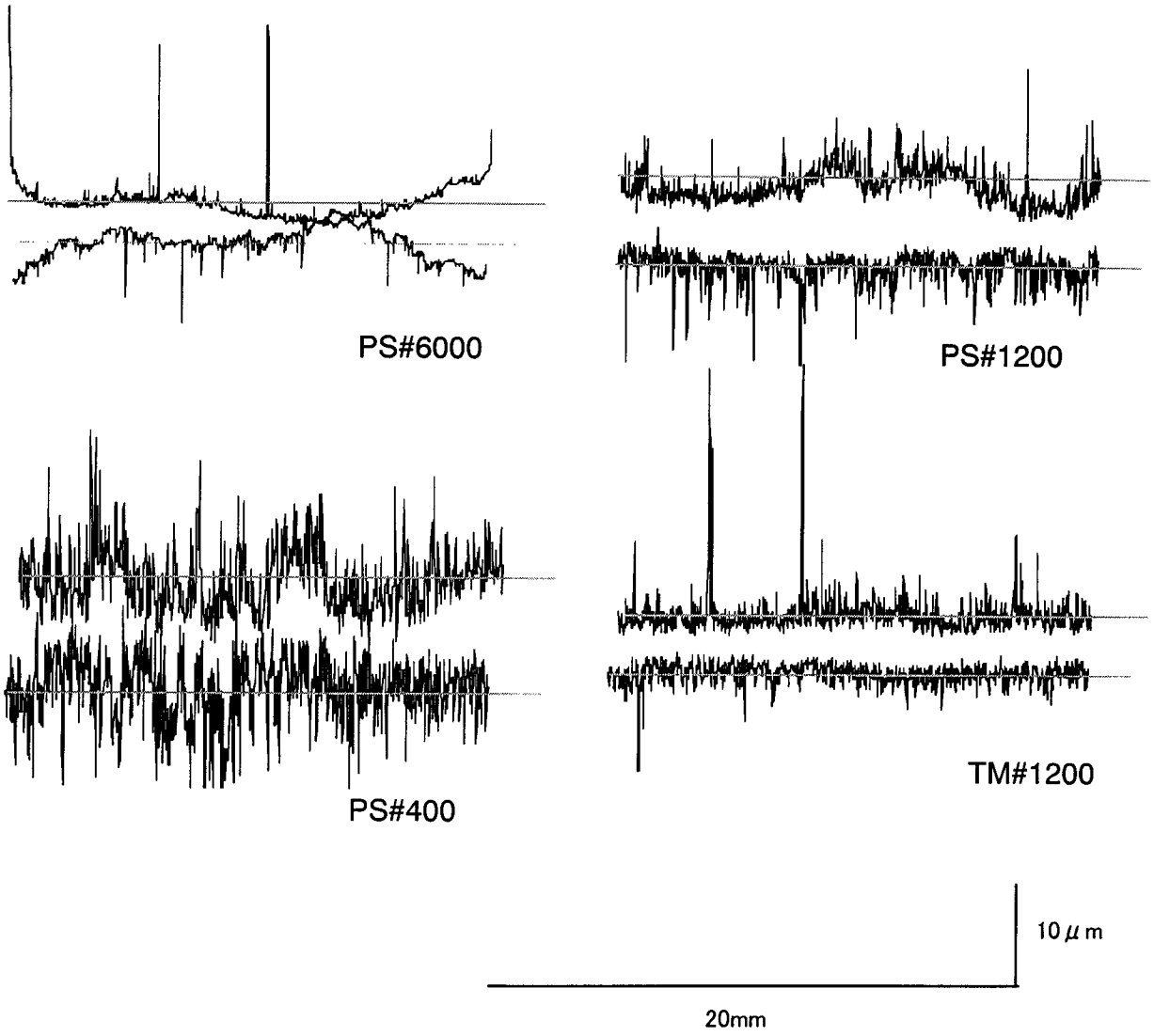

Fig. 6.4. (a) Surface profiles of artificial fractures.

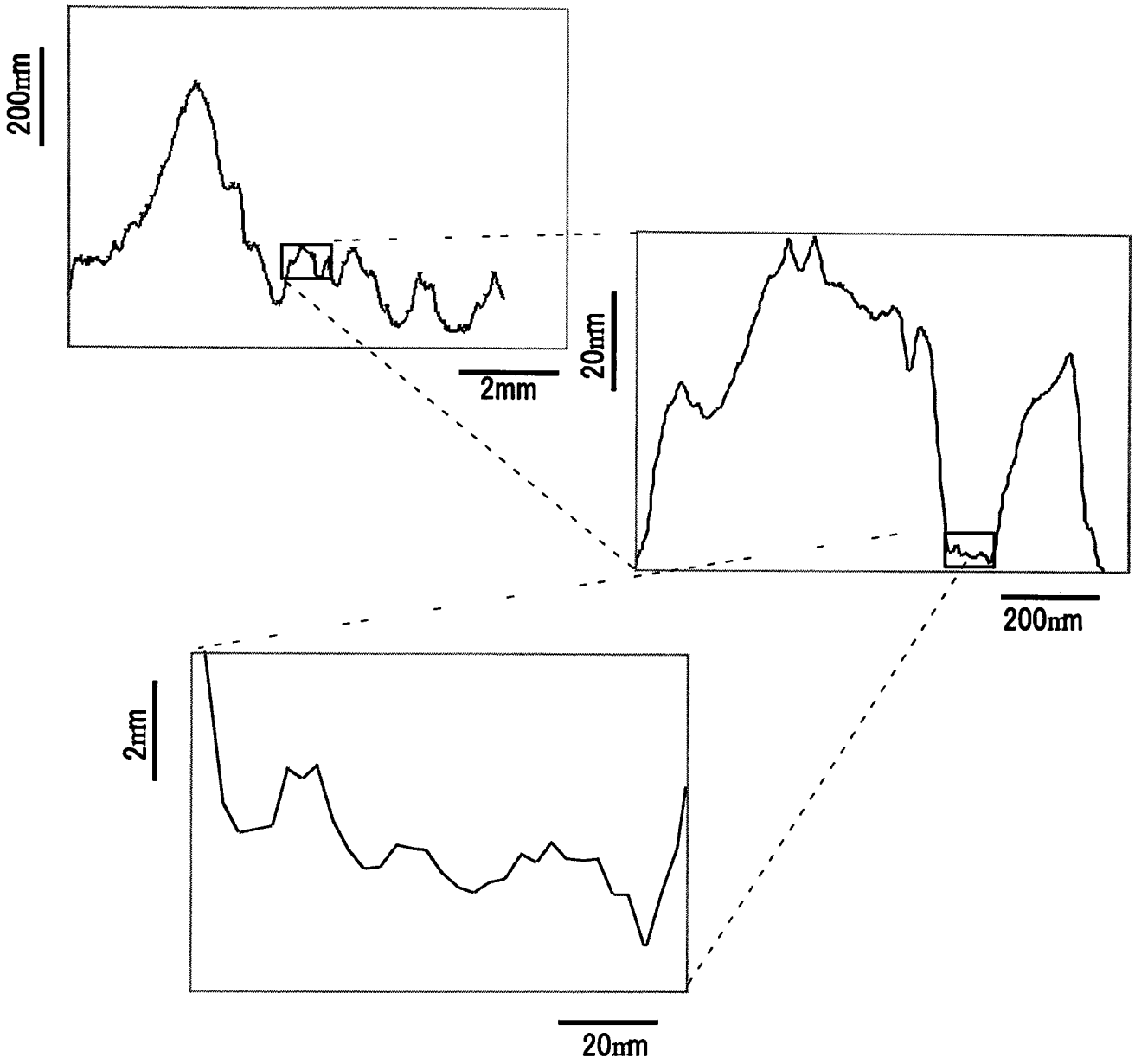

Fig. 6.4. (b) Surface profiles of natural fractures drawn at various scales.

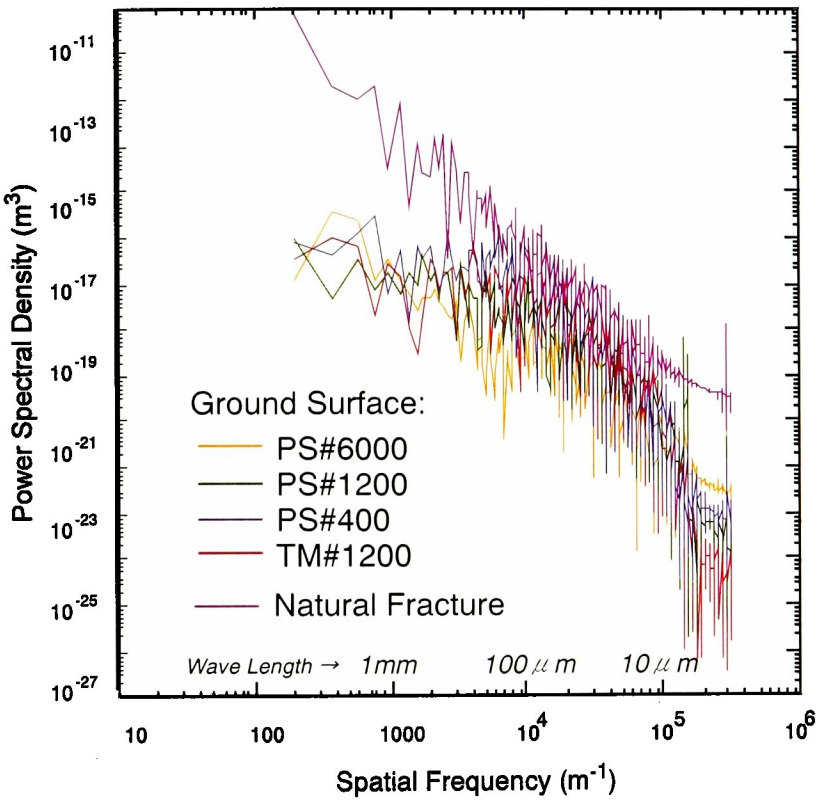

Fig. 6.5. Power spectral density from the surfaces shown Fig. 6.4 (a) and (b).

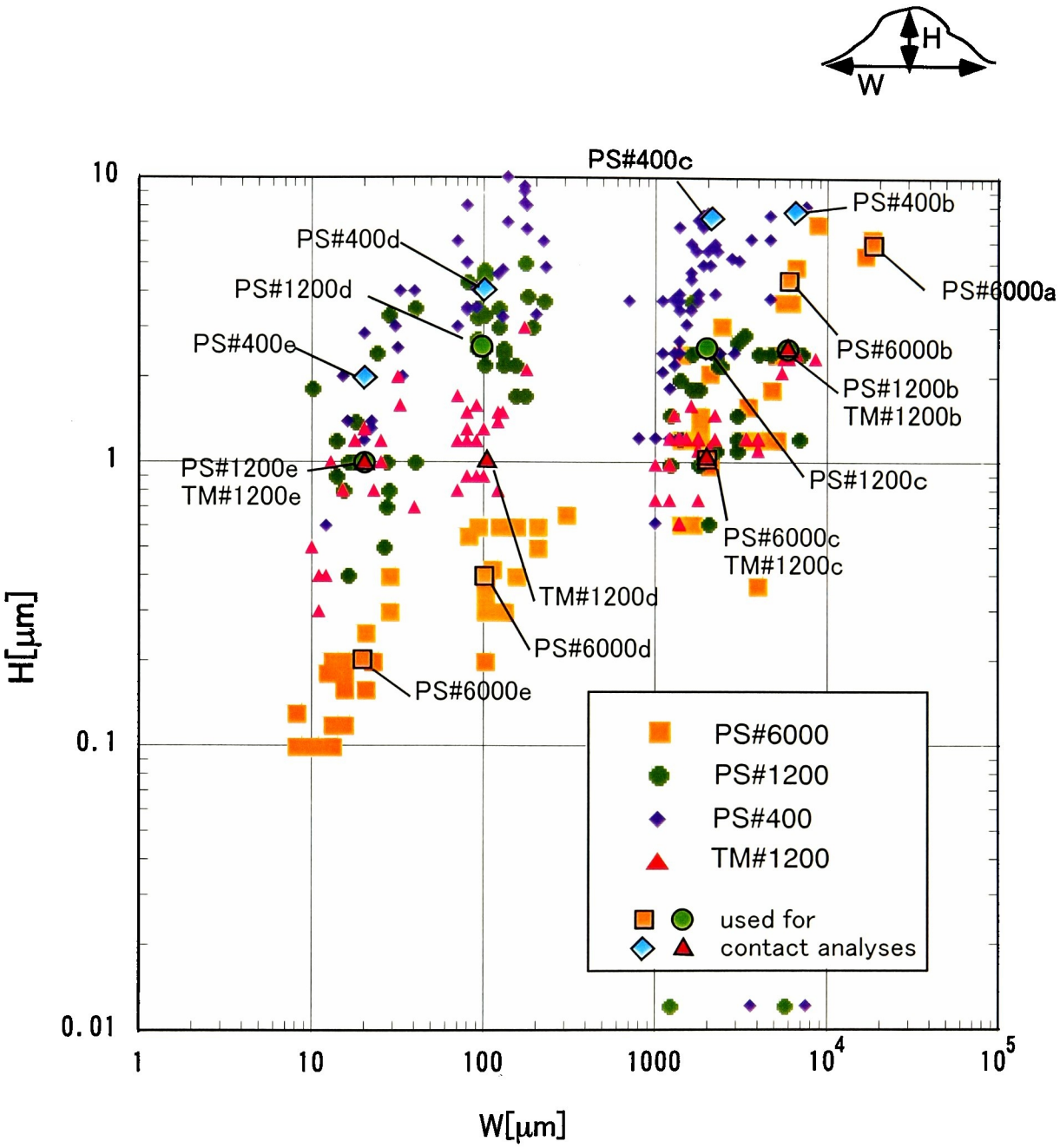

Fig. 6.6. Relation of vertical scale H to horizontal scale W of asperities on surfaces of artificial fractures.

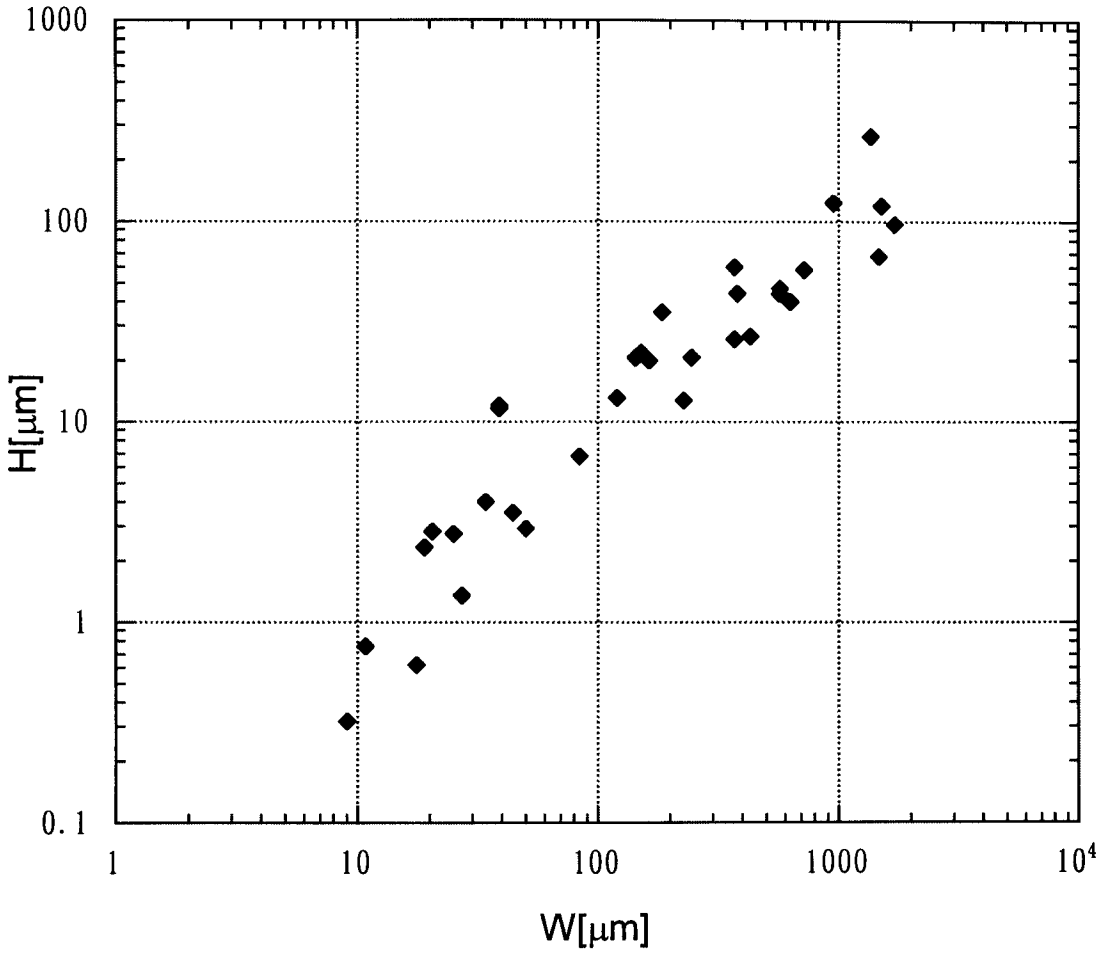

Fig. 6.7. Relation of vertical scale H to horizontal scale W of asperities on surfaces of natural fractures.

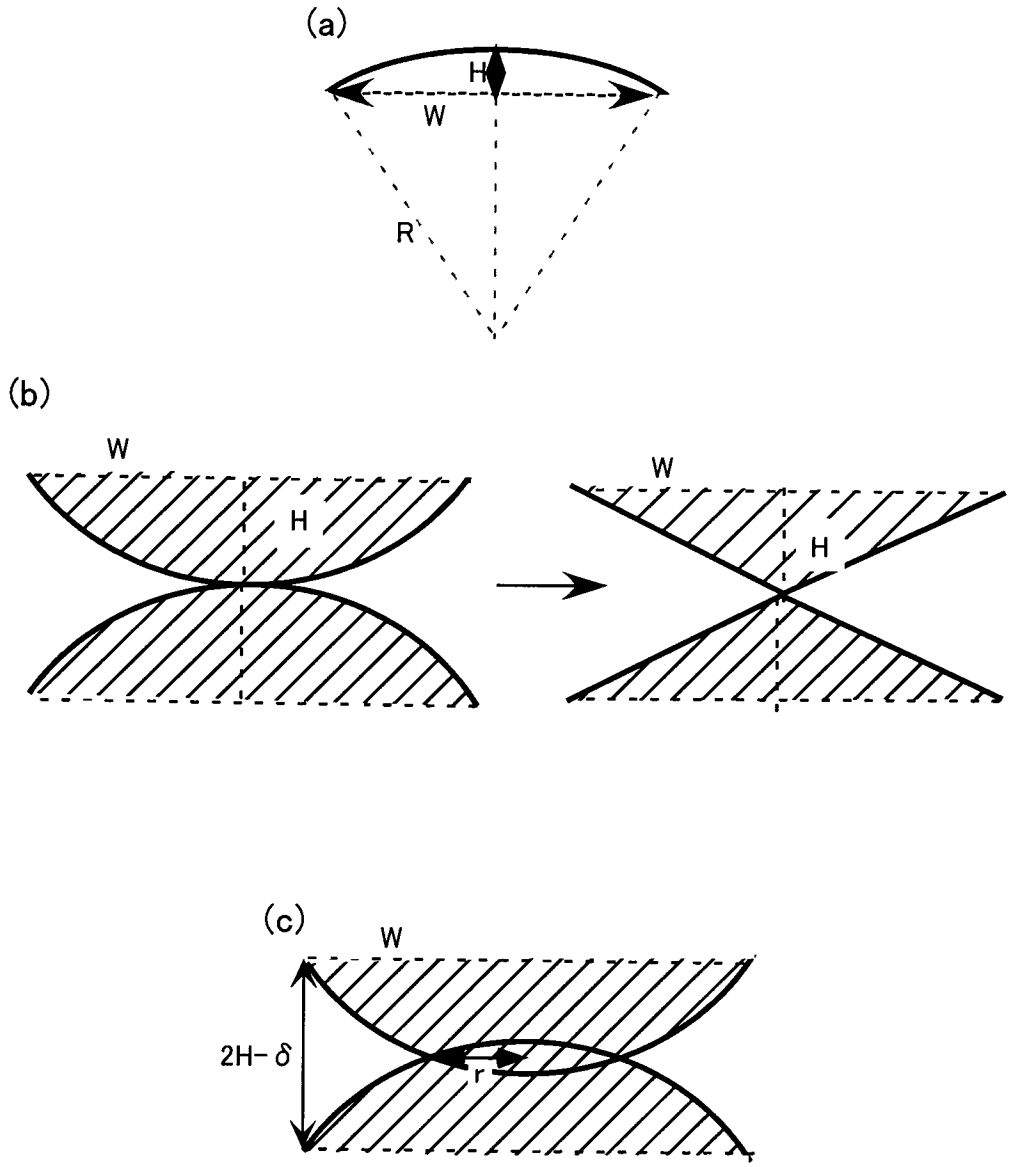

Fig. 6.8. Schematic expressions showing (a) the relation among W, H and R and (b), (c) individual asperity contacts (see text).

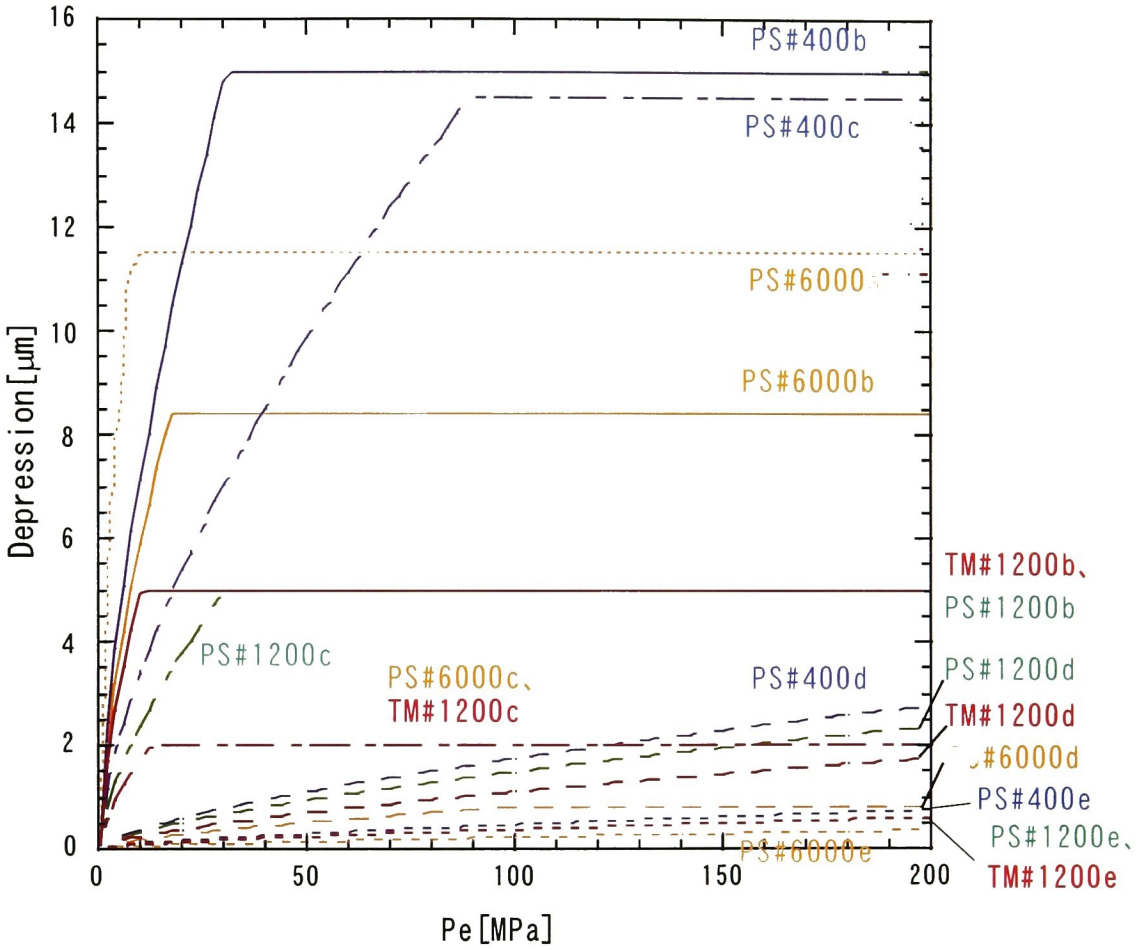

Fig. 6.9. Depression of asperities shown in Fig. 6.6 under loading.

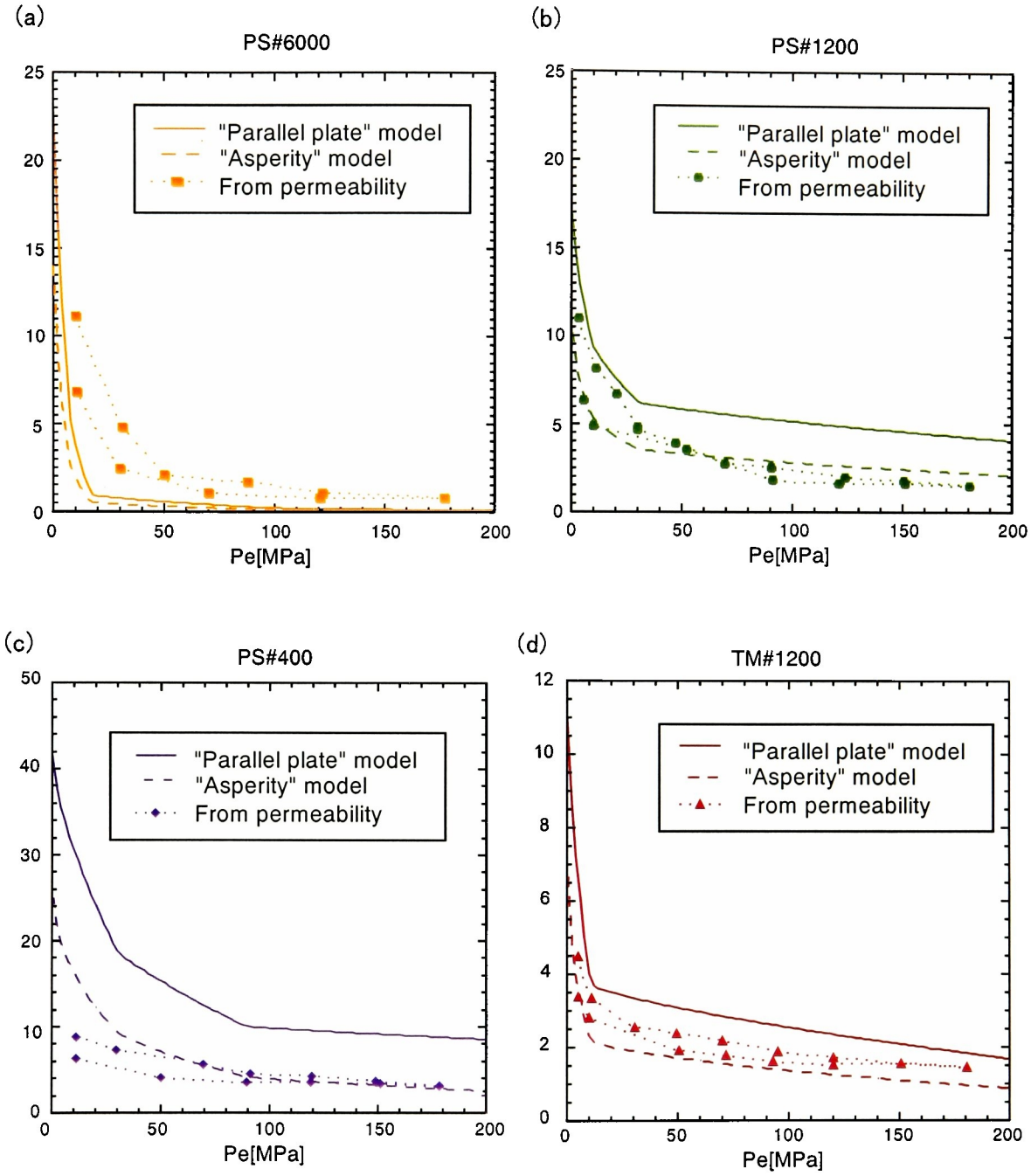

Fig. 6.10. Aperture of artificial fractures estimated from permeability measurements and calculated with contact analyses.

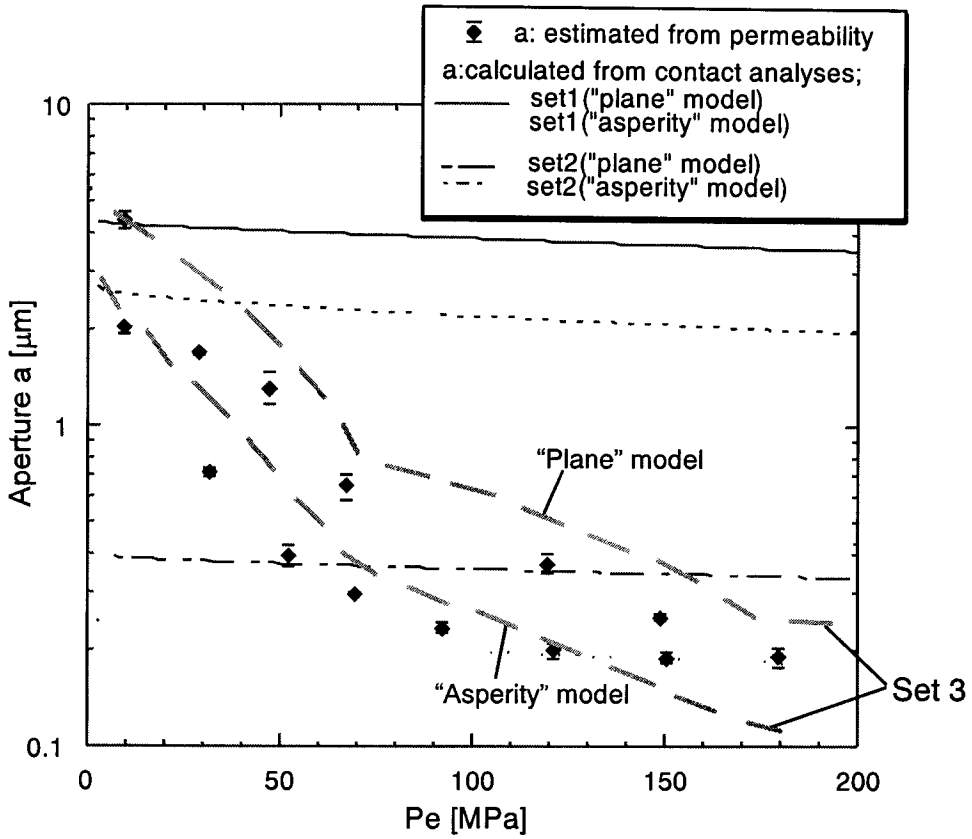

Fig. 6.11. Apertures of natural fractures estimated from permeabilities and the contact analyses, as a function of effective pressure Pe. Sets 1 and 2 are based on the surface profile, however the asperities of set 3 are selected in order to fit the result from the permeability data.

7. DISCUSSIONS

7.1 Permeability structure of the MTL

The fault rock distributions of the Kitagawa and Ankoh outcrops and their vicinities are similar to each other; that is, the fault zone consists of mylonites (about 1000 m wide), cataclasite (about 50 - 200 m wide), of which the area near the gouge zone is cemented by calcite or dolomite, and incohesive fault rocks (about 5 -30 m wide), consisting of discontinuous clayey gouge zones (1 2 cm wide), a black sandy gouge zone (- 2 m wide) and breccia zone of Sambagawa rocks (Fig. 7.1). Sambagawa cemented cataclasite is adjacent to the black gouge zone at the Ankoh outcrop. The distributions of permeability are also close to each other. The results of permeability measurements indicate that permeability of incohesive fault rock samples is larger than that of other fault rocks and host rocks from the MTL in the Kitagawa and Ankoh areas (Fig. 7.1). From this result, the incohesive fault rock zone of the MTL is suggested to act as a conduit around this study area at least above a few kilometers depth, although the permeability measured in this study is that of the sample scale and larger scale structures, such as outcrop scale fractures, must be considered for more detailed discussion. Clayey (sticky) fault gouge zone has permeability as low as 10^{-19} m^2 at high effective pressures, but such an impermeable fault gouge is developed very locally and does not constitutes a continuous zone, which differs from the clayey gouge observed at the active faults (Mizoguchi et al., 2001).

Permeable black gouge zones are found at both the Kitagawa and Ankoh outcrops, which may characterize the permeability structure of the fault zone around these areas. Thin-section observations show that the gouge consists most be of clay minerals and that the structure of the host rock is destroyed. This suggests that, after deformation during fault activity, the fault gouge was consolidated by compaction and/or deposition of calcite and dolomite cement which then brecciated during later deformation. This type of fault rock structure may be characteristic

of fault zones which have evolved for long periods of time at shallow depths. This process has also been inferred from observations on the MTL cataclasites 250km far along strike by Wibberley and Shimamoto (2002).

From the permeability distribution shown Fig. 4.5, subsurface fluid flow around this study area is estimated to concentrate in the fault gouge zone at the MTL. However, because permeability measured in this study is that at the scale of the core sample, larger scale structures such as outcrop-scale fractures are not considered, and this estimated structure is that of 'matrix permeability', and might be lower than the larger scale permeability. In particular, the permeability results indicate that the host rock of the fault rocks along the MTL is impermeable, therefore the fractures in them might play important roles as fluid conduits. In order to estimate the permeability of rock containing fractures, it is important to study the characteristics about distribution of fractures (e.g. the size distribution, anisotropy of directions, and density) and those of the permeability of a single fracture (e.g. dependency on size, roughness stress and temperature). In addition to considering scale, there are many other matters which have to be considered for evaluating the actual permeability structure of the fault zone. One of them is the dependency of permeability of fault gouge on the maximum depth at which samples have been. Temperature and the existence of water might influence the permeability strongly, which are related to the mechanism of rock deformation, the interaction of pore fluid with pore surface (Faulkner & Rutter, 2000), dissolution and deposition of minerals. Furthermore, the permeability of the fault zone might evolve with continued fault activity. For example, the permeability of cataclasite measured in this study might differ enormously from that just after crushing by fault motion.

7.2 Evolution of permeability structure under deformation

The permeability evolution of cataclasite during deformation differs entirely from that of black gouge. Therefore, the permeability structure of fault zone under differential stress may

vary enormously from that under hydrostatic stress (Fig. 7.2). At low strains, the permeability structure may be similar to that under hydrostatic stress, that is, cemented cataclasite is more impermeable than black gouge. As the deformation evolves, the permeability of black gouge and cataclasite probably decrease initially. When the differential stress becomes close to the failure stress, the permeability starts to increase, probably because of the production of cracks and increase in their connectivity. The failure occurs when the deviatoric stress exceeds the strength of cataclasite, and then the permeability may become almost stable, probably being higher than that under hydrostatic stress. On the other hand, the permeability of black gouge may decrease during deformation and become almost stable or decrease slowing even during inelastic deformation. The permeability of these rocks perhaps does not change so much just after the differential stress decreases with the fault sliding, but may return to the initial value by the release of deformation, compaction or cementation, for example. In summary, if not only gouge but also cataclasite deforms until the failure happens, as deformation evolves, the permeability of black gouge may decrease, whereas that of cataclasite may increase, so the difference in permeability between them reduces, or the cataclasite may even become more permeable than the black gouge. To make more realistic model of the permeability structure evolution model during the cycle of fault activity, future studies must cover, at least, the effect of large shearing deformation within fault zones, effects of temperature, complete evaluation of the effects of fractures at deeper conditions, mechanical and chemical cementation of fault rocks during interseismic period.

We should keep in mind that the permeability measured in this study is that of sample size. The permeability and strength of cataclasite larger than the sample probably are influenced from the cracks or subsidiary faults in it. For more precise discussion about the permeability of whole cataclasite area under deviatoric stress, the permeability of such cracks or faults under shear stress or sliding should be taken into account.

The results of permeability measurements under hydrostatic stress show that black gouge shows hysteresis of permeability to effective pressure. If the permeability of black gouge decreases mainly because of rearrangement of grains and/or grain size reduction, it seems to be almost impossible for permeability to recover without any external action. Therefore the permeability may be around the value of when the gouge experienced its maximum differential stress during the cycle of fault activity. When the cohesion of black gouge is increased by compaction or cementation by minerals, or the grain rearrangement and size reduction decrease the permeability enormously, the deformation possibly makes the permeability increase by brecciation or producing shear structure as demonstrated in shear experiments of gouge by Zhang and Cox (2000).

7.3 Permeability of natural fractures under pressure

From the result that the ratio of vertical size to horizontal size of apertures on natural fracture surface is almost constant for wide range of the aperture size, possibly there is a relationship between the size of fracture and the aspect ratio of asperity on it, which may be supported by the relation of the profile length on natural fracture surfaces to the power spectral density of the topography investigated by Power et al. (1987). If such relations are revealed, the permeability of natural fractures on various scales under normal pressure probably can be estimated by the method shown in this study. However, needless to say, the surfaces of natural fractures under pressure may fit to each other more or less. Therefore, if the measurements of the aspect ratio of asperities such as shown in this study can be done for composite topography of the pair of surfaces, more actual evaluation of fracture permeability can be expected.

7.4 Pressurization of pore fluid during deformation

Previous studies have suggested that pressurization of pore fluid during deformation may possibly happen if the permeability of the shear strain concentrating zone is low enough. When

such pressurization is large, it may influence the shear strength of the fault strongly.

Mase and Smith (1987) discussed precisely thermal pressurization. Frictional heating by faulting causes thermal expansion of pore fluid in shear strain concentrating zone. When the rate of the expansion is larger than the escape rate of fluid flow from the zone and the expansion rate of pore volume, the pressure of the fluid flow may increase effectively. The escape rate depends strongly on permeability of the shear strain concentrating zone. As discussed before, clayey gouge which has low permeability exists in the MTL fault zone studied in this study, however it does not constitutes a continuous zone. Thermal pressurization is unlikely in this incohesive fault zone unless clayey gouge is formed pervasively at deeper parts of the MTL around the area studied here. However, for more precise discussion about the pressurization, we have to study the permeability evolution of the shear strain concentrating zone under high strain and high strain rate.

The results of permeability evolution of fault gouge during deformation in Chapter 5 (Fig. 5.2, 7.2) suggest other mechanism of pore fluid pressurization. If the continuous decrease of permeability of gouge during deformation reflects the decrease of pore volume, when the escape rate of pore fluid in the gouge is low enough comparatively the rate of pore volume reduction, the pore pressure may increase. The possibility of this mechanism also depends strongly on the permeability of fault gouge.

7.5 Permeability structure of fault zone from shallow to deep parts and its evolution during seismic cycle

From the results of this study, I discuss the permeability structure of fault zone from shallow to deep parts and its evolution during seismic cycle (Fig. 7.3).

Incohesive fault rock domain

Previous studies have described the permeability structure model of fault zone at the

depth where incohesive fault rocks distribute (Caine et al., 1996). In that model, at the center of fault zone, which is called "fault core", we can observe comparatively impermeable clayey gouge. Such gouge zone does not distribute continuously in the MTL fault zone studied here. During deformation, the permeability of incohesive rocks may decrease continuously with compaction, rearrangement of grains and/or grain size reduction. When incohesive rock consolidates too much, its permeability may increase with the failure. If shear strain or strain rate put on fault gouge is too high, possibly the permeability show different evolution from that observed in this study.

Next to fault core, there is "damage zone", where crack and/or small fault distribute dense, and the damage zone is permeable. From the results of this study, I can not evaluate the permeability of damage zone precisely. During deformation, the density and/or size of crack may increase, and this may make the permeability larger. The permeability also may increase strongly when cracks slide and the discrepancy between topographies of the crack surfaces becomes large.

Cataclasite domain

In this study, the permeability of cataclasite does not differ from that of host rock or less than it, and the permeability increases during deformation. However, in the actual case, the permeability depends on how it decreases during inter-seismic stage. If the permeability does not change so much during the stage, it may not increase so much during deformation, or may decrease as the case of fault gouge. In order to evaluate how the permeability decreases, the mechanism of compaction and cementation of minerals during inter-seismic stage should be investigated.

Mylonite domain

The permeability of mylonite measured in this study does not differ from that of host rock or less than it. There is a evident anisotropy which the permeability parallel to the

foliation is higher than that perpendicular to that. However, from the results of this study, I can not estimate the permeability under high temperature under which mylonite is activate and its evolution during plastic deformation.

Future task for understanding more precisely permeability structure and its evolution

As shown above, there are many things which must be investigated to understand more precisely the permeability structure of fault zone and its evolution during seismic cycle. Especially, the followings should be evaluated exactly:

1. The effect of temperature.
2. The relationship between deformation and manner of fluid flow.
3. Permeability of rocks in which cracks distribute complicatedly.
4. The mechanism of compaction and cementation during inter-seismic stage.

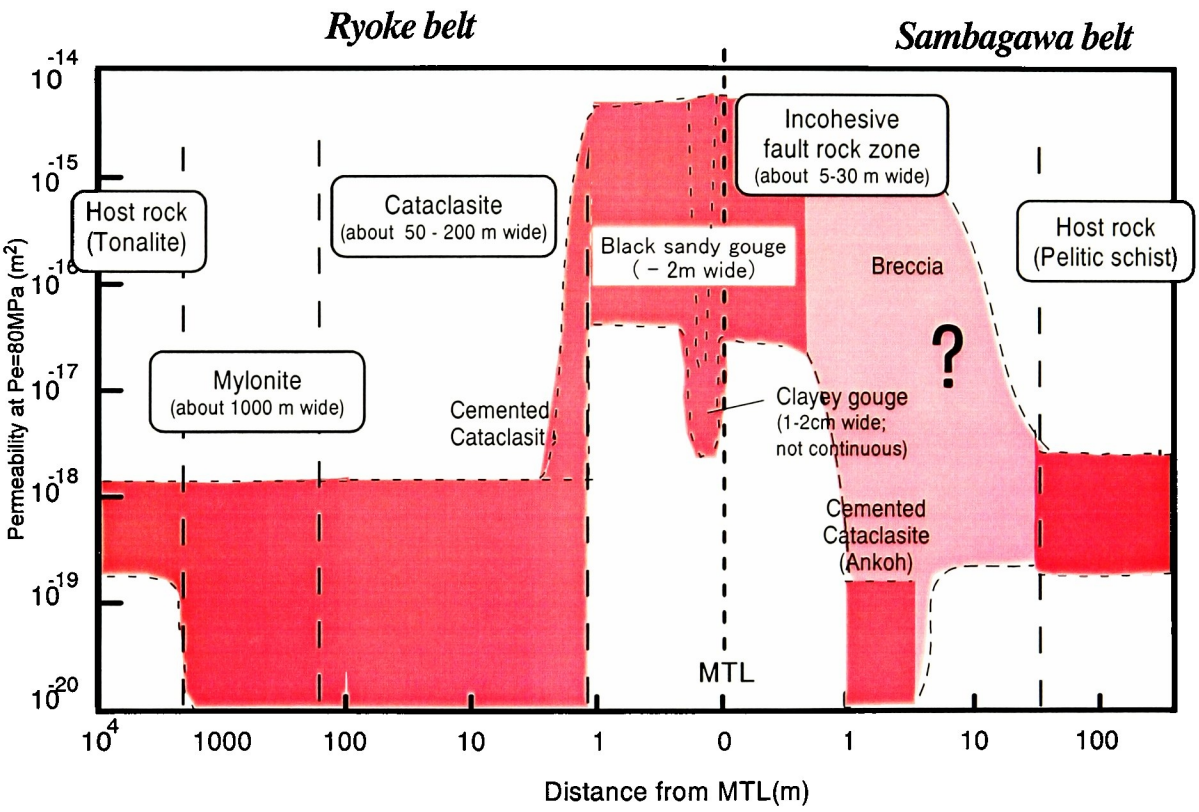

Fig. 7.1. Distribution of fault rocks and permeability structure model along the MTL at Ohshika mura.

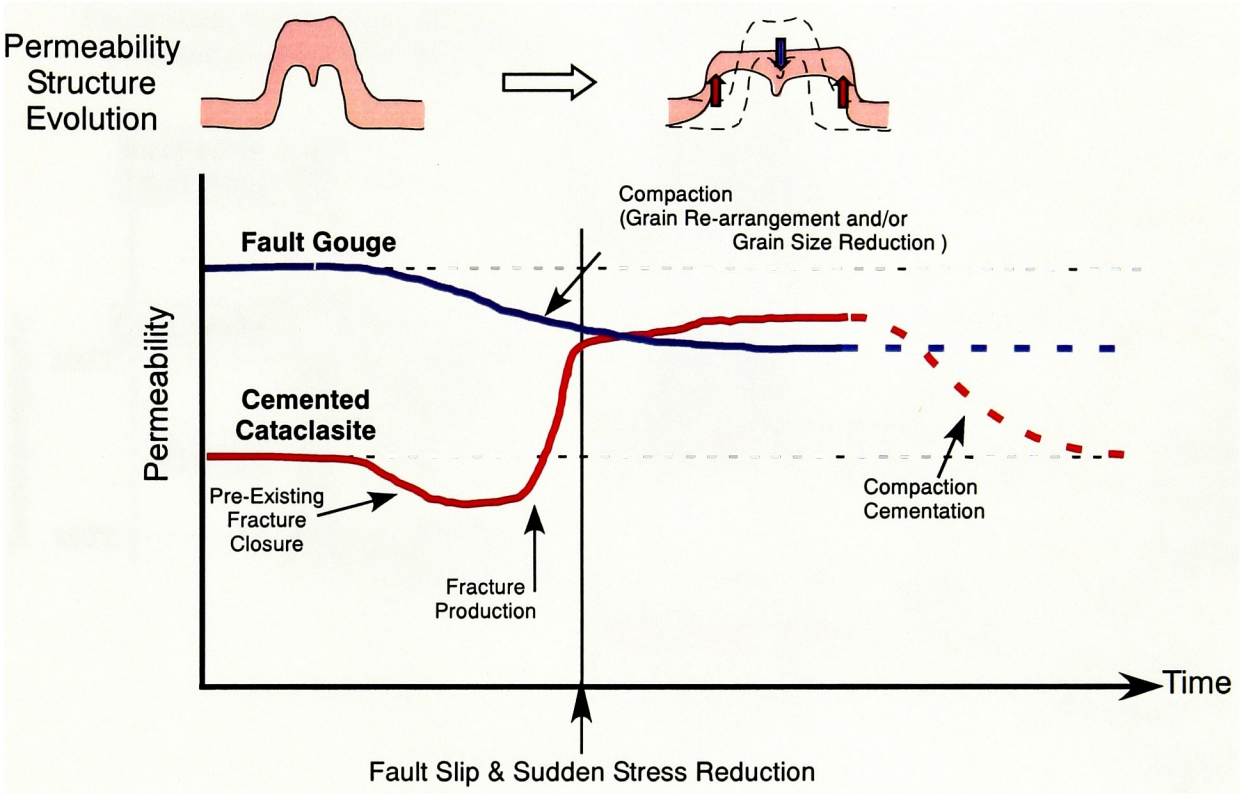

Fig. 7.2. Schematic diagram showing the model of the permeability evolution of fault gouge and cemented cataclasite during the cycle of fault activity.

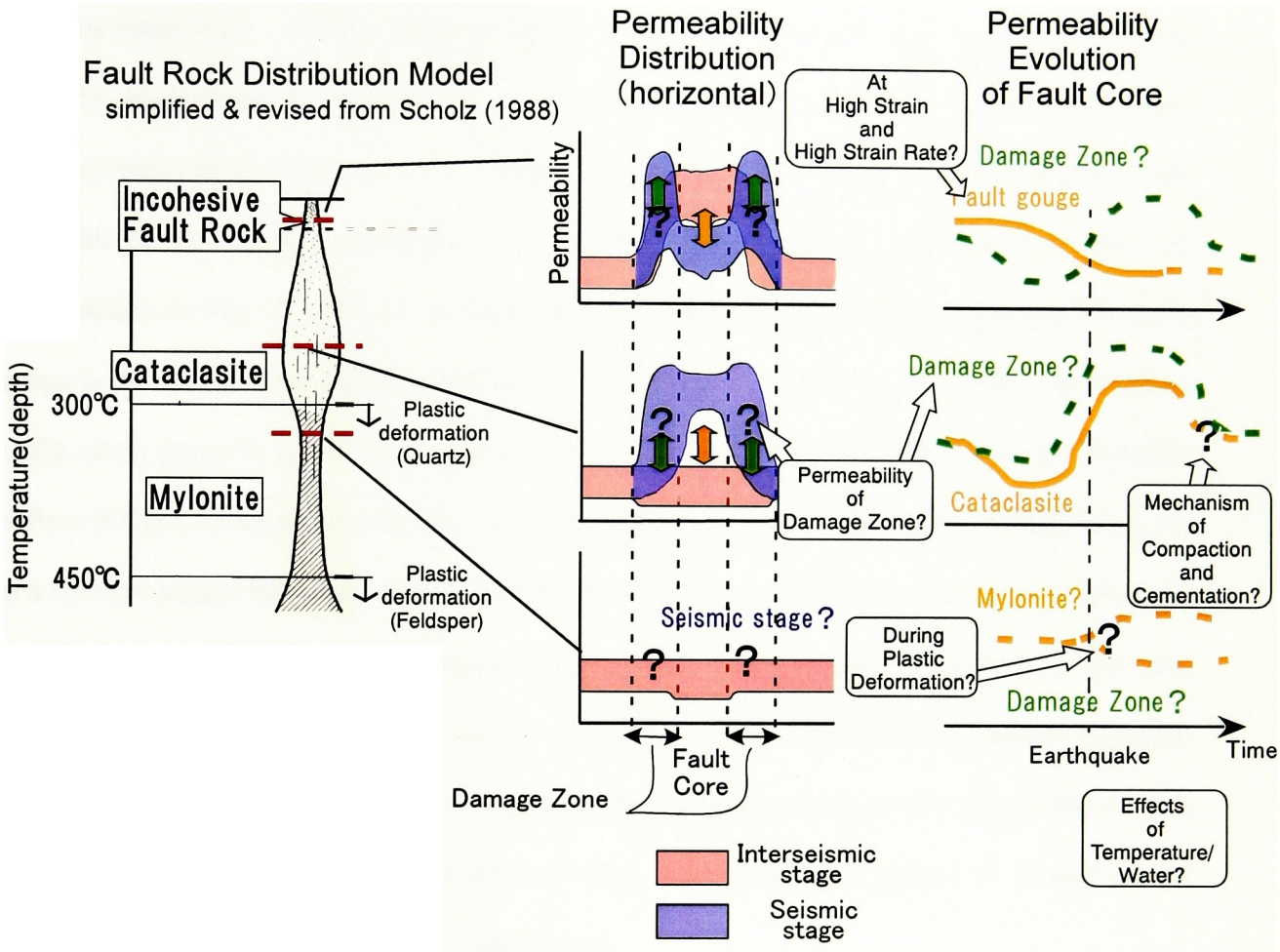

Fig. 7.3 Schematic model of permeability structure of fault zone from shallow to deep parts and its evolution.

8. CONCLUSIONS

Fault rocks are present at the Kitagawa and Ankoh outcrops and their vicinities in the following way, from the MTL contact outward, clayey gouge zone 1 to 2 cm thick is surrounded by black sandy gouge in a zone $\sim$ 2 m thick. The Sambagawa rocks along the MTL are brecciated. Further from the MTL contact is a cataclasite zone, of which the area near the gouge zone is cemented by calcite or dolomite, and mylonite. From the mineral compositions and the structure of the black gouge zone, The gouge can be produced from consolidated or partially cemented fault gouge. Clayey (sticky) fault gouge zone has permeability as low as 10^{-19} m^2 at high effective pressures, but such an impermeable fault gouge is developed very locally and does not constitutes a continuous zone. The permeability of the sandy gouge is more than 2 orders larger than that of cemented cataclasite and mylonite at Pe = 80MPa. From this result, the incohesive fault rock zone of the MTL is suggested to act as a conduit around this study area at least above a few kilometers depth. Incohesive fault rocks exhibit large hysteresis upon pressure cycling and samples tend to remember the low permeability values at the largest pressure, suggesting nearly permanent compaction of gouge and breccia. Whereas cataclasites and mylonites display moderate hysteresis suggesting closing and opening of fractures upon pressure cycling. Thus the past history is important for evaluating permeability of incohesive fault rocks.

The results of the permeability measurements under deviatoric stress with a constant deformation rate showed the characteristic permeability evolution under effective pressure between 10 and 80 MPa of the specimens from the Ryoke cataclasite cemented by calcite and the black gouge consisting of clay minerals collected from the MTL outcrop. When the deviatoric stress increases and becomes close to the failure stress, the permeability of the cataclasite increases maybe because of the production of cracks and increase of their

connection. After failure and sudden decrease in differential stress, the permeability becomes higher than that before deformation. However the permeability of the gouge decreases gradually and becomes almost constant as the deformation evolves. These results suggest the possibility that the permeability structure of the fault zone along the MTL evolves dramatically during the cycle of fault activity. They also indicate that the evolution of permeability structure strongly depends on the deformation mechanism of fault rocks, which is controlled by the depth of deformation.

In general, apertures under normal stress between ground surfaces in pelitic schist and tonalitic mylonite estimated from measured permeability were similar to those estimated from the contact analyses of fracture surface topography deformation. This supports the possibility of estimating permeability of a single fracture under normal stress from the topography data of its surfaces. However, for natural fractures the methods gave different results when the matching of topographies of opposite fracture walls needed to be estimated. In such a case, the composite topography of both surfaces should be taken into account. Hertzian contact theory indicates that the dependency of permeability on normal stress is related to the ratios of vertical and horizontal size of asperities composing the topography of fracture surfaces. Therefore, if the relation of the surface topography and the fracture size is determined for natural fractures, it may be possible to evaluate the permeability of fractures on various scales.

ACKNOWLEDGEMENTS

The author would like to express his sincere thanks to Professor Toshihiko Shimamoto of Kyoto University for many critical discussion, critical reading of the manuscript and encouragements.

The author is grateful to Dr. Akito Tsutsumi of Kyoto University for valuable discussion and helpful advice. The author would like to express his appreciation to Dr. Christopher A. J. Wibberley for sincere discussion, critical reading of the manuscript and correction of my English.

The author wishes to thank Mr. Fumihiro Hara for precious information of the field works and providing the experimental samples. The author is also grateful to Mr. Kazurou Kawamoto for giving useful information and at the permission of sampling at the MTL outcrops and referring literatures in the MTL museum.

The author would like to thank Mr. Takehiro Hirose and Mr. Kazuo Mizoguchi for various discussions and help with the experiments. The author thanks all his colleague of the Experimental Rock Deformation Laboratory for their encouragement. The author also thanks his room mates for their helpful manner.

I thank my parents for a lot of spiritual and financial support and encouragement.

REFERENCES

Bernabe, Y., The effective pressure law for permeability during pore pressure and confining pressure cycling of several crystalline rocks, *J. Geophys. Res.*, 92, 649-657, 1987.

Brace, W. F., J. B. W. Paulding and C. Scholz, Dilatancy in the fracture of crystalilne rocks, *J. Geophys. Res.*, 71, 3939-3953, 1966.

Brace, W. F., J. B. Walsh and W. T. Frangos, Permeability of granite under high pressure, *J. Geophys. Res.*, 73, 2225-2236, 1968.

Brown, S. R. and C. H. Scholz, Closure of randam elastic surfaces in contact, *J. Geophys. Res.*, 90, 5531-5545, 1985.

Brown, S. R., Simple mathematical model of a rough fracture, *J. Geophys. Res.*, 100, 5941-5952, 1995.

Caine, J. S., J. P. Evans and C. B. Forster, Fault zone architecture and permeability structure, *Geology*, 24, 1025-1028, 1996.

Evans, J. P., C. B. Forster and J. V. Goddard, Permeability of fault-related rocks, and implications for hydraulic structure of fault zones, *J. Struct. Geol.*, 19, 1393-1404, 1997.

Faulkner, D. R. and E. H. Rutter, Comparisons of water and argon permeability in natural clay-bearing fault gouge under high pressure at 20 ℃, *J. Geophys. Res.*, 105, 16415-16426, 2000.

Fischer, G. J. and M. S. Paterson, Measurement of permeability and storage capacity in rocks during deformation at high temperature and pressure in *Fault mechanics and transport properties of rocks*, edited by B. Evans and T.-F. Wong, pp. 213-252, Academic Press Ltd, 1992.

Hara, I., K. Shyoji, S. Yokoyama, M. Arita and Y. Hiraga, Study on the southern marginal shear belt of the Ryoke metamorphic terrain-Initial movement picture of the Median Tectonic Line., *Earth Sci.*, 31, 204-217, 1977.

Hara, I., K. Shyoji, Y. Sakurai, S. Yokoyama and K. Hide, Origin of the Median Tectonic Line and its Initioal Shape, *Memoirs of the Geological Society*, 18, 27-49, 1980.

Huenges, E. and G. Will, Permeabiity, bulk modulus and complex resistivity in crystalline rocks in *Fluid movements element transport and the composition of the deep crust*, edited by D. Bridgewater, pp. 361-375, Kluwer Academic Publishers, 1989.

Johnson, K. L., *Contact mechanics*, Cambridge University Press, Cambridge, 1985.

Kranz, R. L., J. S. Saltzman and J. D. Blacic, Hydraulic diffusivity measurements on laboratory rock samples using an oscillating pore pressure method, *Int. J. Rock Mech. Min. Sci. Geomech. Abstr.*, 27, 345-352, 1990.

Lockner, D., H. Naka, H. Tanaka and R. Ikeda, Permeability and strength of core samples from Nojima fault of the 1995 Kobe earthquake in Proceedings of the international workshop on the Nojima fault core and porehoke data analysis (USGS open-file report oo-129, GSJ interim report No. EQ/00/1), edited by H. Ito, K. Fujimoto, H. Tanaka and D. Lockner, pp. 147-152, 2000.

Mase, C.W. and L. Smith, Effects of frictional heating on the thermal, hydrological, and mechanical response of a fault, *J. Geophys. Res.*, 92, 6249-6272, 1987.

Matsushima, N., New Interpretation of Medean Tectonic Line of the Akaishi Mountain Lands, in Japan, *Bulletin of Iida city museum*, 4, 113-124, 1994.

Michibayashi, K. and T. Masuda, Shearing during progressive retrogression in granitoids:abrupt grain size resuction of quarts at the plastic-brittle transition for felspar, *J. Struct. Geol.*, 15, 1427-1432, 1993.

Michibayashi, K., Syntectonic development of a strain-independent steady state grain size during mylonitization, *Tectonophysics*, 222, 151-164, 1993.

Mizoguchi, K., T. Hirose and T. Shimamoto, Permeability structure of Nojima branch fault at funaki, Hokudan-cho, *Chikyu Monthly*, 31, 58-65, 2000.

Mogi, K., Effect of the intermediate principal stress on rock failure, *J. Geophys. Res.*, 72, 5117-5131, 1967.

Morrow, C. A., Z. Bo-Chong and J. D. Byerlee, Effective pressure law for permeability of Westerly Granite under cyclic loading, *J. Geophys. Res.*, 91, 3870-3876, 1986.

Power, W. L., T. E. Tullis, S. R. Brown, G. N. Boitnott and C. H. Scholz, Roughness of natural fault surfaces, *Geophys. Res. Lett.*, 14, 29-32, 1987.

Sakamoto, M., Fault displacement topography along the Median Tectonic Line in the Akaishi Mountains, *MTL*, 2, 103-110, 1977.

Seront, B., T.-F. Wong, J. S. Caine, G. B. Forster and R. L. Bruhn, Laboratory characterization of hydromechanical properties of a seismogenic normal fault system, *J. Struct. Geol.*, 20, 865-881, 1998.

Takagi, H., Cataclastic deformation on mylonitic rocks along the Median Tectonic Line Example in Kami-Ina district, Nagano Prefecture, *Academic studies (Biology · Geology) issued ammually by the school of education*, Waseda University, 32, 47-60, 1983.

Takagi, H., Mylonitic rocks along the Median Tectonic Line in Takato-Ichinose area, Nagano Prefecture, *Jour.Geol.Soc.Japan*, 90, 81-100, 1984.

Takagi, H., Implications of mylonitic microstructures for the geotectonic evolution of the Median Tectonic Line, central Japan, *J. Struct. Geol.*, 8, 3-14, 1986.

Tanaka, H., H. Takagi and M. Inoue, Mode of cataclastic deformation and hydrothermal alteration of the fault rocks and history of fault activity along the Median Tectonic Line, central Japan, *The Journal of the Tectonic Research Group of Japan*, 41, 31-44, 1996.

Walsh, J. B., The effect of cracks on the uniaxial elastic compression of rocks, *J. Geophys. Res.*, 70, 399-411, 1965.

Wibberley, C. A. J. and T. Shimamoto, Internal structure and permeability of major strike-slip fault zones: the Median Tectonic Line in W. Mie Prefecture, S.W. Japan, *J. Struct. Geol.*,

in press, 2002.

Yoshioka, N. and C. H. Scholz, Elastic properties of contacting surfaces under normal and shear loads 1. Theory, *J. Geophys. Res.*, 94, 17681-17690, 1989.

Zhang, S. and S. F. Cox, Enhancement of fluid permeability during shear deformation of a synthetic mud, *J. Struct. Geol.*, 22, 1385-1393, 2000.

Zhu, W. and T.-f. Wong, The transition from brittle faulting to cataclastic flow: permeability evolution, *J. Geophys. Res.*, 102, 3027-3041, 1997.

Zoback, M. D. and J. D. Byerlee, The effect of microcrack dilatancy on the permeability of Westerly granite, *J. Geophys. Res.*, 80, 752-755, 1975.